Adipic Acid Production: Process Modeling of the Benchmark and Two Electrochemical Approaches

A Process Systems Modeling Prospective

Masters Thesis

Edward Yeo

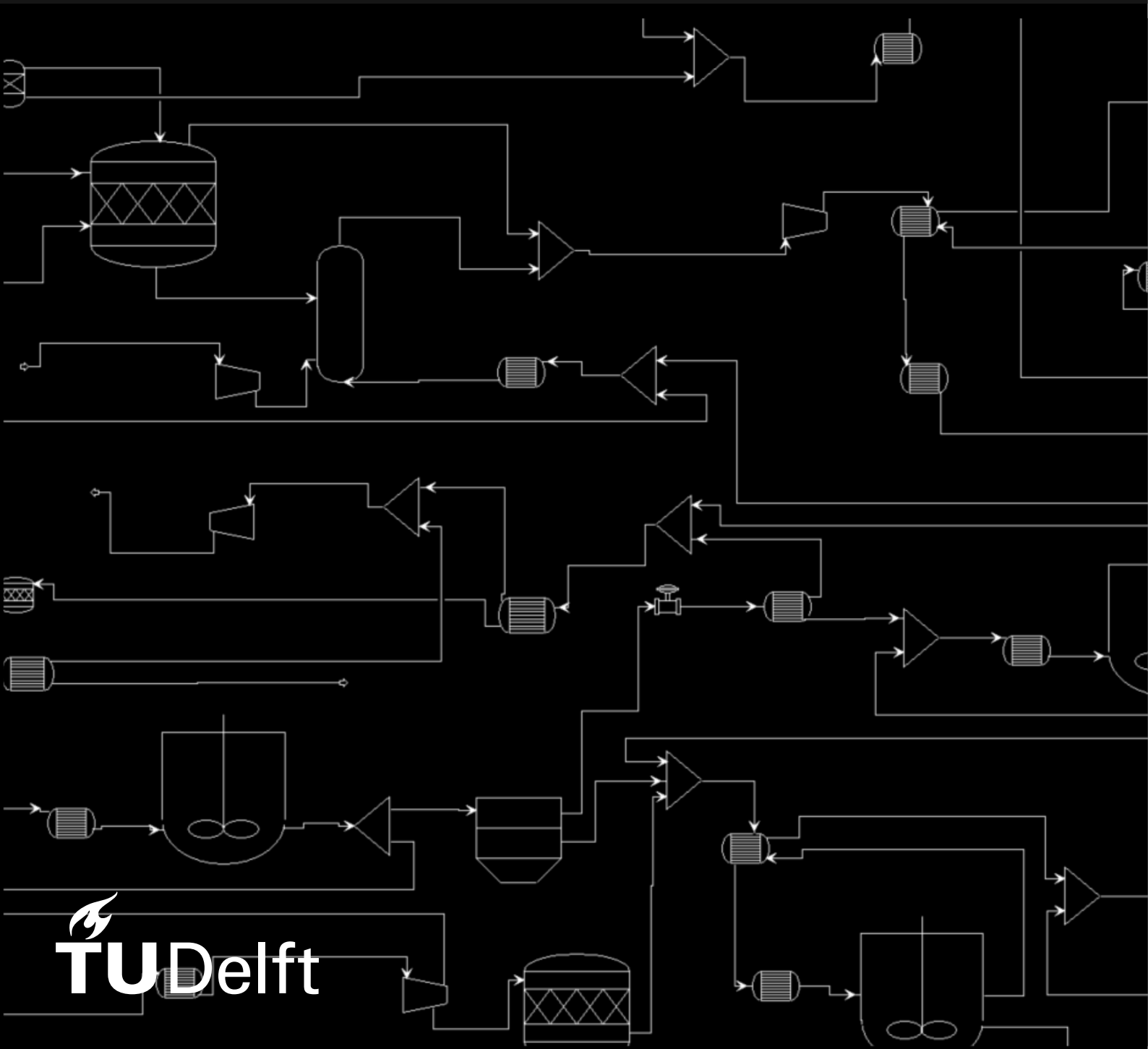

TU Delft

Adipic Acid Production: Process Modeling of the Benchmark and Two Electrochemical Approaches

A Process Systems Modeling Prospective

by

Edward Yeo

to obtain the degree of Master of Science in Mechanical Engineering
at the Delft University of Technology,

Student number:	6052886
Project duration:	December 3rd, 2024 – August 29th, 2025
Thesis committee:	
Chair:	Prof. dr. ir W. de Jong
TU Delft, supervisors:	Dr. Shahid Khan
	Dr. O. Moultos
	Dr.ir. L. Cutz
External examiner:	Prof.dr. P. Osseweijer

An electronic version of this thesis is available at http://repository.tudelft.nl/.

TU Delft

Preface

This thesis was completed as part of my graduation project in the Mechanical Engineering Masters degree, track Energy Process and Flow Technology. The completion of this degree would not have been possible without the huge support from many people.

First and foremost my family. Although not always obvious, your daily check-ins and calls blunted some of the sharper edges of this masters experience and I am so grateful for your emotional and financial support. Aan Oupa, ek sê dankie dat jy my hierdie geleentheid gegee het wat jy geweier was. Ek hoop om dit eendag oor te laat gaan.

I would like to thank my supervisors Wiebren and Shahid. Their assistance in understanding technical decisions and pointing me in the right direction was vital. My discussions can sometimes be all over the show so thank you for your patience and consistent engagement with my ramblings. Your knowledge and understanding in your respective fields are unparalleled and I wish you well in all your future endeavors.

To the countless cool Delft people that I am lucky enough to now call friends, you have been the most eye-opening and fun aspect of this experience in the Netherlands. From ice cream walks, to debates on Italian food, and from countless games of Frisbee, to failed surf missions. If KLM had more baggage allowance, I'd pack you all in.

Edward Yeo
Delft, August 2025

Abstract

Adipic Acid Production: Process Modeling of the Benchmark and Two Electrochemical Approaches - A Process Systems Modeling Prospective

Adipic acid (AA), a critical precursor for nylon-6,6 and other industrial applications, is currently produced at over 3 million tons annually, with projected revenues reaching $6 billion by 2030. However, an alternative to the dominant industrial process, accounting for 95% of global production, has been sought due to inefficiency and significant environmental impact. This conventional route relies on petroleum-derived benzene as a feedstock and involves multiple hydrogenation and oxidation steps, notably utilizing nitric acid, which produces stoichiometric amounts of nitrous oxide (N2O)—a potent greenhouse gas. Furthermore, the high energy feedstocks like benzene, hydrogen, and nitric acid contribute significantly to Scope 3 emissions.

Given these concerns, there is a strong incentive to develop more energy-efficient and environmentally suitable processes. This thesis addresses the gap in comprehensive techno-economic assessments of emerging alternatives, which often overlook practical implementation challenges such as downstream separation, feedstock pretreatment, and overall carbon footprint.

The overarching research question guiding this study is: ”How do various electrochemical based alternatives to current AA production compare on an economic and emissions basis from a process systems modeling prospective?”. To this end, two promising alternatives were selected for evaluation through the key performance indicators of; profitability in the form of minimum selling price (MSP), emissions based on kg $CO_{2equivalent}$, and material efficiency based on the excess ratio of theoretical main feedstock to actual main feedstock.

The first modeled process was that of the conventional route. This was done to ensure a consistent feedstock price component in the final adipic acid cost across all assessed production methods, thereby providing valuable validation for modeling assumptions. Furthermore, it serves as a benchmark for comparing the economic and emissions performance of various electrochemical-based alternatives, offering insights into their relative strengths and weaknesses. The results attained were consistent with those of literature, with a minimum selling price of $1.58/kg

The first alternative route employs an electrocatalytic oxidation cell to replace the nitric acid oxidation step of the conventional process. Experimental work of previous researchers was used to create an approximate model of the cell and the electrodialyzer used for the recovery of KOH electrolyte. This was implemented within Apsen Plus along with upstream and downstream processing. The resulting model and subsequent TEA predicted an adipic acid price of $2.33/kg or a %45 increase over the results of the conventional route. However, assuming the use of renewable electricity, the CO_2 equivalent emissions dramatically reduced by half when compared to the conventional process.

The second alternative was the use of biomass based fermentation and subsequent electrochemical oxidation to produce a adipic acid alternative of similar value to industry. Once again, the experimental work of previous researchers was used to predict a final minimum selling price of around $3.97/kg; however, these results are highly susceptible to variations in input parameters. Both alternatives showed lower emissions when compared to the conventional process.

Contents

List of Figures

List of Tables

Nomenclature

Abbreviation	Definition
AA	Adipic acid
ADSB#	Absorption column (followed by number)
ANE	Cyclohexane
BEN	Benzene
BPM	Bipolar membrane
CAPEX	Capital expenditure
CEM	Cation exchange membrane
CEN#	Centrifuge (followed by number)
CEPCI	Chemical Engineering Plant Cost Index
CHA	Cyclohexanol
CHN	Cyclohexanone
CMPR#	Compressor (followed by number)
COL#	Column (followed by number)
COP	Coefficient of performance
CRYS#	Crystallizer (followed by number)
CS	Carbon Steel
CW	Cooling water
ECH	Electrocatalytic hydrogenation
ECO	Electrocatalytic oxidation
ED	Electrodialysis
F#	Flash separator (followed by number)
FCI	Fixed capital investment
GA	Glutaric acid
GHG	Greenhouse gas
HX	Heat exchanger
KA	Ketone-Alcohol
KPI	Key performance indicator
LPS	Lower pressure steam
M#	Mixer (followed by number)
MA	Muconic acid
MPS	Medium pressure steam
MSP	Minimum selling price
NPV	Net present value
OPEX	Operational expenditure
R#	Reactor (followed by number)
RHE	Reference hydrogen electrode
S#	Spliter (followed by number)
SS	Stainless steel
STP	Standard temperature and pressure
TEA	Techno-economic assessment
TUR#	Turbine (followed by number)
USD ($)	United States Dollar
V#	Let down valve (followed by number)
3tHDA	Trans-3-hexenedioic acid

Symbol	Definition
A	Area
E_{cell}	Reservable cell potential
E_{total}	Total cell potential
F	Faraday constant
j	Average current density
K_c	Reaction quotient
n_{AA}	Amount of product produced
P	Productivity
Q	Total charge passed
Q_{COLD}	Energy dumped to cold sink
R	Gas constant
t	Time
T_{COLD}	Temperature of cold sink
T_{HOT}	Temperature of hot source
z	Number of electrotrons involved
ΔH	Heat of reaction
Δg_o	Net change in gibbs free energy
η	Efficiency

1 Introduction

1.1. Background

Adipic acid (AA) is the common name for butane-1,4-dicarboxylic acid ($HOOC(CH_2)_4COOH$) and is an important precursor monomer to industrially synthesize polyurethane, plasticizers, food additives and, most commonly, nylon-6,6. The annual production of AA exceeds 3 million tons and with the growing global demand for nylon-6,6 in the manufacturing industry, AA revenue is expected to reach $6 billion by 2030, from a current market size of $4.9 billion [1].

The use of this precursor chemical has become widespread, but the manufacturing process remains inefficient and polluting, with 95% of global production coming from a complex process involving petroleum-derived benzene (BEN) as a feedstock and multiple hydrogenation and oxidation steps. There are several issues with this process. Firstly, an important intermediate oxidation step is performed with nitric acid, as a result, 3 tons of N_2O are produced for every 10 tons of AA produced [2]. This N_2O, along with other N_XO_X compounds need to be either emitted into the environment, where they are known to cause significant global warming effects, or they require expensive and complex decomposition into less harmful materials [3, 4]. The second main issue is the need for high energy feedstocks that are currently not produced sustainably. BEN, hydrogen (H_2) and nitric acid (HNO_3) represent significant sources of scope 3 emissions in the current industrial process [5, 6, 7]. There is therefore a great incentive to find a more energy efficient and environmentally suitable processes with several proposed methods showing potential for improvement.

The use of alternative feedstocks such as butadiene or phenol have been tested and even implemented, however for economic reasons these routes have not replaced the conventional route [8, 9]. Certain proposed methods involve the utilization of alternative oxidants, such as hydrogen peroxide, to carry out the oxidation step or alternative oxidation reaction steps to remove the need for nitric acid; however, these routes suffer from high oxidizer costs and several other drawbacks [10].

Electrocatalytic oxidation (ECO) is an alternative to the use of nitric acid and is an area of active research [11, 12, 13, 14, 15, 16]. ECO can be operated at mild temperatures and utilize renewable electricity and water to oxidize the KA oil intermediate. This process does not produce large amounts of unwanted byproducts and can in fact be used to produce the hydrogen needed in the initial BEN hydrogenation reaction. Although very promising, the current research is primarily centered around electrode catalyst design and performance and little work has been done in assessing the practical feasibility of these methods based on the current state of the art. [17, 11]

Another area of AA production research is biomass based fermentation carried out with engineered bacterium. There are several routes which have been studied to various degrees. The direct fermentation of AA from biomass has been shown to be economically viable if high enough AA concentrations and yields can be achieved [18]. However the issue of low concentration in fermentation broth is of serious concern and fermentation and subsequent hydrogenation of a more easily fermented intermediate has

been an active area of research, specifically muconic acid (MA) as an intermediate [19, 20, 21, 22]. The subsequent hydrogenation of the MA can be achieved with MA separation from the fermentation broth and traditional catalytic hydrogenation, or with the direct electrochemical hydrogenation (ECH) of the MA in the fermentation broth. The ECH of MA in the fermentation broth presents an opportunity for significant cost savings due to reduced separation costs as well as reduced scope 3 emissions over the traditional catalytic hydrogenation method. [18, 23]

1.2. Motivation

With large amounts of research being conducted into the use of electrochemical based alternatives in the production of AA, it is useful to assess and compare how these technologies are practically implemented into industry. Factors such as downstream separation and feedstock pretreatment are often not considered when research is conducted into novel techniques [24], however these need to be assessed to determine the research progress and real world feasibility of these techniques.

For example, ECO catalyst performance has been heavily researched but only one simplified techno-economic assessment (TEA) by Liu et al. [11] can be found in literature. The same can be said for biomass based routes, with Gunukula et al. [18] and Dell'Anna et al. [19] representing some of the few TEAs found in literature. The latter being the only example of a biomass based ECH TEA found in literature.

It is the goal of this thesis to widen the view of understanding of these electrochemical based techniques and allow for better understanding of the important and less important factors determining technology feasibility. Consideration will be given to upstream and downstream processing of materials as well as the carbon footprint of the materials and processes employed.

1.3. Research Questions

Overarching question: How do various electrochemical based alternatives to current AA production compare on an economic and emissions basis from a process systems modeling prospective? To answer this overarching question, the following questions should be addressed by comparing the key performance indicators, (KPIs), of profitability, emissions and material efficiency, which are defined in Section 3.2.

- What is the benchmark economic and emissions performance of the current industrial process and what are its areas for improvement?
- What is the performance of electrochemical based alternatives and what conditions need to be met to achieve this performance?
- Under which minimum conditions would electrochemical based alternatives be competitive with the current industrial process in a Northern European context?

1.4. Thesis Chapter Breakdown

This report follows the steps taken in completing this project, starting in chapter two with a literature review. Here the know intricacies of the studied processes are documented along with important information on possibly useful techniques and emission/cost information. Chapter three deals with the methodology used in the execution of the project. This includes relevant assumptions as well as conceptual process design. Chapter four will detail the final process design and results of the techno-economic assessment. Finally chapter five and six will present a discussion, answer research questions and provide recommendations for future work.

2

Literature review

2.1. Current Industrial Adipic Acid Production

2.1.1. Process Description

The current dominant industrial process for AA production is a nitric acid oxidation process in which BEN is used as a feedstock with several process steps. 95 to 98% of global production utilizes this process as shown with the red highlighted path of Figure 2.1 [25, 26, 27]. Whilst alternative routes exist, as shown in Figure 2.1, they are utilized less due to AA selectivity and equipment cost reasons.

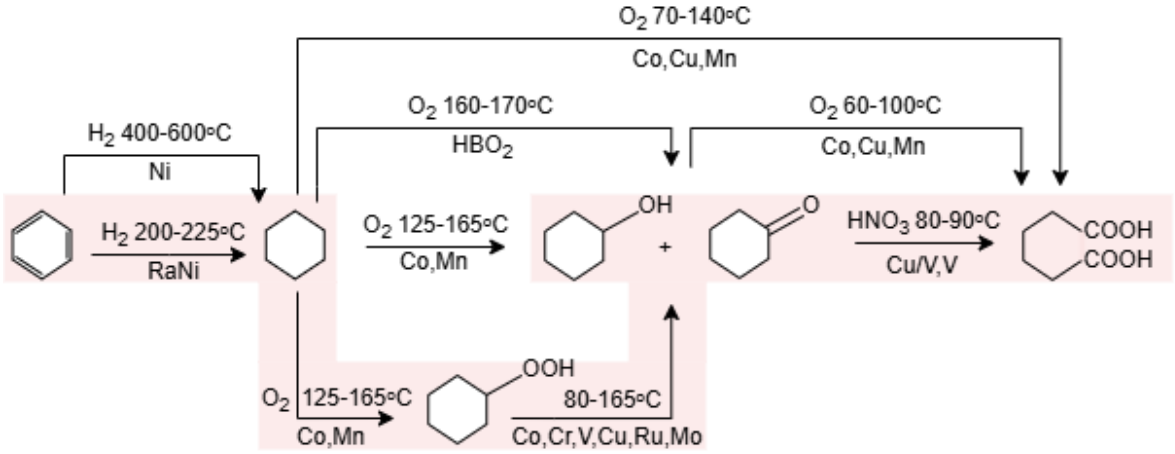

Figure 2.1: AA industrial production pathways

2.1.2. Process History

The current process for the use of BEN feedstock was first developed in the 1930s after a rise in Phenol costs incentivized the development of alternative manufacturing processes [25]. The oxidation of KA oil in the third step of this process was originally done with air, however Du Pont developed the Nitric Acid oxidation process in the 1940s, which improved product yields and conversions. The reaction mechanics of this process were first studied in 1956 and since then, major work has been done to optimize and mature the process. [8]

2.1.3. Process Steps

The first step in this process is the hydrogenating of petroleum-derived BEN to cyclohexane (ANE) and this is highly exothermic, with $\triangle H$ = -214 kJ/mol. There are two main industrial practiced hydrogenation processes. In process one, hydrogenation is performed in a bubble column reactor in the presence of a Raney nickel catalyst. Temperatures are usually between 200-225°C and pressures around 50 bar [28]. A secondary vapor phase reactor is also employed to achieve the final conversion as shown in Figure 2.2.

Process two is done in the gas-phase in the presence of a Ni or noble metal catalyst packing, at around 400 to 600°C and 25-30 bar. Careful control of reaction temperature and residence time is crucial to avoid equilibration between ANE and methylcyclopentane, an unwanted byproduct. To this effect, many processes employ a finishing reactor to reduce residual BEN and methylcyclopentane to less than 100 ppm and producing nearly pure ANE. [28, 29]

It is reported that carbon monoxide and sulfur compounds, common impurities in the hydrogen and BEN supply, can lead to catalyst deactivation. Therefore the hydrogen is commonly passed through a caustic scrubber and a methanator to remove these impurities [28, 29]. BEN often contains Dienes, Olefins,and Sulfur Compounds as impurities as well as other non-organic compounds. A two stage hydrogenation process is often used, in which the dienes are hydrogenated to olefins in a mild first stage. In the second stage, the olefins and sulfur compounds are removed under more severe conditions. Saturation of the BEN aromatics is not a concern as the ANE byproduct is utilized in the AA production process [30].

BEN to ANE:

$$C_6H_6 + 3H_2 \rightarrow C_6H_{12} \qquad \Delta H = -214kJ/mol_{BEN} \tag{2.1}$$

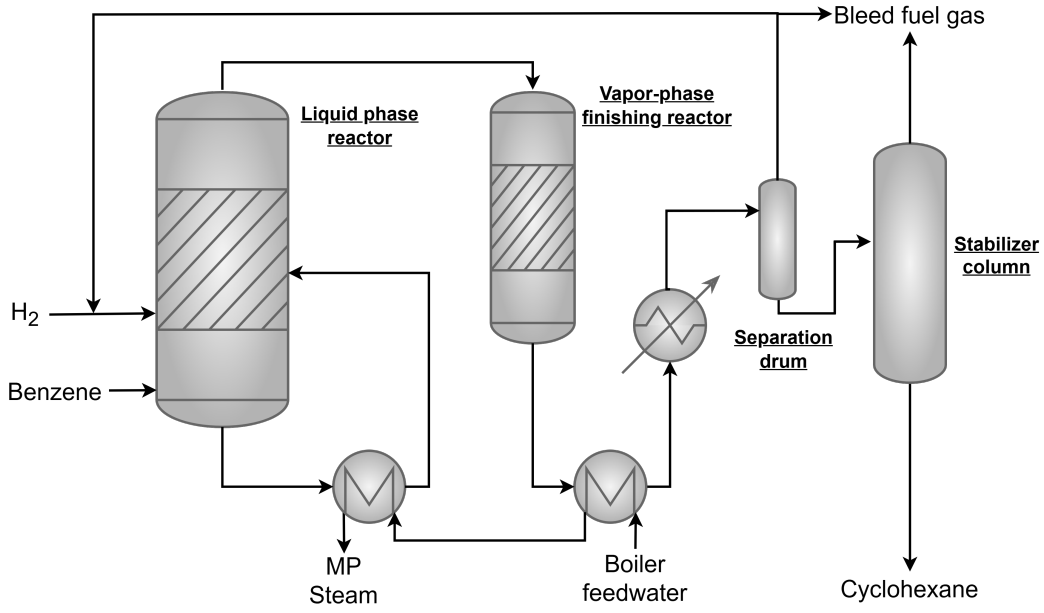

Figure 2.2: Industrial BEN to ANE process

Step two involves oxidising ANE with air in the presence of a cobalt catalyst to produce ketone-alcohol (KA) oil, which consists of Cyclohexanol (CHA) and Cyclohexanone (CHN). The oxidation of ANE to KA oil is performed in the liquid phase at 8-15 bar and 125-165°C, and involves the intermediate cyclohexyl hydroperoxide as shown in Equation. 2.2. Due to KA oil oxidizing more readily than ANE, the ANE oxidation is heavily limited to reduce unwanted KA oil oxidation byproducts and maintain selectivity of around 80-85 %. As a result, the single pass ANE conversion for these reactors are low (10-12%).[31] Decomposition of the cyclohexyl hydroperoxide performed in a separate reactor under milder conditions, while the unreacted ANE is recycled, as shown in Figure 2.3.

The two main byproducts, glutaric and succinic acid are extracted with aqueous alkali and the remain KA oil can be distilled to 99.5% purity by distillation and normally has a ketone alcohol ratio of 3.5:1 [2, 32, 28, 33]. There has been substantial research into the use of boric acid to assist in the oxidation of ANE. However the higher costs of dealing with this acid as well as the cost of the additional equipment is not offset by the additional raw material savings from higher selectivity [27].

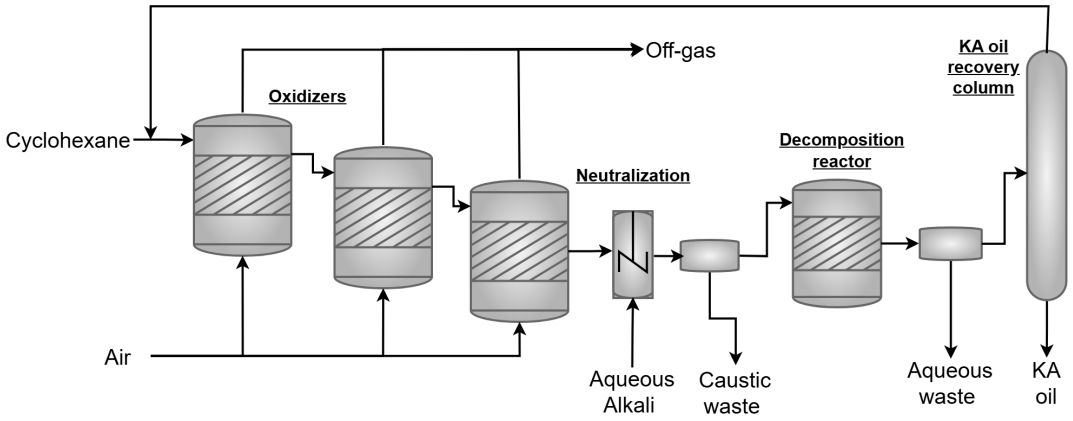

Figure 2.3: Industrial ANE to KA oil process

ANE to KA Oil (unbalanced):

$$\begin{aligned} &C_6H_{12} + O_2 \rightarrow (CH_2)_5COOH \\ &\rightarrow HOCH(CH_2)_5 + (CH_2)_5CO + H_2O \qquad \Delta H \approx -294kJ/mol_{ANE} \end{aligned} \tag{2.2}$$

In step three, the KA oil is oxidized with excess HNO_3 to produce AA according to Equation 2.3 with a typical conversion yields of between 92 and 96% [25, 26, 8].This step is shown in Figure 2.4. Typical HNO_3 concentrations of 50-65% are used with an HNO_3 excess of from 3:1 to 1000:1. This is done to improve yield but also to control the reaction temperature as the reaction is highly exothermic, around 6300 kJ/kg of AA. The reaction temperature and pressure are relatively mild, at 60-80°C and 1-3 bar, respectively. Several catalysts are used in this reaction, namely, copper and vanadium derivatives and at various concentrations below 1%. Typical byproducts include glutaric and succinic acid.[2, 12, 26]

KA oil to AA (unbalanced):

$$\begin{aligned} &HOCH(CH_2)_5 + (CH_2)_5CO + HNO_3 \\ &\quad \rightarrow HOOC(CH_2)_4COOH + N_2O + NO + NO_2 + H_2O \qquad \Delta H \approx -700kJ/mol_{AA} \end{aligned} \tag{2.3}$$

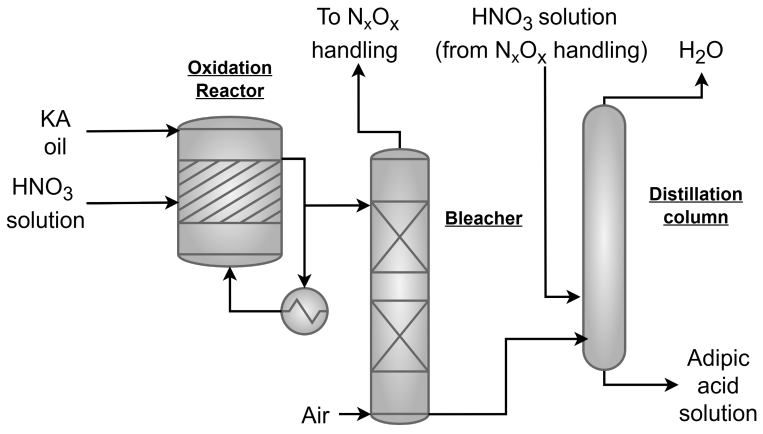

Figure 2.4: Industrial KA oil to AA process

Table 2.1: AA solubility in water solution

Temperature (°C)	Solubility limit (M)
5	0.035186
10	0.070373
15	0.105559
40	0.281492
60	0.422238
80	0.562984
100	0.70373

Finally, the AA crystallizes as the product solution cools according to Table 2.1 [34]. The AA can be purified by means of recrystallization as shown in Figure 2.5 [28, 35]. The AA solution is first run through a crude crystalizer to crystallize and remove as much AA as possible. The remaining solution is then distilled and concentrated before being cooled and the AA allowed to crystallized once more in the purge crystallizer. The remaining HNO_3 solution is separated from heavy wastes and then set back to the KA oil oxidizer. Due to the high purity requirements of AA, a secondary refined crystallization is used to remove impurities before the AA is separated and dried at a purity of around 99.6%. [28, 8, 36].

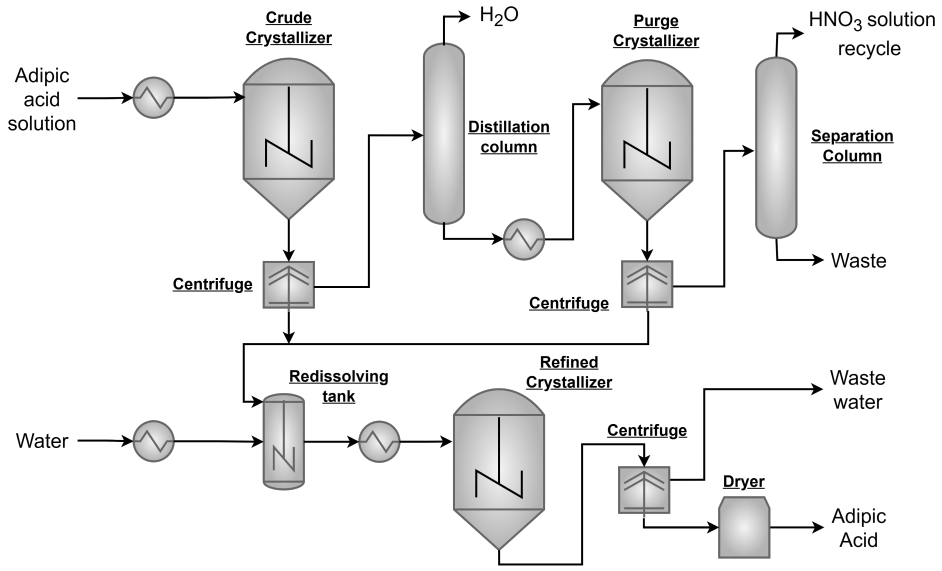

Figure 2.5: AA crystallization process

2.1.4. Abatement Technologies for NO Emissions

The current industrial synthesis of AA produces stoichiometric amounts of NO compounds and specifically N_2O, as shown in Equation 2.3. The molar ratio of N_2O: NO_2 is around 1:1 [27]. The N_2O needs to either be emitted to the atmosphere, where it is known to have serious negative environmental effects, or decomposed. This decomposition can be done catalytically or thermally and there have been several processes developed by the major AA producers. The thermal decomposition process entails the mixing of air into the NO stream. This stream is then oxidized to allow NO_x compounds to be recovered as nitric acid. The remaining N_2O stream is sometimes mixed with natural gas, if the N_2O concentrations are low, and then combusted to N_2 and O_2 and the heat is recovered for process steam.[3].

The catalytic decomposition process is the more common method used, with large scale producers Invista, Rhodia, Asend and BASF all employing it to some degree [27, 3]. The process can take multiple forms however Figure 2.6 displays the process that was made public by BASF in 1997. The NO_x com-

ponents of the exhaust gas are recovered as nitric acid in an initial absorption column. The remaining N_2O is catalytically decomposed in stages to produce process steam and N_2 and O_2 [37]. Decomposition conditions vary significantly depending on catalyst type and stream composition. However, N_20 abatement rates of effectively 100% have been achieved in some configurations [27, 38].

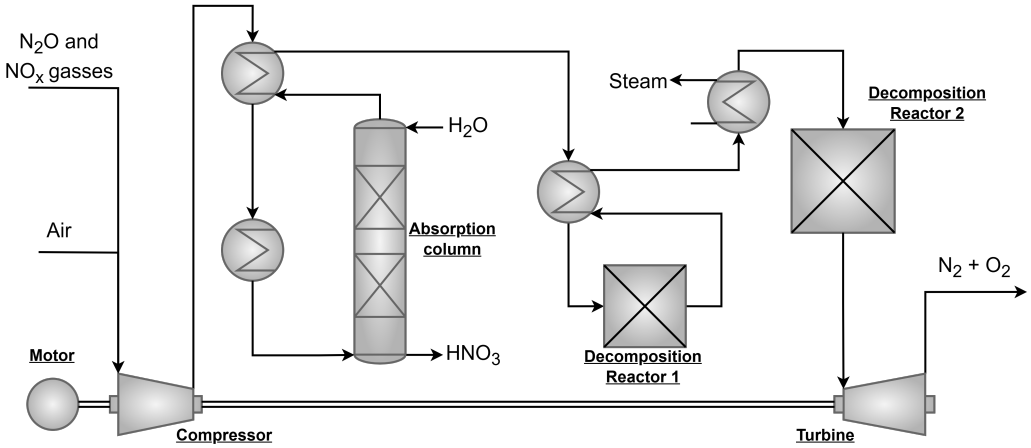

Figure 2.6: BASF catalytic N_2O decomposition process

2.1.5. Conventional Process Energy Considerations

The majority of reactions in the conventional production process are exothermic, as shown in Equations 2.1, 2.2 and 2.3. This is largely due to the large chemical potential of BEN and H_2, the two main feedstocks. Therefore the main reactions do not require external heat but will require heat removal. This heat removal is optimized to produce valuable process steam as shown in Figure 2.2 [29, 39].

The main energy consuming steps within the conventional process are the air compression for the ANE oxidation step, shown in Figure 2.3 and the heating requirements of the distillation columns in the AA crystallization steps shown in Figure 2.5.

2.1.6. Conventional Process Emissions

The largest emissions of the conventional AA production process is in the form of scope 3 emissions due to the large chemical potentials of the main feedstocks. The scope 3 emissions for hydrogen sourced from steam methane reforming, the most common source of hydrogen, are about 5.2 $kgCO_2e/kg_{H_2}$ [6]. While the scope 3 emissions of BEN feedstock is hard to determine as it is largely produced in conjunction with other chemicals but it has been estimated around 1.2 $kgCO_2e/kg_{BEN}$ [5]. The scope 3 HNO_3 (60% in H_2O) emissions are roughly 3.9 $kgCO_2e/kg_{HNO_3}$ [7].

Electricity generation emissions within Europe average around 0.2 $kgCO_2e/kWh$ [40] and although not a significant proportion of the energy consumption, the electrical energy scope 2 emissions, derived from compressors, pumps and cooling water (CW), is not negligible.

Although historically the scope 1 emissions from the release of N_2O were large, the AA industry has been successful at and developing and implementing abatement technologies and thus scope 1 emissions have decreased steadily over the past several decades. [3, 27].

2.2. Electrocatalytic Synthesis of Adipic Acid

As discussed previously, the oxidation of KA oil with Nitric acid can lead to large amounts of N_2O emissions. These emissions are either expensive to abate or are released and cause environmental harm. A cleaner and possibly more efficient means of oxygenating KA oil is ECO. ECO can be operated under mild conditions and utilize renewable electricity and water to produce AA form KA oil [11]. The use of ECO can also provide an on site supply of H_2 which could further reduce costs through the negation of the need for caustic scrubbers and methanators, as well as reduce scope three emissions

of the BEN to ANE process.

The use of ECO for has been studied for two decades with the main challenges being a low current density and competitive oxygen evolution reaction OER. Lyalin and Petrosyan reported a NiOOH catalyst which was able to achieve a 47% AA yield and a current density of 6 mA cm^{-2},in 2004 [41]. Further work increased yield/Faradaic efficiency (FE) and increased current densities to around 30 mA cm^{-2}[12, 13]. More recent work by Liu et al. has shown significant improvements in catalyst design, with current densities reaching industrially relevant levels of around 300 mA cm^{-2} and FEs around 80% [11].

The reported feasible costs of AA produced by ECO was 2.43 $\$kg^{-1}$ in a 2024 initial TEA by Liu et al. [11].

2.2.1. Process Description

ECO Process Description

Generally, the large scale ECO of KA oil is conducted in a continuous flow membrane electrolyser in a aqueous solution of KOH and KA oil. Experimental results by Liu et al. showed that the optimal concentrations for KOH and pure CHN solution is around 1 M and 0.4 M, respectively [11, 12]. However industrially produced CHN is seldom produced alone as discussed in Section 2.1 and separation of CHN and CHA is nontrivial due to the thin separation envelope shown in Figure 2.7 and the valuable CHA will still need to be further processed.

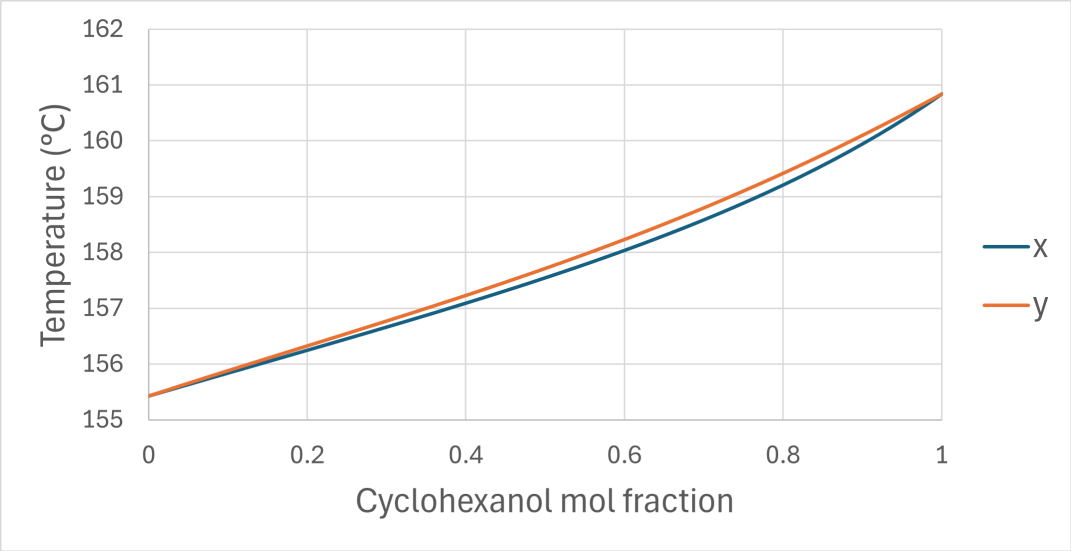

Figure 2.7: Binary diagram between CHA and CHN. (1 bar, NRTL-HOC equation of state) [42]

It is therefore important that the ECO electrolyser is capable of CHA electrooxidation to CHN as shown in Equation 2.4 as well as the subsequent CHN electrooxidation to AA as shown in Equation 2.6 [2, 12].

Overall CHA electrooxidation to CHN:

$$HOCH(CH_2)_5 \rightarrow (CH_2)_5CO + H^2 \tag{2.4}$$

CHA Anodic half reaction:

$$HOCH(CH_2)_5 + 2OH^- \rightarrow (CH_2)_5CO + 2H_2O + 2e^- \tag{2.5}$$

Overall CHN electrooxidation to AA:

$$(CH_2)_5CO + 3H_2O \rightarrow HOOC(CH_2)_4COOH + 3H_2 \qquad E_O = 1.152V \tag{2.6}$$

CHN Anodic half-reaction:

$$(CH_2)_5CO + 6OH^- \rightarrow HOOC(CH_2)_4COOH + 3H_2O + 6e^- \qquad E_O = 1.152V vs RHE \tag{2.7}$$

The use of ECO will result in the production of hydrogen at the cathode according to the following cathode half reaction.
Cathodic half-reaction:

$$2H_2O + 2e^- \rightarrow H_2 + 2OH^- \qquad E_O = 0VvsRHE \tag{2.8}$$

There are several parameters of a ECO electrolyser that are of importance when assessing their performance. The first one is average current density, j ($mAcm^{-2}$). This is a measure of how much electrolyser surface area will be required to transfer a certain amount of charge at a given potential, and is a function of the total charge passed, Q, the total area, A, and the reaction time, t. This has a large impact on the capital investment required for any electrolyser plant.

Average current density:

$$j(mAcm^{-2}) = \frac{Q(C)}{A(cm^2) \times t(s)} \times 1000(mAA^{-1}) \tag{2.9}$$

The next important parameter is Faradaic efficiency, FE. This is a measure of the amount of electrical energy that goes into the desired product. FE is a function of the amount of AA produced, n_{AA}, the charge passed, and the number of electrons involved in the reaction, z_{AA}. Ohmic losses, unwanted OER, and all other losses and byproduct production will reduce the FE.

Faradaic efficiency:

$$FE(\%) = \frac{n_{AA}(mol) \times z_{AA} \times F(Cmol^-1)}{Q(C)} \times 100\% \tag{2.10}$$

Finally, productivity, P, is similar to the average current density and is a measure of the surface area required to produce the desired amount of product. Productivity:

$$P(molcm^{-2}s^{-1}) = \frac{n_{AA}(mol)}{A(cm^2) \times t(s)} \tag{2.11}$$

Using the parameters discussed above, the various reported AA ECO configurations can be assessed. The setup information and performance of published results are given in Table 2.2.

Electrolyte Separation Process Description

The separation of AA from the alkaline electrolyte mixture is non trivial. Due to the high-pH environment, there is dissociation or deprotonation of organic acids such as AA and the formation of the conjugate base and water. This is a significant issue as potassium adipate recovery, in the form of the desired AA, from conventional separation techniques is not feasible [17]. The recovery of AA therefore requires protonation of the potassium adipate. This can be done in two ways;

Firstly through the neutralization of the electrolyte with a strong acid such as sulfuric acid, as shown in Equation 2.12. This is a costly process as all KOH is neutralized and although the K_2SO_4 salt has some value, it does not compensate for the feedstock costs of KOH and H_2SO_4 [11, 17].

$$KOOC(CH_2)COOK + H_2SO_4 \rightarrow HOOC(CH_2)COOH + K_2SO_4 \tag{2.12}$$

The second method, shown in Figure 2.8 and suggested by Zhenhua Li, employs electrodialysis (ED), to recover the carboxylate and separate the KOH for reuse. This method employs a cation exchange membrane (CEM), two bipolar membranes (BPM) and an electric field to transfer the KOH to another carrier fluid and allow the AA_{2-} to be converted into AA [12]. Although ED is well studied [43, 44], no detailed literature on an ED setup for AA separation from electrolyte could be found. The work by Ramdin et al. highlighted considerations for the process modeling of a ED protonation and distillation of a formate solution [44], many of which are likely to be encountered in the application to AA. Firstly, although the current density, current efficiency and membrane costs can dominate the CAPEX of the

Table 2.2: Reported ECO setup configurations and results

Ref	Reactor type	Catalysts	Temp (°C)	Membrane type	Electrolyte	Year	Cell voltage (V)	j (mA cm^{-2})	FE (%)	Productivity (μmol $cm^{-2}h^{-1}$)
[11]	MEA	NiV-LDH -NS	STP	AEM (FAA-3-50)	1M KOH 0.4M CHN	2024	1.76	300	82	1536
[12]	Membrane-free flow cell flow cell	$Ni(OH)_2$-sds/NF sds/NF	STP	NA	0.5M KOH 0.05M CHN 0.05M CHN	2022	1.8 1.9 2.0	22 28 42	35 20 12	48 35 31
[13]	H-cell	2%Cu-$Ni(OH)_2$/NF	STP	AEM (FAB-PK-130)	1M NaOH 0.075M CHN 0.025M CHA	2022	1.8	70	NA	NA
[14]	H-cell	$Cu_xNi_{1-x}(OH)_2$/CF	STP	BPM	1M KOH 0.1M CHN	2024	3.9 4.2 4.6	27 30 35	92 84 70	154 157 152
[15]	Flow cell	Co_3O_4/GDY GDY	STP	PEM	1M KOH 0.4M CHN 0.4M CHN	2024	1.6 1.9 2.2	50 100 180	63 50 45	196 311 504
[16]	Flow cell	$Cu_3Co_2O_4$/NF	50°C	BPM	1M KOH 0.075M CHN 0.075M CHA	2024	1.7 2.2 3.0	50 100 200	70 65 52	218 404 647

ED, these costs are smaller than the OPEX costs associated with the electricity consumption. It also highlighted that distillation of the electrolyte after ED is likely to be expensive. This is especially true for AA when considering that only a two chamber ED setup is likely possible due to no commercial adipate membranes being available. This means that meaning-full product concentration improvements within the ED cell is not possible [44].

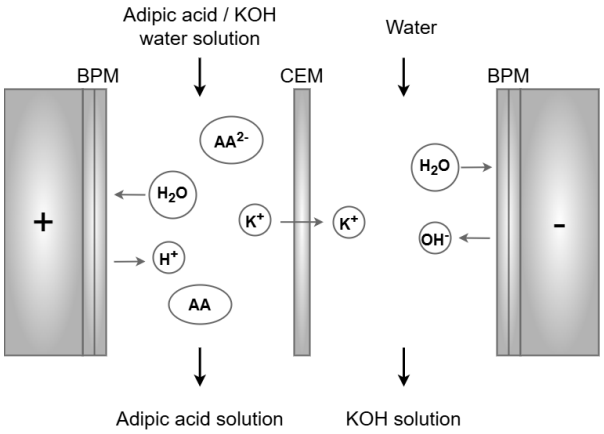

Figure 2.8: Zhenhua Li proposed ED setup for AA separation from electrolyte. [12]

After separation of the KOH ions, the water solution containing the AA, impurities and unreacted CHN needs to be separated. This is normally done through discoloration by activated carbon and subsequent distillation and crystallization. [15]

2.2.2. Electrocatalytic Oxidation Energy Requirements

The energy consumption of the ECO production step is largely in the form of electrical energy expended when passing current over the total cell potential, although it is important to note that the energy considerations when synthesizing KA oil and separating AA are still relevant considerations as these steps will still need to be performed. There are several losses which need to be considered and are generally given in the form of additional potentials as shown in Equation 2.13 [45].

$$E_{total} = E_{cell} + |\eta_{ohmic}| + |\eta_{s,anode}| + |\eta_{s,cathode}| + |\eta_{conc,anode}| + |\eta_{conc,cathode}| \tag{2.13}$$

- $\mathbf{E_{cell}}$. If a ECO process was completely reversible, the total potential, that is thermodynamically required to perform ECO, would be given by the the reservable cell potential E_{cell} as shown in the Nernst Equation 2.14. Where F is the Faraday constant with a value of 96 485 C mol^{-1}, Δg_o is the net change in Gibbs free energy, z is the number of electrons transferred and K_c is the reaction quotient between products and reactants, Equation 2.15.

$$E_{cell} = -\frac{\Delta g_o}{zF} - \frac{RT}{zF} ln(K_c) \tag{2.14}$$

$$K_c = \frac{activity_{products}}{activity_{reactants}} \tag{2.15}$$

- $|\eta_{\mathbf{ohmic}}|$. The ohmic loses are due to the charge transfer within the electrolyte, membrane and electrodes of the cell. The ohmic loses are an important industrial consideration [45] and are dependent on cell temperature, design/layout and current density, with Ohm's law ($V = I \times R$) stating that a higher current density will result in a large ohmic overpotential.
- $|\eta_{\mathbf{s}}|$. Each half-reaction will have an activation barrier that needs to be overcome for the reaction to proceed. This potential is dependent catalyst material on each electrode and thus novel catalysts that can lower this overpotential are being continuously sought.

- $|\eta_{\mathbf{conc}}|$. Each half-reaction will consume reactants and produce products at the surface of the electrodes. This leads to a concentration gradient within the electrolyte of the cell due to mass transport limitations. Based on Equation 2.14, it can be seen that an increase in Kc can lead to higher cell potentials. However, this is generally not of concern as mass transport is normally rapid enough, at reasonable current densities, to avoid significant overpotentials.

The reversible cell potential can not be lowered by the use of optimal electrode materials and cell design, however the right most term of Equation 2.14 can be strategically altered to optimize for process efficiency. Specifically the cell temperature and pressure, as well as reactant concentrations can be changed.

One possibly desired operational change away from room temperature and pressure is that of increased ECO pressure to negate the need for hydrogen compression when fed back to the BEN hydrogenation reactor. Although the increase of cell pressure will result in additional cell potential, as shown by the right most term of Equation 2.14, as well as additional liquid pressurizing, the savings on reduced hydrogen compression energy and equipment costs have shown to make the higher pressure economical [46]. Assuming a BEN hydrogenation at 50 bar and a electrolyser operating at room temperature (25°C), the additional electrical energy supplied to the cell would be roughly 9.66 kJ/mol$_{H_2}$. However, assuming a typical isentropic efficiency of 55%, motor efficiency of 90% and a two stage compressor, the expected electrical energy requirement for mechanical compression is 26.3 kJ/mol$_{H_2}$ [47]. Or 170% more than the higher pressure electrolyser.

An additional benefit of higher cell pressures is the reduction in parasitic OER due to the larger rightmost term of the Nernst equation. Although the reversible potential for CHN oxidation increases by 50mV under 50 bar of pressure, the OER potential increases by 75mV under 50 bar. Therefore the higher pressure will reduce OER relative to the desired CHN oxidation reaction. The CHA oxidation has the same gas molar ratios as the water hydrolysis and thus is not preferentially enhanced.

The internal resistance of the cell may also be reduced due to smaller H_2 bubbles and improved species transport with the electrolyte [46]. However this is unverified for KA oil oxidation. Gas permeation through the membrane can be an issue at higher pressures but this is generally only an issue above 100 bar [46].

2.2.3. Electrocatalytic Oxidation Process Emissions

The scope 1 emissions of the ECO process are likely to be larger than that of the conventional process employing N_2O abatement technology due to the large energy requirements of the post ECO separation [17].Scope 2 emissions are larger due to the ECO, however this also implies that if a cleaner source of electricity is used to produce AA, it would have a greater impact on the ECO method than on the conventional method.

Scope 3 emissions of the ECO process should be reduced due to the removal of H_2 as a feed stock and HNO_3 as an oxidizer. There are however new sources of scope 3 emissions due to the KOH electrolyte and possible H_2SO_4 neutralization acid. The scope 3 emissions of KOH and H_2SO_4 is roughly 0.77 kgCO_2e/kg$_{KOH}$ [48] and 0.14 kgCO_2e/kg$_{H_2SO_4}$ [49], respectively.

2.3. Biomass Based Adipic Acid Production

2.3.1. Background

Biomass-based chemical manufacturing is an important part of global efforts to reduce the environmental footprint of our current industrial chemical industry. However, direct competition with fossil fuel-based production is generally not feasible if low oil and gas prices are maintained [19]. In an effort to catalyze research and development into these areas, in 2004 the US Department of Energy released a report of value-added chemicals most likely to benefit from novel biological pathways [50]. Over the two decades since that report, it has become clear that a combination of chemical and biological transformation of these building block chemicals is required. This involves biologically converting biomass into platform molecules with genetically engineered microbes and further diversification into value-added chemicals using chemical catalysis. [51].

One such value added chemical is trans-3-hexenedioic acid (t3HDA). t3HDA is a monounsaturated diacid which has been shown to be a valid AA substitute with additional desired properties, including chemical resistance and hydrophobicity when used in Nylon synthesis. [19, 20, 51, 52]. The synthesis of t3HDA is can be performed through the fermentation of biomass into muconic acid (MA), and subsequent electrochemical hydrogenation to t3HDA. MA can also be catalytically hydrogenated to traditional AA.

2.3.2. Muconic Acid Production

MA can take the form of cis,cis-, trans,cis- or trans,trans-muconic acid, with the cis,cis- being the most commonly biologically synthesized. MA is a di-olefinic, c6-dicarboxylic acid. Fermentation of biomass to MA and subsequent synthesis of AA was pioneered by Draths and Frost in the 1990s and involves the use of a specialized bacterium to produce MA through various pathways [53]. Many types of bacterium and strains of bacterium are proposed for the multitude of biomass feedstocks, including but not limited to Corynebacterium glutamicum [54], Escherichia coli [23], Saccharomyces cerevisiae [19, 51, 55] and Pseudomonas putida [56, 57].

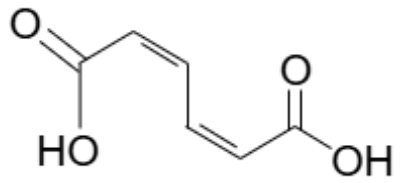

Figure 2.9: Muconic acid molecular structure

Biomass Feedstocks

- **Glucose:** Glucose derived from sugar and corn has been proven to be a valid feedstock in MA production. Glucose is a monosaccharide sugar and a subcategory of carbohydrates. Glucose can be obtained from many plant sources, but a common source is in the form of lignocellulose-derived hydrolysate. [19, 51, 56, 58]
- **Lignin:** Cellulosic biomass is increasingly being converted into liquid transportation fuels, this will greatly increase the availability and usability of the remaining 15 to 40% of the plant matter that is unconverted. This fraction is called lignin and is an aromatic polymer that provides structural integrity to plants.[59]. Ahn et al. proposed a Lignin separation process [60]. [22, 57]
- **Benzoate:** Benzoate salts are the salts of benzoic acids. There are several common types, with sodium benzoate being the most widely used as a food preservative E211. Although effective in producing high-titer fermentation broths [61], benzoate is a relatively expensive feedstock at 1.4 $ / kg. [62, 63]
- **Algae based lignin:** Currently, the use of algae for conversion to renewable biofuels focuses on the use of the lipid fraction for fuel conversion. This leaves the carbohydrate-rich aqueous phase for high-value co-production. Although a promising feedstock option, not enough work has been done to optimize for high productivity and yield of algae-based fermentation. [64]
- **Catechol:** Although multiple studies have been conducted, Catechol's toxicity and high cost render the feedstock unsuitable for large scale MA production.[65]
- **Glycerol and Methane** have been shown to be possible feedstocks, however, very low MA titers, yields and productivity render these impractical.[66, 67]

Current Achievable Muconic Acid Yields and Productivity

Although multiple sources of fermentation feedstock are available, there are several important indicators as to the viability of each feedstock.

- The first is simply the cost of the feedstock multiplied by the highest recorded conversion factor or yield. It is clearly not economically viable to produce MA from 100% conversion of a feedstock that is more expensive than MA. Likewise, it is not economical to use a feedstock that is only marginally cheaper than MA but with low yield.

- The next important consideration is achievable concentrations or titers of MA. Separation costs can make up a significant portion of total costs and thus minimizing downstream separation requirements is important. [20, 56]
- The final important consideration is fermentation productivity or amount of MA per liter broth per hour. This provides an indication as to how much fermentation volume capacity will be required. Fermentation tanks can be large and capital intensive, thus it is important that the productivity of each liter of fermentation broth is maximized. For example, a fermentation process that achieves high titers but takes multiple days, is less attractive than a slightly lower achievable titer that can take a few hours.[56, 20]

It can be seen in Table 2.3 that the most competitive feedstocks are Glucose and Benzoic acid. These are the only two with significant titers as well as good productivity and reasonable cost.

Table 2.3: Comparison of titers, yields and costs of muconic acid fermentation

Biomass feedstock	Titers (gL^{-1})	Productivity ($gL^{-1}h^{-1}$)	Yield % (c-mol,c-mol^{-1})	Paper	Feedstock cost ($\$kg^{-1}$)
Glucose and xylose	47.2	0.49	50	[56]	0.489 [56]
Lignin	6.6	0.138	97	[57]	0.088 [68]
Na-Benzoate	0.56	0.02	28	[62]	1.42 [63]
Benzoic acid	44	2.1	90	[61]	1.02 [69]
Glycerol	2	0.027	15	[66]	0.98 [70]
Algae hydrolysate	13	0.25	27	[64]	-
Methane	0.012	-	25	[67]	0.2 [71]

Muconic Acid Separation and Purification

Once the fermentation broth has reached its maximum titer and larger solids have been removed by filtration or centrifuge, there are several methods for conversion of MA to AA. The first and more traditional method is the use catalytic hydrogenation. This requires a very pure MA supply as fermentation broths containing various biogenic impurities present in fermentation broths have been shown to poison precious metal catalysts. With either reversible and/or irreversible deactivation [72]. Extensive separation and purification of the MA from the fermentation broth is therefore required to remove these compounds before downstream chemical conversion. Common impurities found in glucose based broths are Na (15 600 ppm), S (1220 ppm), P (3680 ppm), K (1320 ppm), Cl (297 ppm) and N (301 ppm) [73].

The MA purification process proposed by Vardon et al. is a four step process shown in Figure 2.10 [73]. Firstly a 10 kDa microfiltration was performed to remove proteins from the broth. This step results in a 2.3% loss in MA. Next, activated carbon is used to remove trace colour compounds from the broth at a loading of 5 g L^{-1}. Activated carbon is a suitable absorbent due to its low cost and effectiveness at removing impurities [74]. Vardon then employes pH/temperature shift crystallization at pH 2, 1atm and 5°C. The precipitated MA crystals are then dried in a vacuum oven for 48 h. Achieving an 86% recovery. At this point the MA is at 97.7 % purity, below the 99.8% required for AA polymer applications. In the final treatment step, ethanol is used to dissolve the MA and pass it through a 0.2 µm PES membrane. Due to the poor ethanol solubility of broth salts, the majority of these impurities are extracted. After this final step, the MA in solution is at 99.82 % purity [73]. This solution can be used further in MA hydrogenation without recrystallization or the MA can be recrystallized as a final product.

2.3.3. Muconic Acid to Adipic Acid

Catalytic Hydrogenation

As mentioned previously, there are several ways to hydrogenate MA to AA and the more conventional approach is catalytic hydrogenation. The starting point of this process is that of the ethanol MA solution attained in the process discussed previously. As shown in Figure 2.11 Excess hydrogen is supplied to the bottom of a trickle bed reactor in which the ethanol MA mix is run over a packed catalyst. Multiple catalyst types have been proposed with various degrees of effectiveness and degradation. Mokwatlo et al. and Vardon et al. suggested a 2% and 1% Rh on activated carbon catalysts, respectively [56,

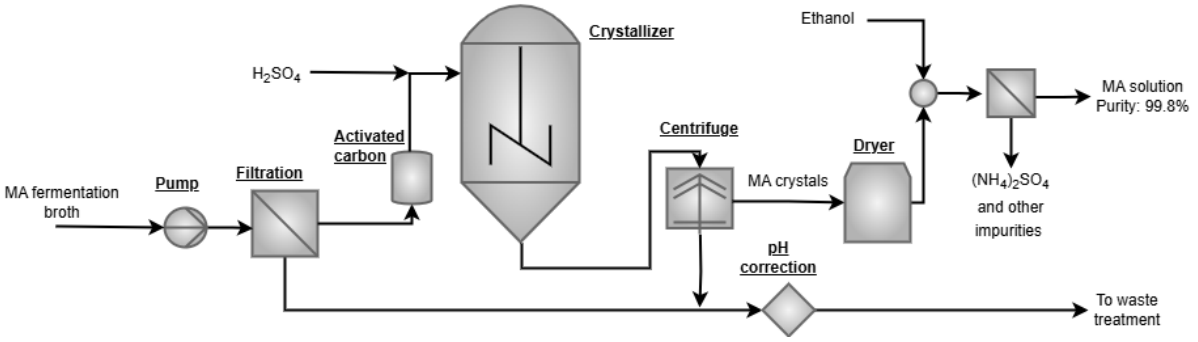

Figure 2.10: Muconic acid separation process

73], while Settle et al. suggested employing atomic layer deposition of AL2O3 onto Pd/TiO2 for a good combination of reactivity and reduced leaching [75]. Reaction temperatures range from 25 to 85°C and pressures range from 1 to 35 bar [76, 56, 73]. Larger reaction pressures allow for greater mass transfer between the catalyst and hydrogen; however, it also requires more specialised equipment and feedstock compression. The excess hydrogen is recycled, and the ethanol AA mixture is drawn from the bottom of the vessel and the AA is evaporatively crystalized. This process has been shown to achieve almost 100 % MA to AA conversion. [56, 73]

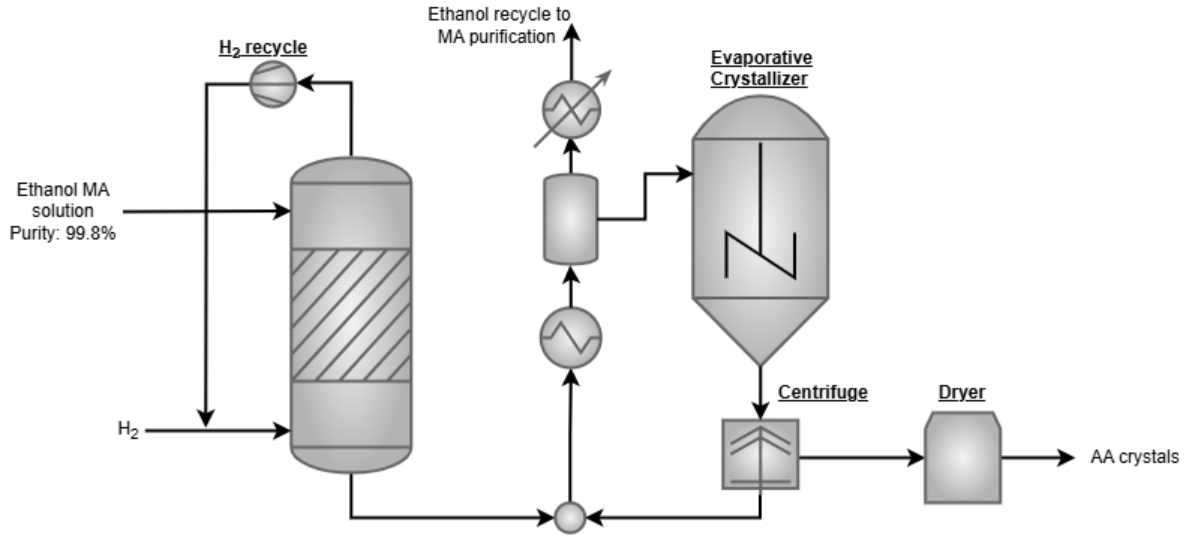

Figure 2.11: Muconic acid catalytic hydrogenation process

Electrocatalytic Hydrogenation

The second proposed way of hydrogenating MA to AA is electrocatalytic hydrogenation, ECH. The use of ECH is of interest to due to several reasons:

- MA need not be completely separated from the fermentation broth. Traditional catalytic hydrogenation suffers from catalyst deactivation from impurities such as broth salts. Therefore, MA needs to be separated to high purity levels before hydrogenation. This is an expensive process that can constitute a large portion of AA final cost [56]. ECH can be done with minimal solids removal. Thus, reducing a costly separation step.
- The need for an external source of hydrogen is removed. Although green hydrogen is predicted to be widely available in the future [6]. The majority of hydrogen produced today is from the SMR process and is thus a large scope 3 CO_2 emission source.
- Electrolysers are generally considered safer to operate when compared to large traditional hydrogenation vessels. Especially when considering the difficulties in hydrogen transportation [77].

This could reduce safety costs of small scale operations.

The reaction pathways for ECH of MA are shown in Equations 2.16, 2.17 and 2.18. The production of AA and/or t3HDA is dependent on cathode material choice within the electrolyser, pH of fermentation broth during ECH and cathode geometry [23].

MA to t3HDA overall reaction:

$$MA + H_20 \rightarrow t3HDA + \frac{1}{2}O_2 \tag{2.16}$$

Anodic half-reaction:

$$2OH^- \rightarrow H_2O + \frac{1}{2}O_2 + 2e^- \tag{2.17}$$

Cathodic half-reaction to t3HDA:

$$MA + 2H_2O + 2e^- \rightarrow t3HDA + 2OH^- \tag{2.18}$$

Using the overall reaction shown in eqn.2.16 and the ECH mechanism suggested by Dell'Anna et al., industrial-relevant current densities (200 to 400 mA cm^{-2}) were achieved by employing a neutral broth pH and a high MA titer. Pb or Bi (bismuth) cathodes were used to achieve good activities and it was found that Bi has minimal degradation or leaching into the broth. Reasonably large FEs of between 20-70% were attained [19].

Patel et al. have shown experimentally that the ECH of MA to conventional AA is feasible. However, low FEs (18% on Pd/C cathode) are found and this ECH has not yet been done with actual fermentation broth and it is possibility that the mechanism for full hydrogenation to AA due to nano particle geometry will degrade with fermentation broth impurities. [23]. The overall reaction for the ECH of MA to AA is shown in Equation 2.19.

MA to AA overall reaction:

$$MA + 2H_20 \rightarrow AA + O_2 \tag{2.19}$$

Biomass Based Acid Separation

Once MA has been hydrogenated to t3HDA or AA, the final product needs to be separated from either the ethanol AA solution, in the case of catalytic hydrogenation, or from the fermentation broth, in the case of ECH. In the case of catalytic hydrogenation, this is done with evaporative crystallization, as discuss previously.

In the ECH process there is a four step process of separating and purifying AA as shown in Figure 2.12. The first step after ECH is the use of an ion exchange resin to remove the majority of the ammonia and ion impurities while achieving between 97-99% product retention [20, 19]. The next step is to dose the solution with H_2SO_4 to lower the pH and thus solubility of AA in aqueous solution. This mix is then allowed to crystallize in a temperature controlled agitated crystallizer. Finally, the AA crystals are recovered with a vacuum drum filter and likely further air drying.[19, 20]

2.3.4. Biomass Based Adipic Emissions

The sources of CO_2 or CO_2 equivalent (CO_2e) emissions for the biomass based AA production is split between feedstock scope 3 emissions, heating/separation energy scope 1 or 2 emissions and, in the case of catalytic hydrogenation, hydrogen feedstock scope 3 emissions. The feedstock scope 3 emissions are due to production, transportation and pretreatment and are around 2 $kgCO_2e/kg_{AA}$ for catalytic hydrogenation. Scope 1 and 2 emissions for heating and electrical consumption can vary widely based on location and energy type, however it has been suggested that this can account for about 1.5-3.0 $kgCO_2e/kg_{AA}$. An important consideration of the biomass based production route, is that of carbon uptake. AA consists of 6 carbon atoms and thus the CO_2 emissions that would have occurred if the biomass was left to decompose can be subtracted from total emissions. If this is done, the total CO_2e emissions for biomass based AA production is estimated to be 1.9-2.7 $kgCO_2e/kg_{AA}$. [56, 78, 79]

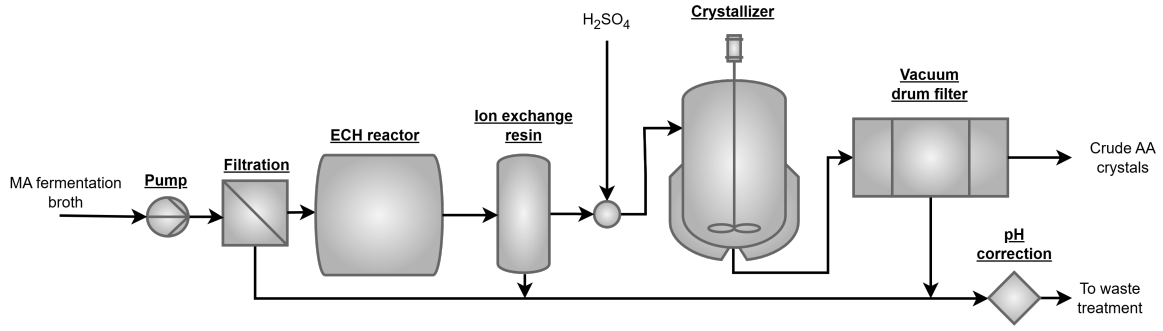

Figure 2.12: Separation process for electrocatalytic hydrogenation of muconic acid

2.3.5. Biomass Based Adipic Acid Cost

The cost of MA fermentation and subsequent catalytic hydrogenation to AA has been estimated to be in the range of $2.88 to $4.69 per kg [56, 78, 79]. The cost breakdown varies based on specific process properties but feedstock costs are shown to account for about 50% of production costs. The next largest cost is capital costs due to large fermentation and MA/AA separation requirements. The costs associated with MA hydrogenation to AA and subsequent AA purification are low, between $0.18 and $0.25 per kg.[56] This is due to the fermentation broth being separated from MA before hydrogenation and thus the majority of separation cost are seen before hydrogenation.

Fermentation and ECH costs for the ECH process represent $0.17 and $0.22 per kg of high purity product, respectively. Final 3tHDA cost, based on simplified TEA was assessed to be around $1.75 per kg.[19]. Sugar feedstock remains the main cost driver, as in most industrial bio processes, however the waste stream treatment costs are significantly higher than in catalytic conversion, due to the large amounts of unseparated fermentation broth after AA extraction.

Based on sensitivity assessments, the most important cost parameter is fermentation titers and MA yields. A raising of titers will lower fermentation CAPEX as well as separation costs. An increase in MA yields would allow for less feedstock, the main cost driver, to be utilized. [56]

3
Methodology

This chapter aims to provide details of the methods used in this thesis. A discussion on the selection of processes for study is presented, followed by an overview of the implementation methods of the selected processes. The inputs and outputs for each process are defined and core assumptions and design decisions are laid out. The reaction rate equations used for each reactor or electrolyser are presented and a short discussion on the accuracy of each assumption is given.

3.1. Process Selection

Based on the literature review and consultation with academic supervisors, three processes were selected for modeling and TEA. These processes were selected due to their feasibility, diversity of techniques, as well as literature availability.

3.1.1. Conventional Industrial Method

The first studied AA synthesis process was the current industrial scale AA production route. Although the majority of the global production of AA utilities this route and therefore the AA cost of this route is relatively well known, it was modeled here for three important reasons:

- First, the cost of AA is highly dependent on the feedstock price [27], namely BEN and hydrogen. Thus any difference between the current feedstock price and the feedstock price at the time of a reported AA price, will render the AA price inaccurate. By completely modeling the current industrial process, the feedstock price component of the final AA price can be assured to be the consistent for all assessed production processes. The final non feedstock cost breakdown percentages can then be compared against the bulk of the previously reported work, most of which was done in the 20th century [8, 33, 29]. This will provide valuable validation of many of the modeling assumptions, many of which are made for all studied processes.
- The current industrial process is a good benchmark to compare other processes against. The cost and emissions breakdown of the current industrial process offers insight into the weaknesses and strengths of alternative methods. Comparison against the incumbent also allows for possible future tweaking and replacing of selected process steps.
- N_2O abatement technology and implementation continues to improve and thus the AA industry is quickly becoming less polluting while still utilizing the current industrial process [27]. Therefore the current industrial process, with the additional N_2O abatement units is a valid and important contender in the search for the most cost and environmental efficient process, and should be fully understood when looking at alternative processes.

The PFD for this process is shown in Figure 3.1 and it can be seen that there are multiple inflow and outflow streams. The main feedstock inflows of this process is BEN, hydrogen, nitric acid, water and air. BEN is the main building block of AA in this process and thus constitutes the main feedstock. The purity of the various feedstocks is important in the production of AA, a commodity chemical that requires very high final purity levels. The main byproducts of the current industrial process are fuel gas from bleeds, process steam, caustic waste, waste water and N_xO_x emissions. These by products either have value as a co-produced product, or they require additional resources to handle and are a waste product. The

downstream treatment of these waste streams are out of the scope of this project but the economic and environmental cost of these streams are accounted for.

3.1.2. Electrocatalytic Oxidation (ECO)

The next studied industrial method is that of ECO. This process has garnered considerable interest in recent years due to its ability to eliminate N_2O and acid waste stream production [2, 12, 11, 14, 15]. The ECO process is also attractive as it can be implemented into excising AA production processes without significant alterations to the other process steps, thus allowing existing plants to pilot and retro fit for the ECO process.

Although large amounts of research into catalyst performance and possible overall cell performance has been conducted, there has been little research into the integration of ECO into existing AA production pathways. Thus the economic and environmental effects of heat integration, hydrogen recycling and other practical considerations are not well assessed. [17]

The scope of this process is similar to that of the incumbent industrial process, with BEN being the main input and AA crystals being the main output. However the ECO process does not require an external source of hydrogen for BEN hydrogenation to ANE, due to hydrogen being co-produced at the cathode, and does not require a KA oil oxidizer due to the oxidation at the anode. [11].

3.1.3. Biomass Based with Electrochemical Hydrogenation

The production of t3HDA (AA alternative) from biomass based sources has been selected for study as it is an area of intense research [64, 56, 23] and the first test scale production plant is under construction by Toray and PTT Global Chemical [80]. The main benefit of this process is the renewable and non fossil derived feedstocks as well as the possible reduction in toxic waste.

The main feedstock for this process is the biomass derived non-edible sugars. Although there are several possible feedstock types, as shown in Table 2.3, the fermentation process is highly dependent on many factors and thus the capex and opex of the muconic acid intermediate production is out of the scope of this project. The work by Mokwatlo et al. [56] will be used for a input feed cost estimate of cleaned fermentation broth. Because ECH will be employed to hydrogenate MA, the output of this process will be t3HDA, the bio enhanced version of AA. Although there is likely additional value in t3HDA as a precursor to Nylon with special properties [52], for the purposes of this study, t3HDA is assumed to have the same sale value as conventional AA.

3.2. Basis of Design and Key Performance Indicators

This chapter defines and documents the basis of design (BOD) for the processes studied and key performance indicators (KPIs) to conceptually design and assess the AA production processes assessed in this project.

3.2.1. Key Performance Indicators

There are many types of KPIs on which the performance of a system can be evaluated. Several of these are only applicable further down the design stage, such as control and operation or maintenance efficiency [81]. However, three common KPIs can be assessed in this work:

- **Profitability:** Probably the most common overarching KPI for any industrial process, profitability is the measure of financial reward for performing any action. In this project it will be measured through a comparison of the minimum selling price (MSP) of AA, ($/kg$_{AA}$). The MSP is the price at which AA needs to be sold in order to achieve a net present value (NPV) of 0. This incorporates the time value of money through the use of an expected rate of return discussed in Section 3.4.2. NPV of the processes is not used as it is dependent on market prices which are volatile and the electrochemical alternatives are likely to have very negative NPVs.
- **Emissions:** The assessment of process green house gas (GHG) emissions as a KPI allows for an understanding of some of the environmental impact of a process. It is also increasingly being used to assess the risk and implications of regulatory changes [82]. A process with high GHG emissions is more likely to require modifications or pay for carbon credits in the future, should

regulations and standards change. The GHG emissions will be measured as the CO_2, or CO_2 equivalent, emissions per kilogram of AA ($kg_{CO_2}e/kg_{AA}$). In this project, all scope 1, 2 and 3 emission sources of a production process are assessed and combined.

- **Material efficiency:** The production of AA through any process will result in some waste and byproducts being produced. Therefore in order to assess a process's efficiency of converting feedstocks into final AA product, the ratio of theoretical AA production, with 100% yields, to actual AA production will be compared ($kg_{AA_{actual}}/kg_{AA_{100\%}}$). Other factors such a water consumption will also be assessed.

3.2.2. Scale Selection

An important consideration is that of scale of production. Certain process will employ vessels and equipment that benefit from scale up, while other equipment, such as electrolysers, will rather scale out and thus not benefit from economies of scale. A brief discussion production scales for each process is presented below.

- **Conventional industrial route**
  The production capacity of the conventional industrial route was found to range from small pilot plants to the largest 400 kt/a plants. This route is a well studied and mature process with the core mechanisms being relatively unchanged since the 1950s [28]. Therefore it is reasonable to assume that the scale of any new production site would be similar to that of existing modern production facilities. Invista (formally DuPont) is the largest producer of AA, with two large production facilities in North America producing roughly 260 kt/a each [1, 83]. Previous studies have used a production capacity of 400 kt/a [84, 35] while many existing plants operate at around 100 kt/a [8].
- **ECO route**
  Although significant research has been devoted to ECO of KA oil to AA as shown in Table 2.2, there are no examples of large scale plants in operation. Based on the assumption that the ECO process could be retro fitted to an existing AA plant and for the sake of simplified comparison, the plant capacity of a ECO route is assumed to be similar to that of the conventional route.
- **Biomass based route**
  The biomass based AA production route with ECH has not yet been implemented on an industrial scale. However, in 2024 Toray and PTT Global Chemical agreed to construct a pilot scale plant to assess the feasibility of AA production through biomass fermentation and subsequent conventional hydrogenation [80]. The use of biomass limits the size of a single production plant due to the transport limitations of raw biomass materials and large size requirements of the fermentation tanks. For this reason, the plant capacity was capped at 120 kt/a, in line with previously studied sizes [56].

For the reasons discussed above, the final production capacity of **100 kt/a** was chosen as a fair representation of a realistic plant capacity for all processes.

3.2.3. Plant Location

The plant location can have a large impact on raw materials, infrastructure and skilled workforce availability, as well as a wide range of geopolitical implications. The location of the hypothetical plant within this project will be in the Rotterdam industrial area in the Netherlands. This allows for several key advantages:

- **Outsourced utilities:** Utilities such as electricity and process steam are assumed to be available and thus need not be produced on site or have extra transmission Capex costs.
- **Skilled labor:** Labor costs are assumed to not included typical costs associated with remote plant locations such as staff housing and transportation.
- **Cold CW:** Due to the low water temperature of the North Sea, the available CW temperature is lower than that which is typical for a more inland plant. This can allow for significant performance improvements in processes which operate at moderate temperatures and pressures.

3.2.4. Feedstock Parameters

The feedstock and required AA purity levels for the various feedstocks are given as follows:

- **H_2:** Hydrogen is commonly supplied at levels above 99.5% on a mole basis [85]. Therefore this is taken as the feedstock purity with the remainder approximated as inert Argon.
- **BEN:** The BEN supply to AA plants is typically polymer grade BEN which is 99.9% pure with < 1 ppm sulfur. In this work, the BEN supply is assumed to be 99.9 % pure with the remainder being the commonly found impurity toluene.
- **HNO_3 and H_2SO_4:** The nitric and sulfuric acid solution supplied is assumed to comprise of only the acid, acid ions and pure water. The most common impurity of nitrogen dioxide is not of concern as this is produced as a byproduct of the process and thus will be handled in the ECO process.
- **KOH solution:** Due to the regeneration of KOH in the ED separation step, there will be minimal continual KOH added to the system and there should be minimal build up of impurities. However, common impurities such as potassium carbonate and sodium hydroxide are still each assumed to be 1% of total KOH feedstock mass.
- **Biomass:** The impurities found in biomass fermentation broth can range significantly. In this work the fermentation is not modeled directly but rather the experimental results of previous papers will be used to assess selectively and yield of the various products and byproducts. Therefore the biomass purity is of little concern in this work and the composition of the main components within the broth feedstock will be taken from the fermentation literature from which the ECO results are taken. In this case, the compositions reported by Dell'Anna et al. [19].
- **Air and water:** Although never pure in practice, impurities in air and water supplies can vary widely and thus and problematic impurities are assumed to have been removed before use. Thus these feedstocks are assumed pure. Air inlet pressure is considered atmospheric, 1 bar.
- **AA/t3HDA purity requirement:** Purity grades for AA vary, however due to AA use in food and polymer production, they are high. In this project, purity requirements are assumed to be 99.5% wt [28, 8].

3.2.5. Process Flow Diagrams

The process flow diagrams (PFDs) display the main process steps for each process types studied in this project as well as the main feedstocks utilized.

Conventional Route

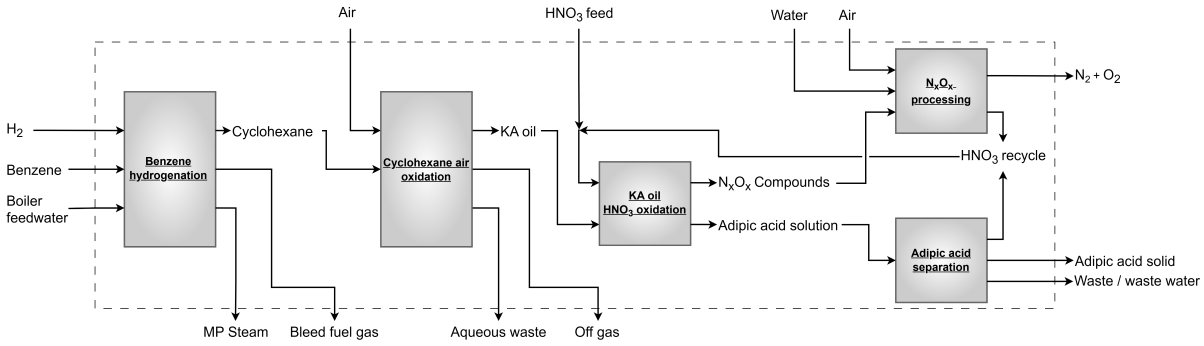

Figure 3.1: Process flow diagram of the conventional AA production process

The PFD of the conventional route is shown in Figure 3.1. As discussed in the literature review, this is a mature process and wide spread, with the majority of global AA production following this process with various minor alterations.

BEN is the major feedstock and is hydrogenated with H_2 to produce ANE. This reaction is conducted at high temperatures and pressure and is highly exothermic. It is therefore common practice to recover excess heat in the form of useful medium pressure steam, (MPS) [29]. To ensure almost complete conversion of BEN, the H_2 gas is circulated in excess and recycled within the hydrogenation step.

Due to this recycling of H_2, there is also the possibility of inert gas accumulation and this needs to be removed, in this case, with a bleed of fuel gas (a flammable mixture of H_2 and other impurities). Bleed ratios are very dependent on feedstock purity and composition and thus a variable hydrogen feed to bleed ratio will be used [39].

The ANE is then oxidized with air to produce KA oil. In order to maintain final yields of between 70% and 90%, a low single pass conversions of ANE is used. This leads to large recycles and thus large Capex and separation costs for this step [33].

Finally the KA oil is oxidized with nitric acid to obtain an AA solution. The Nitric acid is normally between 50-60% concentration and added in excesses of between 3:1 and 1000:1. This is done to improve AA yield, which is normally above 90%, and to absorb and regulate the heat generated by this highly exothermic reaction.

The use of nitric acid as an oxidizer leads to the production of stoichiometric amounts of N_xO_x compounds. These need to be either be recovered with water in the form of nitric acid and catalytically decomposed to N_2 and O_2, or released into the environment. In this project, the N_xO_x compounds are covered and decomposed. The final AA and nitric acid solution is then concentrated and cooled, allowing the AA to crystallize and be removed and dried.

ECO Route

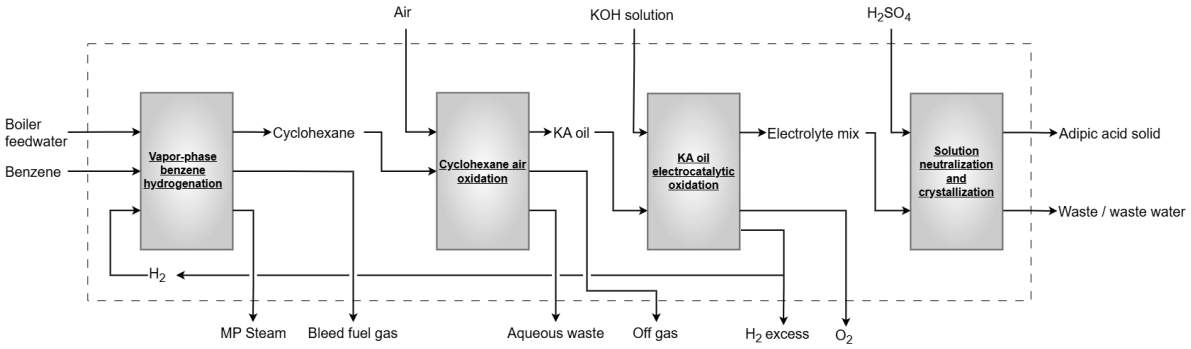

Figure 3.2: Process flow diagram of the ECO AA production process

The ECO route of AA production contains the same first two steps as the conventional route, with the exception of the H_2 being supplied by the ECO process within the system boundary. This will not only reduce feedstock costs, as the hydrogen will not need to be purchased and preprocessed, but will reduce process scope 3 emissions. This is because the the majority of hydrogen on the market today is produced with the polluting steam methane reforming process [86].

As shown in Table 2.2, the ECO step requires the use of a KOH solution to dilute the KA oil and create a conductive electrolyte. The H_2 is produced on the cathode and AA along with smaller amounts of O_2 are produced at the anode. This O_2 production is due to the parasitic OER as discussed in the literature review, however this may actually be a beneficial. As shown in Equation 2.4 and 2.6, the molar H_2 to AA production is between 3:1 and 4:1. In the ideal case, the BEN to ANE hydrogenation requires a H_2:BEN molar ratio of 3:1. and thus the ECO would produce enough H_2. However the effects of non ideal bleeds and yields within the first parts of the process will increase the amount of BEN that needs to hydrogenated without the subsequent increase in H_2 production. Thus the use of OER at the anode could be used to ensure enough hydrogen is available for the BEN hydrogenation.

Biomass Based Route

The production of AA from biomass based sources starts with the fermentation of biomass feedstock with specialized bacterium. These bacterium can produce varying concentrations of MA as shown in Table 2.3 and are usually grown in a seed train before being added to the main fermentation units. These fermentation units are large tanks in which air is bubbled through to allow for aerobic digestion. The fermentation broth is then clarified through a filter and centrifuge where the solids are collected and sold as Distiller Dried Grains with Solubles (DDGS). This process cost is highly dependent on

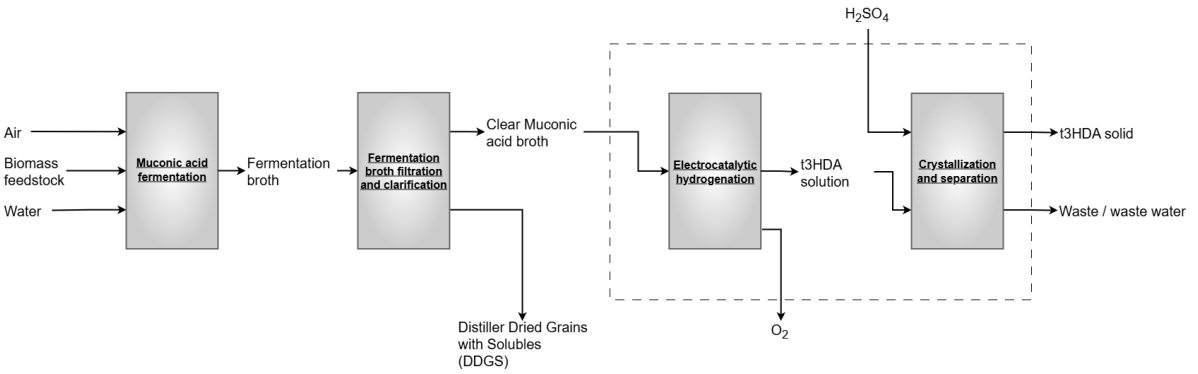

Figure 3.3: Process flow diagram of the biomass based t3HDA production process

equipment sizes and thus residence times and several other complicated parameters. For this reason, the fermentation of MA is out of the scope of this project.

The clean fermentation broth is electro catalytically hydrogenated to t3HDA. The t3HDA solution is then dosed with sulfuric acid to lower the pH of the broth to 1.2 and the t3HDA is crystallized and separated out. A second recrystallization step is used to further purify the t3HDA.

3.3. Aspen Modeling Approach

This section documents the details arising from the modeling of the various process steps in Aspen plus. Equations of state and material properties are discussed, followed by the considerations and assumptions used for the modeling of various unit operations

3.3.1. Equations of State and Material Properties

The equation of state used to model the process steps within the Aspen models is an important decision. Accurate material properties and interactions ensure realistic material and energy transfer, and thus realistic process modeling. The Aspen methods assistant manual recommends utilizing the UNIQUAC and NRTL activity coefficients model for the liquid phase interaction and the Nothnagel or Hayden-O'Connel (HOC) model for vapor phase association. This is due to organic acids forming dimers in the vapor phase and thus requiring special attention to account for their non ideal phase behavior [42]. Similar work involving the process modeling of the separation process for the carboxylic acid formic acid, by Ramdim et al., employed the NRTL-HOC model and validated this against experimental data [44].

Experimental data for the AA vapor phase behavior is not available, however, unlike formic acid which has a similar volatility to the water solvent, AA has a low relative volatility and thus is not expected to be significantly present in the vapor phase. Therefor perfect modeling and experimental validation of the AA vapor phase behavior is less important. For this reason, the NRTL activity coefficients model for the liquid phase and the Redlich-Kwong model for vapor phase association was used. Where required, electrolyte interactions are modeled with Henry's law.

t3HDA properties present a challenge. There are no property models for t3HDA as it is a relatively novel molecule. Within this project, the JOBACK method of property estimations is used for t3HDA enthalpy of formation. There is however no implemented property estimation method within Aspen that can estimate t3HDA enthalpy of solution and its ions' behavior. For this reason, the properties of standard AA and AA^+/AA^{2+} ions were assumed for the crystallization and separation steps of t3HDA production.

3.3.2. Reactor Modeling

Realistic reactor modeling presents a major challenge. Catalyst types, operating conditions and performance vary widely for each reactor and the detailed design for each reactor remains outside the

scope of this project. Therefore operating conditions were assumed to within the found ranges within literature. Single pass yields of products and byproducts were taken from literature. Energy and mass balances were maintained with either the reactor heating/cooling duty varying to maintain a set temperature or the outlet temperature changing in a adiabatic case. Sizing for reactors is estimated from typical residence time where possible.

3.3.3. Heat Exchanger Modeling

Where streams need to be cooled or heated from an external utility or where streams are to exchange heat within the system battery limits, the Aspen $HeatX$ block was used. Target hot and cold stream outlet temperatures were specified and limited against a minimum approach temperature of 5°C [24]. The thermal heat transfer coefficients for the various fluids were estimated using typical overall coefficients provided by Towler [39].

The main types of utilities assumed to be available are CW , low pressure steam (LPS), medium pressure steam (MPS), boiler feed water for steam generation and electricity, as shown in Table 3.1. Note that steam generation is assumed to be a negative price as this is a valuable by product. Prices and emissions for steam is assumed to be linked to that of natural gas [87]. Electricity is assumed to be from a renewable source and thus has low emissions [88]. The price of electricity is an important consideration and will be checked in the sensitivity study. The large consumer industrial EU average will be used as a baseline [40].

Table 3.1: Utility properties and price summary

Utility	Phase	T_{lower} (°C)	T_{upper} (°C)	Pressure (barg)	Price ($/GJ)	Emissions ($kgCO_2$/kWh)
MPS	Saturated vapor	174	175	7.9	13.27	0.202
LPS	Saturated vapor	125	124	1.3	11.41	0.202
MPS (generation)	Saturated liquid	174	175	7.9	-12.61	-0.202
LPS (generation)	Saturated liquid	125	124	1.3	-10.84	-0.202
CW	Subcooled liquid	10	15	1	0.14	0
Electricity	-	-	-	-	44	0.050

3.3.4. Separation Column Modeling

There are several distillation columns throughout the studied processes. These columns play a critical role in separation and concentration of various streams and are generally a large component of capital and utility expenses. It is therefore important that they are designed and optimized effectively.

- **Step 1:** Assess the main components of the separation to ensure there are no azeotropes. The presence of azeotropes is dependent on many things, one of which is pressure. For example, in the case of ANE CHN CHA separation, at 26 bar there is an azeotrope between CHA and ANE, however a lower pressure of 5 bar can be used to bypass the azeotrope and allow full separation.
- **Step 2:** Attain the input ratios of main components and find relationship between the the reflux ratio,RR to theoretical number of stages using the Win-Underwood-Gilliland method [89]. This method is implemented by Aspen Plus within the $DSTWU$ column unit. The purity levels are assumed to be 99.5%.
- **Step 3:** Select the number of trays. The required RR decreases with additional trays, however the reductions diminish with each tray. Therefore the number of stages, at which RR comes within 20% of the theoretical minimum, is selected as the real number of reasonable stages. It is also common to add an additional 10% of trays to allow for uncertainties in the design [24]. The feed stage is also given in this step.

- **Step 4:** Using the found feed tray and number of trays, implement a full column model within the $RadFrac$ unit of Aspen Plus. This includes setting up optimizations of reflux and boil-up ratios to attain the desired purity.

3.3.5. Turbomachinery Modeling

There are several locations throughout the studied processes where compressors and turbines are used. These are modeled using Aspen's $COMPR$ block. The outlet pressure is specified and the efficiency of all turbomachinery is assumed to be 72%. If multiple compression stages with inter cooling is required, this is modeled with multiple compressors of equal pressure ratios and heat exchangers between each for inter-coolers. Condensate is drained from these inter-coolers if needed as shown in Figure 3.4. Depending on the application, there could be a cooler before and/or after the compressors.

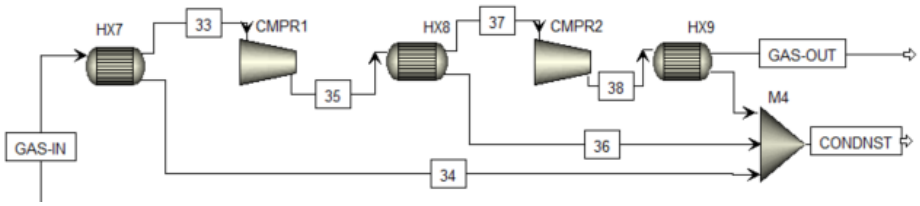

Figure 3.4: Example of possible setup for multistage compression with inter-cooling

3.3.6. Centrifuge Modeling

Centrifuges are modeled using the $CFuge$ block within Aspen Plus. The mechanical duty of the centrifuge is assumed to be 1 kWh/ton of feed [90, 91, 92] and the recovered solid phase is assumed to be 5% liquid by mass.

3.3.7. Crystallization Modeling

As shown in Table 2.1, the exponential increase in AA solubility at higher temperatures indicates that a cooling-type crystallizer would likely be the best option. This crystallizer type has the advantage of not requiring solvent evaporation within the crystallizer and the limiting fouling and heat usage [49]. The crystallizers used in all studied processes are modeled using Aspen's $Crystallizer$ unit block. This block takes the solute solubility as a function of temperature and then calculates the proportion of the solute which will crystallize assuming the solution leaves saturated at a specified temperature [42].

Sizing of the crystallizers for capital cost estimates is not a straight forward task. Crystallization is highly dependent on crystal growth rates under specific supersaturation levels, as well as nucleation rates and agitation levels [39, 49]. The work by Costa et al. and Marchal et al. will be used to estimate a reasonable average resonance time approximation for crystallization [36, 93].

3.3.8. Electrocatalytic Oxidation Modeling

The modeling of the electrocatalytic cells in Aspen was done as a black-box. Aspen has a water electrolysis cell model but does not have a built in general electrolyser modeling unit. Therefore current densities, FEs and voltages from literature sources were used to calculate the equivalent duty and reaction molar extent for a $RStoic$ reactor unit block. This approach is discussed in Section 2.2.2 and an example is shown in Appendix A.

This method was validated with a water electrolysis example. As shown in Figure 3.5, the Aspen $Electrolyser$ block (E1) was set up to with a given voltage and current and the final outlet temperature and composition were compared to that of an equivalent $RStoic$ reactor unit block (R1), with the same net power input, to ensure they achieve the same result. Costing for the electrolyser will be done separately.

3.3.9. Electrocatalytic Oxidation Electrolyte Separation

As discussed in the literature review, there are two possible approaches to the separation of the AA from the electrolyte solution. First the KOH and AA solution can be neutralized with H_2SO_4, the re-

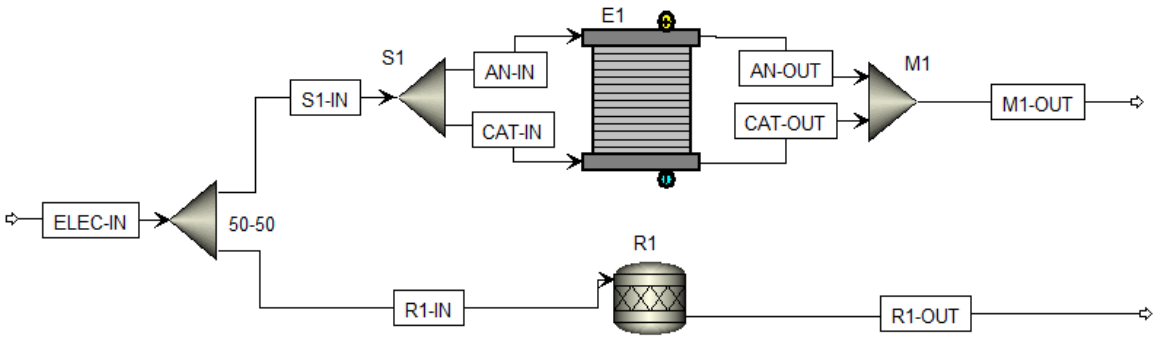

Figure 3.5: Electrolyser approximation validation setup

sulting K_2SO_4 can be crystallized out and the remaining solution concentrated with distillation, and subsequently crystallized. The second approach utilizes ED to fist recover the KOH. The remaining AA solution is then concentrated and separated in the same manner. Although the neutralization option is feasible [11], the use of significant amounts of KOH and H_2SO_4 makes the approach counter to the principles of green chemistry [94]. Therefore the use of ED will be studied for this application.

The implementation will be based on the approach laid out by Ramdin et al. [44], however with several alterations. First the use of a three chamber ED setup is not feasible for AA protonation due to there currently being no commercial anion exchange membrane for adipate ions.Therefore the concentration of AA out of the electrodialyzer is expected be unchanged. Second, due to the large difference in relative volatility of AA and water, a more energy efficient multistage vacuum distillation can be employed to concentrate the AA. Finally, the final AA concentration out of the evaporators will be based on the solubility limit of AA. This process is shown in Figure 3.6.

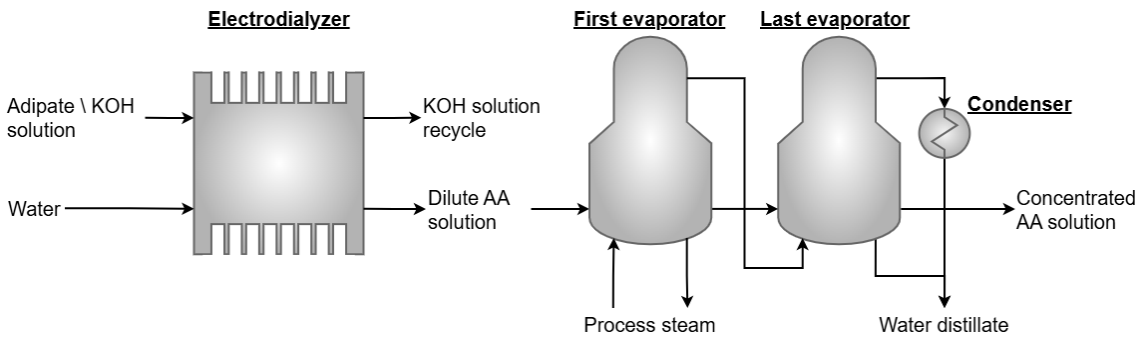

Figure 3.6: Process flow of ED process. Note that number of evaporators can change

3.3.10. Electrochemical Hydrogenation Modeling

Due to the novelty of MA ECH in the fermentation broth, there is minimal understanding of the reaction mechanics of this process. Therefore the modeling of the ECH reactor in this project was done based on the experimental results by Dell'Anna et al. [19]. Current density, faradaic efficiency and applied voltage are used in a calculator block to apply a duty and reaction extents to reactor block within aspen. The optimal operating point was investigated by Dell'Anna and found to be 200 mA/cm^2 with an applied voltage of 5.7 V and a faradaic efficiency of 40%.

3.3.11. t3HDA Separation

The separation of t3HDA from the fermentation broth after ECH can be achieved in several processes:

- The most conventional approach is the use on vacuum distillation to concentrate the t3HDA solution and then crystallization to precipitate out the final crystal product.

- The acid solution can be added to a lower pH through sulfuric acid dosing. As solubility is greatly decreased under acidic conditions around pH 1.2 and low temperatures, around 2°C, the t3HDA can be recovered through precipitation [19, 56].
- Activated carbon or ion exchange resins can be used to first concentrate and remove impurities from the fermentation broth, followed by the traditional vacuum distillation and crystallization [19]. Absorbents are commercially available for a wide range of applications [95].

In this project, the acid dosing method is used. It is the most straight forward and proven method of recovering weak acids in relatively dilute solutions. A prepackaged chiller unit is assumed to operate refrigerant between the reasonable temperature range of -10°C and 20°C. Assuming a mechanical efficiency, η, of 0.8, the electrical duty of this unit is calculated according to coefficient of performance (COP) shown in Equation 3.1 and 3.2

$$COP = \frac{T_{COLD}}{T_{HOT} - T_{COLD}} \tag{3.1}$$

$$Q_{ELECTRICAL} = \frac{Q_{COLD}}{COP * \eta} \tag{3.2}$$

Once the t3HDA is recovered the spent solution will need to be dosed with lime (Calcium hydroxide) to bring the pH back to neutral before it can be sent to waste water treatment.

3.3.12. NO Compounds Recovery Modeling

As discussed in Section 2, the ratio of N_2O to NO_2 emissions for the nitric acid oxidation of KA oil is 1:1 [27]. Therefore the system is modeled to handle this ratio. The air feed in the bleacher is set to attain a 30% N_XO_X mass concentration [4].

The water flow rate to the NO_2 absorption column is set to attain a HNO_3 concentration of 60% wt. While the remaining N_2O is assumed to completely catalytically decompose.

3.4. Techno Economic Assessment Implementation

The cost of equipment, installation, raw materials, etc. are attained through multiple sources and correlations that will be laid out throughout this section.

3.4.1. CEPCI Price Corrections

There is not always updated pricing information for each expense item and thus cost information from previous years must be utilized. These cost values are corrected to current values by using the Chemical Engineering Plant Cost Index (CEPCI) indexes as shown in Equation 3.3. The cost index is published by Chemical Engineering magazine, based on industry/equipment type and location. The current CEPCI value used within this project is 801. [96]

$$\frac{C_1}{C_2} = \frac{INDEX_1}{INDEX_2} \tag{3.3}$$

where:

C_1	= Equipment cost in year 1
C_2	= Equipment cost in year 2
$INDEX_1$	= cost index in year 1
$INDEX_2$	= cost index in year 2

As shown in Figure 3.7, the cost of goods manufactured (COGM) is split into operational expenditure and capital expenditure. These are discussed below and are used to calculate the minimum selling price (MSP) of AA. This is the price at which a profit is made on the production of AA or t3HDA.

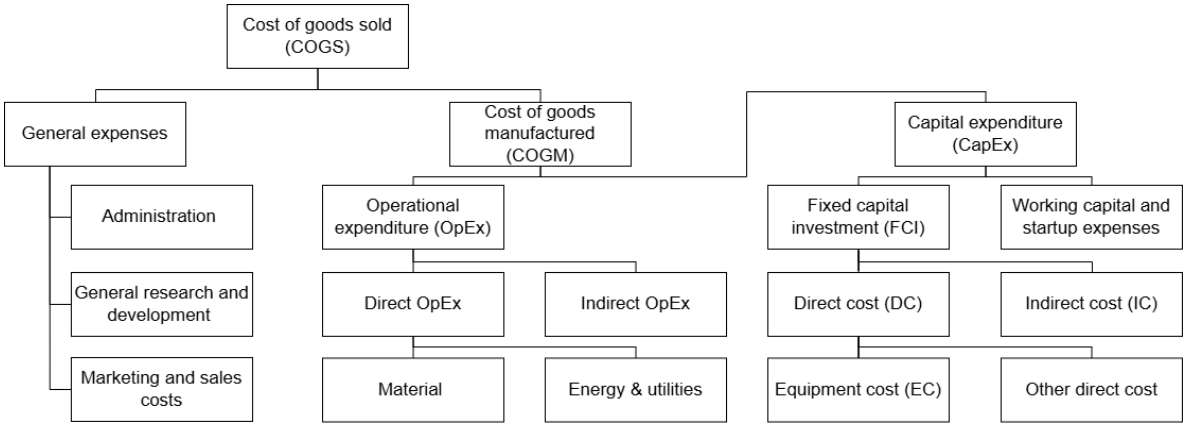

Figure 3.7: Structure of estimated cost of goods sold [97]

3.4.2. Capital Expenditure (CAPEX)

As shown in Figure 3.7, the CAPEX can be broken down into several subcategories. Working capital is the capital of a company which is used in its daily operations [98]. Fixed capital investment (FCI) can be split further into indirect costs and direct costs, the latter consisting of equipment costs and other direct costs.

To quantify the cost of CAPEX per kg of AA produced, the total CAPEX is is annualized with a plant lifetime of 20 years and expected rate of return of 15%, pretax [39]. The plant is expected to have 8000 hours of operational time per year, a typical value [24].

Fixed Capital Equipment Costs:

The delivered cost of specific pieces of equipment is important as it generally affects the estimate for other CAPEX costs. Where equipment or groupings of equipment is widely used and costing estimates are available, these are used. The cost of common equipment with specific dimensions and configurations are estimated using correlations and estimations from literature [39, 24]. Certain types of equipment are too specialized for regular correlation methods and these are either estimated based on the Aspen Capital Cost Estimator (ACCE) estimate or equipment of similar composition and function.

Other direct costs were estimated using the procedure set out by Robin Smith [24] and shown in Equation 3.4. The various cost factors, f_i, are applied to the direct equipment cost, C_{direct}, to estimate the FCI for each item.

$$C_{FCI} = \Sigma C_{direct} f_i \tag{3.4}$$

Cost approach and data for each component

- **Heat exchangers:** As discussed in Section 3.3.3, Aspen is used to size the surface area required for each heat exchanger based on temperature difference and the reasonable transfer coefficients suggested by Towler [39]. This surface area is then converted into a direct cost based on scaling factors and base costs provided by literature [24, 39]. The decision of HX type as well as material is done case by case based on fluids involved, pressures and with engineering judgment.
- **Compressors and turbines:** Compressor and pump costs are estimated using the correlations given by Gavin Towler and Ray Sinnott [39], based on shaft work duty. Because minor pressure changes result in minor shaft power requirements and thus low cost, only equipment with large pressure increases and flow rates are considered. The results of this estimation are compared against vendor prices and found to be reasonable [99].
- **Pumps:** Although there is likely to be extensive use of pumps to move liquids throughout the process, the energy consumption and capital requirements are likely to be low when compared to that of gas compression. Therefor pumping energy and equipment costs are ignored.
- **BEN hydrogenation reactors:** The CAPEX estimate from the hydrogenation reactor of BEN to ANE is based on the work by Garcia et al. in which the hydrogenation process economics of

various liquid organic compounds were studied [100]. The cost estimate of a single stage reactor of 3,5-dibenzyl toluene, which was of comparable sizes and catalyst type, is scaled to attain a cost estimate of $12665 per kmol/h of hydrogen reaction extent.

- **ANE air oxidation reactors:** According to M. Musser in Ullmann's Encyclopedia of Industrial Chemistry, an appropriate residence time of the liquid reactants in the agitated jacketed vessel reactor is 30 minutes [33]. This time is used to calculate the required volume of a reactor which is then costed using correlations in Towler [39]. Catalyst loading of 100ppm [101] costs of $230 per ton feed.
- **ECO reactor:** Previous work by Xiang et al. assumed a CAPEX cost per kW similar to that of a generic water electrolyser [11]. This approach is a good first estimate but does not take into account the very different cost structures of a proton exchange membrane water electrolyser verses a anion exchange membrane electrocatalytic oxidizer. Within this project, the cost estimates of various stack components are taken from the 2020 IRENA report as well as other sources [102] and the final ECO CAPEX is calculated using the structure laid out by Kim et al. [103]. This final cost breakdown is shown in Table 3.2 and is split into Stack components and auxiliary or Balance of Plant (BoP) components. The stack membrane and catalyst lifetime is assumed to be 20000 hours or roughly 2.5 years [102].
- **ECO reactor:** Cost estimation of the ECH reactor is done in a similar manner to that of the ECO reactor, with the BoP items being kW based as shown in Table 3.2. However the stack components are estimated based on a cost of $10 000 per m^2 [20].
- **ED electrolyte recovery:** The equipment cost estimate for the ED setup follows the same assumptions as in Table 3.2, however items which are not present in ED such as catalysts and gas handling are ignored. Reported current densities and voltages are similar to that of the ECO reactor [11, 43] and therefore power density of the ECO reactor and ED equipment should be similar. CEMs are assumed to be 10% more expensive than AEMs [104]. The final cost estimation is therefore estimated to be 512.56 $/kW.
- **Columns:** As discussed in Section 3.3.4, the size and number of trays of each column is determined within Aspen. The cost estimates for these units are then derived by deconstructing the various components of a column. Namely the boiler, condenser, vertical pressure vessel and trays. These items are then costed based on the correlations in Towler [39].

Table 3.2: ECO equipment breakdown. (2025 prices)

	Components	Cost estimation ($/kW)	Reference
Stack components	Porous transport layers	160	[102]
	Small parts (eg. seals)	8.5	[102]
	Stack plates	16	[103]
	Stack assembly and end plates	8.5	[102]
	Membranes	13	[104]
	Catalyst	2.6	[105]
Balance of plant	Power supply	173	[102]
	Solution circulation	76	
	Gas handling	69	
	Heat management	27	
	Manufacturing	28	
Total		**583**	

Working Capital and Contingency

Working capital can consist of, among other things, raw materials for plant start-up, inventories of intermediate and product, money to carry customer accounts, and money to pay payroll during start up. In this work, working capital is assumed to be 15% of total capital investment [24]. Contingency allowance

is added to cost estimates to account for uncertainty in new processes. A common contingency of 10% of installed equipment costs will be used [39].

3.4.3. Operational Expenditure (OPEX)

As shown in Figure 3.7, the OPEX is broken down into indirect and direct costs. Indirect costs consist of labor, maintenance and plant overhead costs, while the direct costs consists of feedstock and consumable materials, and utilities. These costs were estimated as follows:

- **Feedstocks:** The cost and scope three emissions of the main feedstocks for the various processes are given in Table 3.3. These were gathered from the sources referenced within the table. MA in a the fermentation broth was priced based on the work by Mokwatlo et al. The minimum selling price of MA minus the cost of crystallization was used. In other words, the minimum selling price of MA broth predicted by Mokwatlo. [56]
- **Utilities:** The cost of utilities can vary widely based on waste heat availability and location. As discussed in Section 3.3.3, the utility costs shown in Table 3.1 are taken from a variety of sources. The ACCE has reasonable values based for utilities in various global regions and these are used to check the reasonability of these prices
- **Waste disposal:** The cost of waste water disposal is assumed to be $2.2 per ton [39]. Any major toxic contaminates are first neutralized or accounted for. For example, the acidic fermentation broth after t3HDA separation is first neutralized with lime, and the removal of GA from the ANE oxidation process is assumed to be done with KOH and thus the cost or GA removal is equal to the cost of KOH required to neutralize it. This is appropriately included in the cost calculations. Valuable byproducts are assigned a negative disposal value.
- **Maintenance:** The cost of maintenance depends heavily on the type of machinery and the conditions in which it operates. Maintenance is assumed to be 5% of fixed capital investment [24, 39].
- **Labor:** Labor costs depend heavily on the level of automation and process type. Turton suggests the number of operators required for 3 shift rotations can be calculated from Equation 3.5. Where P and N_{np} are the number of solid and non solid processing steps, respectively. [106]
- **Supervision and management:** 25% of labor costs. [39]
- **Insurance:** 1% of installed equipment costs. [39]
- **Plant overheads:** 45% of labor costs. [39]

$$N_{op} = 3 * (6.029 + 31.7 * P^2 + 0.23^* N_{np})^{0.5} \tag{3.5}$$

Table 3.3: Feedstock cost and scope three emissions

Feedstock	Cost ($ kg^{-1}_{pure})	Equivalent CO_2 ($kgCO_2e\ kg^{-1}_{pure}$)
BEN	0.89 [107]	1.2 [5]
H_2	3.49 [108]	5.2 [6]
Water	0.00133 [109]	0
Nitric acid	0.29 [110]	3.9 [7]
Air (N_2+O_2+Ar)	0	0
Potassium hydroxide	0.60 [111]	0.77 [48]
Sulfuric acid	0.13 [112]	0.14 [49]
MA broth (MA content)	1.86 [56]	0.38[56]
Calcium hydroxide	0.14[113]	0.79[114]

3.4.4. TEA Sensitivity Analysis

In order to assess the sensitivity of the results of the TEA, parameters deemed important can be varied in order to understand the effect of changing these parameters on the MSP an CO_2 emissions. These

parameters can either be varied by set percentages or between known limits. The following parameters were checked:

- **Electricity.** The price and CO_2 emissions of the purchased electricity was checked in all three routes. The price was varied from the lowest EU price, 0.0767 $/kWh, to the highest EU price, 0.255 $/kWh. Electricity emissions factor was varied from the cleanest EU electricity, 0.008 kg/kWh in Sweden, to the current Netherlands average of 0.256 kg/kWh. [40]
- **Process steam.** Process steam is used the most in the conventional and ECO routes and their sensitivity to steam price and CO_2 emissions are checked. A best case of free waste heat with no CO_2 equivalence was taken. The worst case was assumed to be steam provided by an older less efficient boiler, running at 60% efficiency. [115]
- **Main feedstocks.** The main feedstock prices and emissions factors for the various routes are assessed. This is done by varying the price between ten year highs and lows (excluding extreme price stocks such as COVID) or between values cited in literature. As will be shown in Section 4.4, nitric acid supply emissions play an important role in conventional route CO_2 emissions. The best case was taken from the average CO_2 emissions of the cleanest 10% of nitric acid plants [116]. Whilst the worst case was taken from the testing results of the worst performing nitric acid plant.
- **Electrochemical reactor CAPEX.** Due to the novelty of ECO and ECH in this application, the CAPEX estimates for these reactors are unlikely to be extremely accurate. The effects of halving and doubling these equipment costs are assessed.
- **ECH FE.** The final FE of the ECH reactor was varied to assess the importance of this parameter as there is room for further optimization, as discussed in Section 6.2.

4

Results

4.1. Process Design Results

In this section, the structure and operation sequence for each of the three studied processes are presented. Major assumptions and operating points are given and the final iterations of the Aspen Plus process flowsheets are shown divided into the main process steps discussed in Figures 3.1,3.2 and 3.3. Generally, the blue, red and green lines represent input, output and tear streams, respectively and further stream details can be found in Appendix C.

4.1.1. Conventional Route Process Design Results

The process flowsheet results for the conventional AA production route is discussed below.

Process Flow Diagrams

As discussed in the previous sections and shown in Figure 4.1, the hydrogenation of BEN and ANE is done at 50 bar and with excess hydrogen which is then recycled with a bleed in the event of any inert build up. The product coming out of reactor 1 is first cooled and the ANE condensed in HX10 to generate 4.8 MW of MPS. The stream is then further cooled and partially condensed with CW and separated in HX11, with a duty of 2.0 MW

Due to low H_2 solubility and immediate recycling, a vigorous separation was not required and as discussed in Section 3.4.2, pressure drops through equipment are not accounted for. In this model, a bleed rate of 1% was assumed and found to have minimal effect on BEN or ANE loss. The bleed is assumed to have value as a fuel gas. Overall selectivity is 100% which is inline with literature [29].

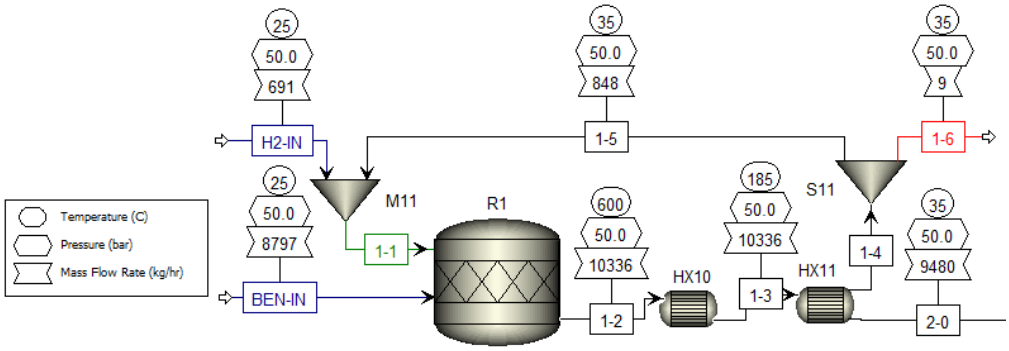

Figure 4.1: Flowsheet of BEN hydrogenation in conventional route

The subsequent ANE oxidation, shown in Figure 4.2, is performed at 15 bar and in two stages, as discussed in the previous sections. Air supply is tuned to achieve desired reaction temperatures of 125°C and is supplied at a 2:1 excess ratio, with CMPR1 and CMPR2. The liquid products of R2 are passed through SP1. This is an idealized separation unit, used to remove GA which is a minor byproduct of this process, at 5% mass fraction of stream 2-1. Although not modeled here, calcium hydroxide is used to form Calcium Glutarate which is then precipitated out of the solution. The cost of

GA removal is therefore largely a function of calcium hydroxide prices and this is accounted for in the TEA.

The products of R2 are then cooled in HX21 before being allowed to complete the reaction according to Equation 2.2 in R3. It is assumed that all cyclohexyl hydroperoxide is converted to KA oil in this step. Aqueous byproduct, which constitutes 4.2% mass fraction of stream 2-5, is then separated with a decanter and sent to waste handling before the remaining KA oil and large excess of unreacted ANE are separated in COL1. COL1 has a partial condenser and operates with minimal reflux but large boilup ratios due to the high boiling point of KA oil and large excess ANE ratios, respectively. These are given in Table 4.1.

The vapor phase of R2 is immediately cooled to 20°C with CW in HX22 to recover 98.5% of the evaporated ANE. The remaining gas stream at 15 bar is passed over an activated carbon bed, SP2, to recover any residual ANE before being emitted to the environment. This carbon bed can be regenerated by periodically releasing the pressure and capturing the ANE through HX23, which is the main 5.2 MW condenser of vapor product from COL1.

Overall selectivity towards KA oil is 81% and ANE single pass conversion of ANE in R2 is 10%. These values are consistent with literature findings [33].

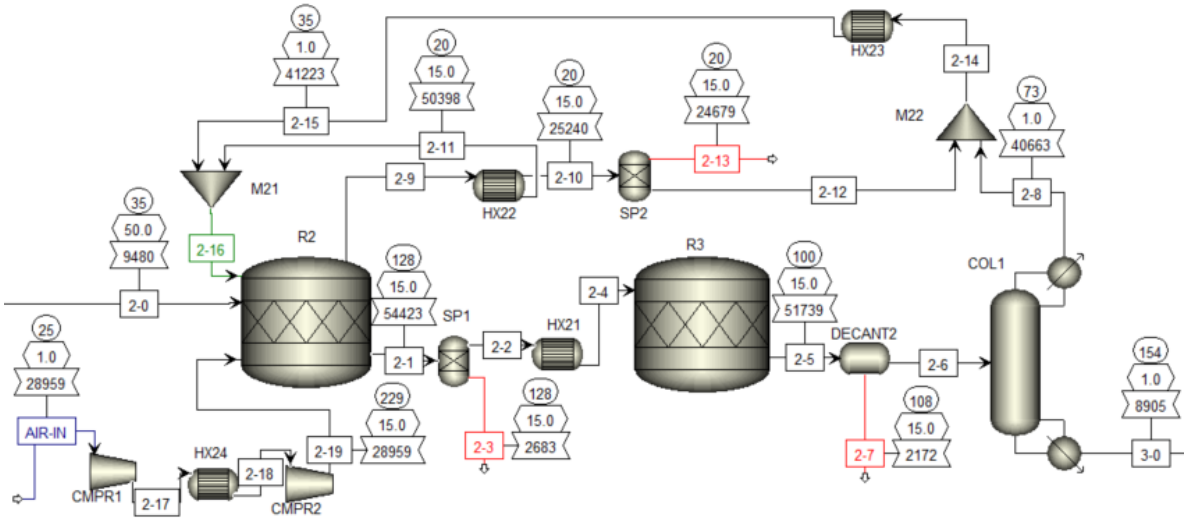

Figure 4.2: Flowsheet of ANE oxidation to KA oil

In step three of the conventional route, shown in Figure 4.3, the KA oil is cooled to 30 °C in HX31 and feed into R4 where it is oxidized with a large excess of HNO_3. The HNO_3 flow rate is used to control reaction temperature and a molar excess ratio of 3.14:1 was obtained, which in within the typical range reported in literature [8].

The liquid product of R4 is then bleached of N_xO_x compounds with air at 3 bar that is controlled to achieve the required stripping with the minimum airflow. The resulting flow of stream 5-0 is comprised of roughly 34% N_xO_x compounds. This is a reasonable composition for catalytic decomposition [4].

Note that stream 3-8 is a return line for HNO_3. The mass concentration of HNO_3 is 60.1% which is effectively the same as the 60 % HNO_3 feed. When comparing 3-1 to 3-8, it can be seen that no minor components of 3-8 pose an accumulation risk. For numerical efficiency reasons, 3-8 is not connected back into R4, but the recycle is accounted for in the TEA

HNO_3 in excess in R4 means that large amounts on HNO_3 needs to be recovered and recycled at 60% HNO_3 from stream 4-0, shown in Figure 4.4. However due to the KA oil oxidation, the ratio of water to HNO_3 is too large after exiting the oxidation step. This means that water needs to be removed from the system in order to maintain the 60% HNO_3 feed after AA and waste products have been removed. This is done through the use of a distillation column (COL2) under low pressure (0.3 bar) conditions to reduce the thermal degradation of HNO_3 at elevated temperatures.

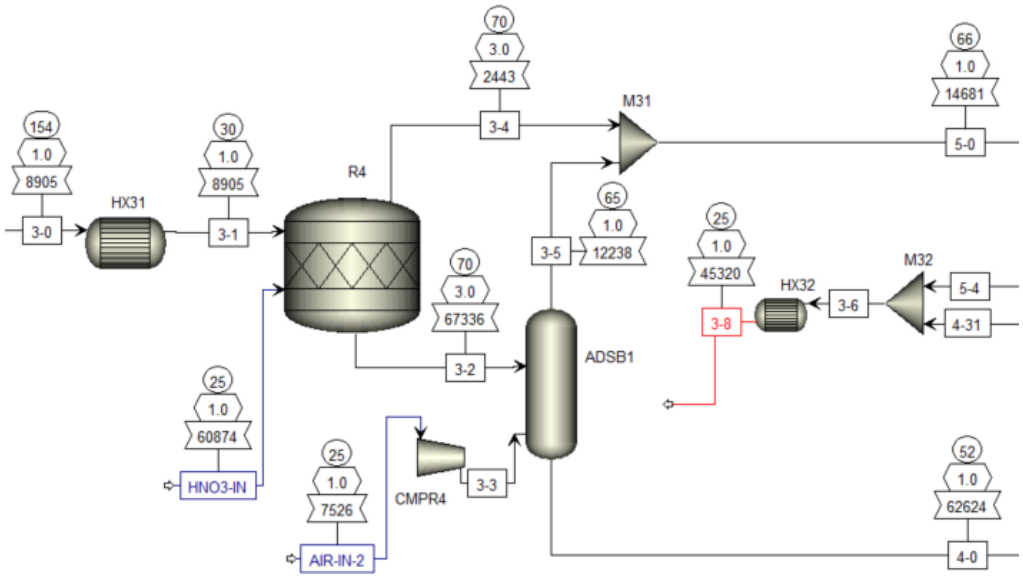

Figure 4.3: Flowsheet of KA oil Nitric acid oxidation to AA

HNO_3 separation can cause difficulties in modeling due to water and HNO_3 exhibiting strong deviations from ideal behavior due to hydrogen bonding, electrostatic interactions, and partial dissociation of HNO_3. For this reason, the Electrolyte NRTL model was used for the HNO_3 and water separations. This model will have slightly different equilibrium predictions to that of the standard NRTL. For this reason two fake blocks have been added to the flowsheet to allow for conversion from one EoS model to another will maintaining stream temperature, pressure and composition. These are EOSCOR1 and EOSCOR3 as seen in Figure 4.4. COL2 recovers 99.74% percent of HNO_3 in the column bottoms with a HNO_3 tops mass fraction of 0.10%.

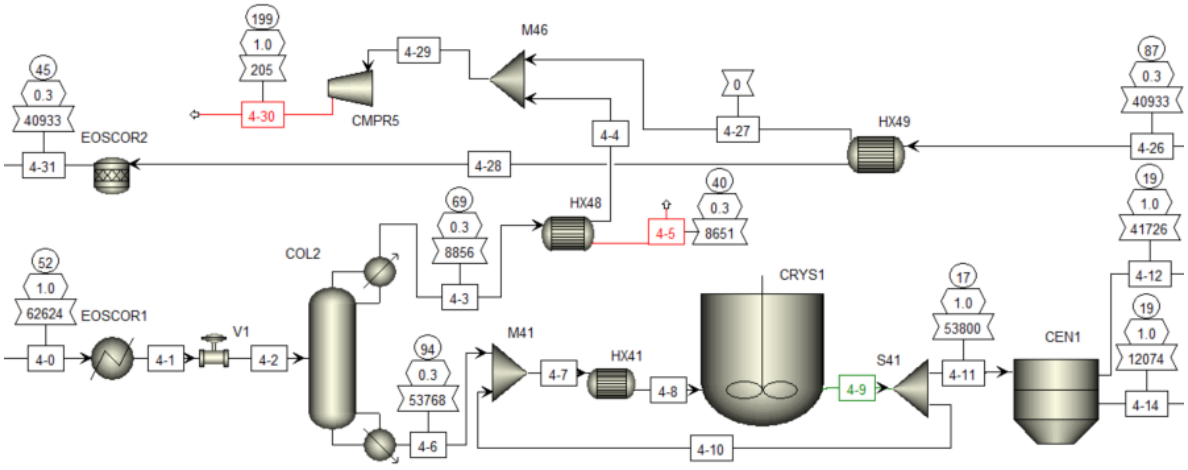

Figure 4.4: Flowsheet AA crude crystallization and EOS interface

Once the required amount of water has been removed, the separation of AA from the mixture is done through cooling crystallization as shown in Figure 4.4 and 4.5. The solubility data as a function of temperature was attained from Aspens built in solubility estimator and used to estimate the amount of AA solids formed under ideal conditions. Although not a perfect approximation, the true crystallization of AA under these conditions is highly complex and out of the scope of this project and thus industrial practice has been followed and assumed to be reasonable.

The AA is crystallized in crude and purge crystallizer CRYS1 and CRYS2, respectively, where 96.7 % and 2.6 % of the AA is recovered, respectively. The remaining liquid is distilled and returned to the

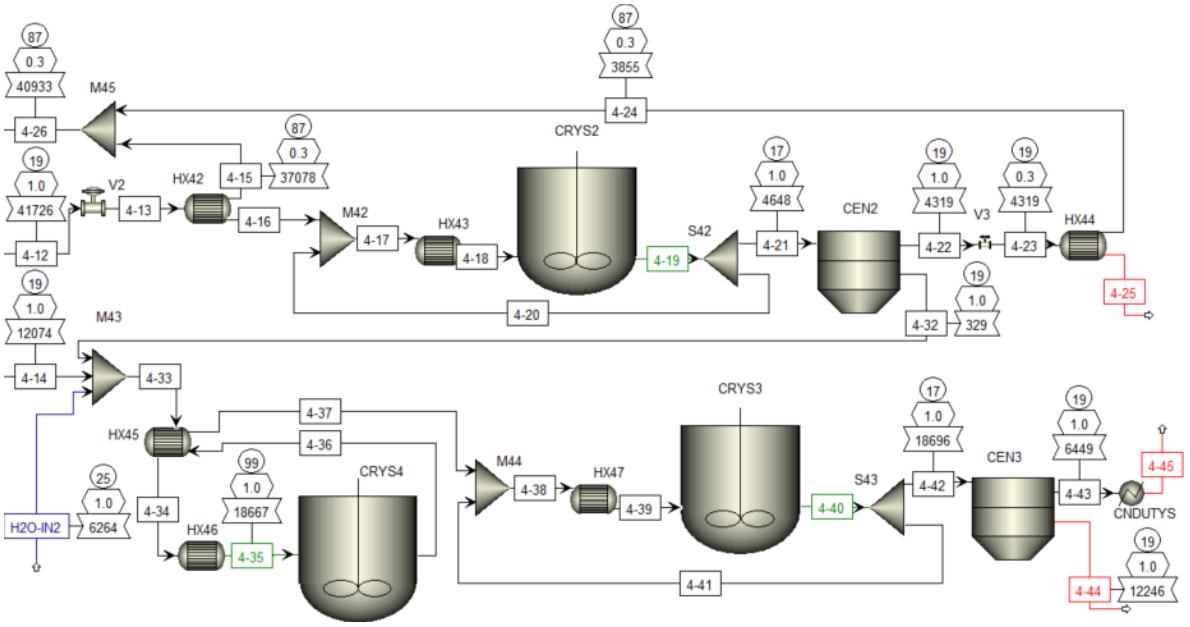

Figure 4.5: Flowsheet AA purge and refined crystallization

reactor leaving a small amount of heavy impurities to be removed in stream 4-25. The AA solids are then dissolved in clean water in CRYS4 and and recrystallized in CRYS3 to achieve a pure product.

Note that CNDUTYS after CEN3 is another fake block and used to ensure the electrical utility duty of the centrifuges is accounted for as there is no option for selecting utility type within the $CFuge$ unit block.

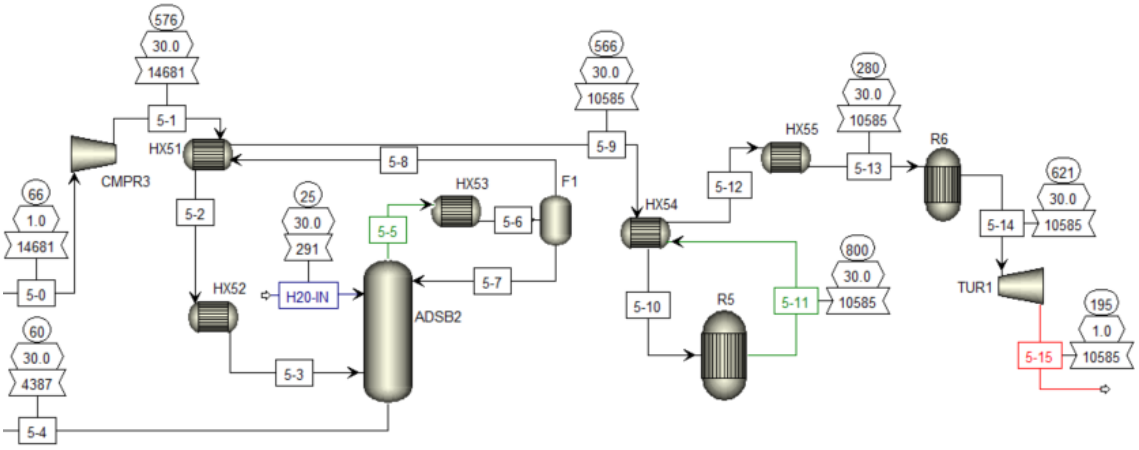

Figure 4.6: Flowsheet N_xO_x decomposition

As discussed in previous chapters, one of the main issues with the use of HNO_3 for the oxidation of KA oil is that there are stoichiometric amounts of N_xO_x compounds. The flowsheet in Figure 4.6 models a potential N_xO_x decomposition process.

The 35% N_xO_x containing gas stream is first compressed to 30 bar in a single stage compressor before being cooled in HX51 and HX52. The NO_2 is then recovered as HNO_3 in a absorption column while the remaining N_2O and NO is decomposed in adiabatic reactors R5 and R6. Heat is recovered in the form of 1.7 MW of MPS generation in HX55 and finally the 30 bar hot gases leave over a turbine which produces 1.3 MW of electrical utility.

Note that no dryer is implemented. This is due to the fact that the majority of AA is produced for the Nylon industry where the wet crystals are immediately added to a solution of 1,6-hexanediamine for

further processing. Some clean rinse water in the solid product after the centrifuge is not an issue and thus the crystals do not need drying.

Equipment Parameters

The resulting heat exchanger and column parameters for the modeling of the conventional route is given in the tables below. Columns tray numbers were found based on the method set out in Section 3.3.4. This as well as the resulting boiler and condenser duties are given in Table 4.1. The column diameter and other internals were sized based on Aspens built in column sizing function. This function uses empirical relationships and the flow rates for each case to estimate appropriate sizes.

Table 4.1: Final optimized column parameters for conventional route

Column	Stages	Diameter m	Pressure (bara)	Boiler duty (kW)	Condenser duty (kW)
1	15	2..0	1	4420	331
2	18	4.0	0.3	13797.6	6719.52

The sizing of absorption and stripping columns was done in a similar manner to that of the distillation columns. However the appropriate packing height and diameter was calculated and shown in Table 4.2.

Table 4.2: Final optimized absorption/stripper column parameters for conventional route

Column	Height	Diameter m	Pressure (bara)
1	12	1.3728	1
2	2.16	0.48089	30

The heat exchanger requirements are shown in Table 4.3. Where required, HX utility type was selected based on minimum requirement. For example, HX46 could be operated on LPS, MPS or electricity but LPS is the cheapest source of heat of these three and thus is utilized. The type of HX and material used is also shown as this impacts costing of the HX.

Table 4.3: CON process HX parameters

Unit	Utility	Duty (kW)	Type	Material
10	MPS-GEN	4874	Shell	cs
11	WTR	2017	Shell	cs
21	WTR	3492	Plate	cs
22	WTR	11506	Shell	cs
23	WTR	5279	Shell	cs
24	WTR	1550	Plate	cs
31	WTR	654	Plate	cs
32	WTR	715	Plate	ss
41	WTR	2731	Shell	ss
42	LPS	17171	Shell	ss
43	WTR	218	Shell	ss
44	LPS	1693	Shell	ss
45	-	891	Shell	ss
46	LPS	66	Plate	ss
47	WTR	1244	Shell	ss
48	WTR	5694	Shell	ss
49	WTR	18046	Shell	ss
51	-	1732	Plate	ss
52	WTR	2086	Plate	ss
53	WTR	143	Shell	ss
54	-	14	Plate	ss
55	MPS-GEN	1717	Plate	ss

4.1.2. Electro Catalytic Oxidation Process Design Results

The process flowsheet and equipment results for the ECO AA production route is discussed below.

Process Flow Diagrams

As discussed and illustrated in Figure 3.2, the first two steps of the ECO process are the same as for the conventional route, with the exception of hydrogen from the ECO process being recycled back to the BEN hydrogenation reactor. For this reason step one and two are not repeated here.

The third step shown in Figure 3.2, ECO, is expanded and shown in Figure 4.7. There are several input (blue) and output (red) as well as recycle (green) lines. There are several important considerations to note here.

- First, as discussed in Section 3.3.8, there is no ECO reactor block in Aspen Plus. Therefore a combination of reactor, separator and calculator blocks have been used to implement the results of Liu et al. [11] with the modification of a small cell voltage increase of 50.1 mV to compensate for the cell operating at 50 bar, as explained in Section 2.2.2. This approximation can be seen as the red dotted square. The separator block is used to split the oxygen and hydrogen which would have already been in two separate compartments in the physical system. The final electrical utility requirement was found to be 32 MW, while producing 89 kmol/h of AA, 322 kmol/h of H_2 and 5.5 kmol/h of O_2 at an outlet temperature of 113°C. An example of this calculation is shown in Appendix A.
- Secondly, the use of KOH as an electrolyte in the ECO of KA oil is wide spread [2, 12, 11]. However, as discussed in the literature review, the neutralization of the AA solution can be expensive and is a very important consideration in terms of overall process cost and complexity [17]. The use of ED was investigated in this project. The two compartment ED setup proposed by Zhenhua et al. [12] and shown in Figure 2.8, was modeled with a simple separation block followed by two heater blocks to model the required electrical duty. This is shown in Figure 4.7 as the green dotted square. With the aid of a calculator block, this approximation should be capable of modeling the separation results and power requirements of a real ED setup. The predicted electrical power requirement was 27 MW. J. Wisniewski reported that the power requirements for a two compart-

ment ED setup is highly dependent on the final concentrate of electrolyte [43]. His experimental results for the separation of NaOH from $NaNO_3$ were used to estimate the similar separation of KOH from AA, including an adjustment for molar mass. It is assumed that Na^+ ions and K^+ ions will have similar CEM permeability for an optimized CEM. The requirement to lower the KOH return concentration in order to minimize power requirements means that it is beneficial to include the top up water and recycled distillate in the concentrate compartment of the ED system.

- Finally for numerical instability reasons recycle streams 4-49 and 4-48 were disconnected but checked to ensure that values were within 5% of the return and no impurity build up was possible.

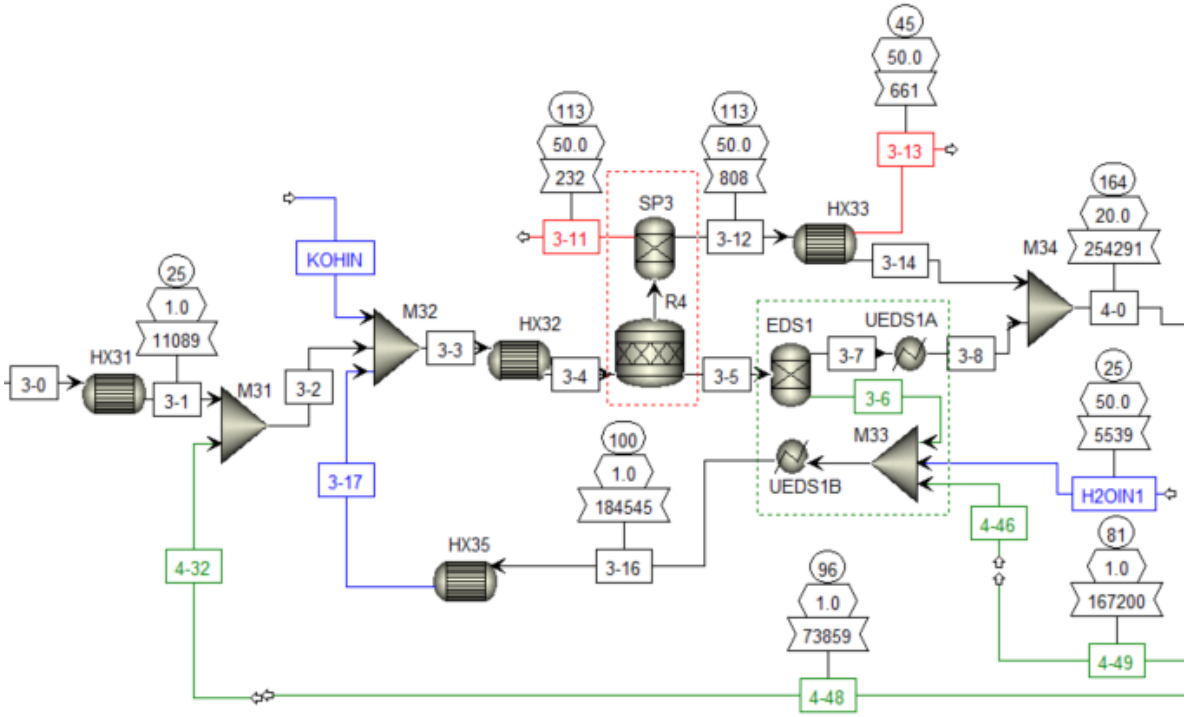

Figure 4.7: Flowsheet of ECO process step

The separation of AA from the remaining solution is conducted in a similar manner to that of the conventional route and is shown in Figure 4.8. However due to the low concentrations of AA, about 6% wt., there is significantly more distillation required to concentrate the AA. This is, however, offset but the ability to use a multi effect distillation system, as unlike HNO_3 which breaks down at temperatures above 80°C and limits the use of multi effect distillation, the electrolyte is stable at higher temperatures. This multi effect distillation is seen in COL2, HX41 and HX42, where valves v1 and v2 are used to lower the pressure from 1 to 0.8 to 0.6 bar, respectively. It is important that there are no incondensable in the solution before distillation as these would hinder condensation and thus the drawing of a vacuum. For this reason it is important to flash the stream before it enters COL2. This is shown in Figure 4.7, block F3.

The use of distillation column, COL2, with a partial condenser allows for recovery of unreacted KA oil from the product stream and, although out of the scope of this project, this could be useful in optimizing of recycles to the ECO reactor.

Following concentration to the solubility limit of 40% AA at 90°C , the solution is cooled to 17°C with CW and allowed to crystallize in the CRYS1, recovering 96% of dissolved AA. The AA crystals are centrifuged out and the remaining solution is concentrated once again at vacuum pressures using the exhaust vapor from the first multistage evaporator. Finally the solution is crystallized again to recover an additional 3% of the AA.

The recrystallization purification step is the same as for the conventional process except the waste water which consists of mainly H_2O and aqueous AA can be recycled through the ED and into the ECO.

Reducing water consumption and recovering uncrystallized product.

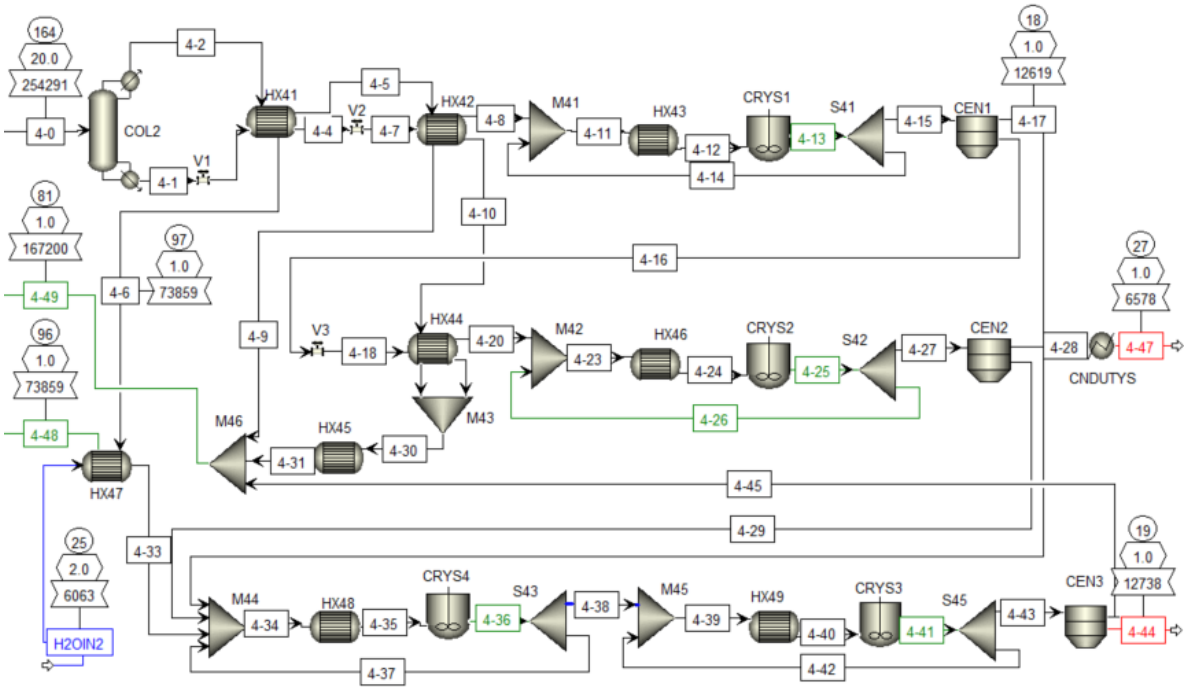

Figure 4.8: Flowsheet ECO AA separation

Equipment Parameters

The final equipment parameters for the ECO route are given in this section. It can be seen in Table 4.4 that the boiler duty of COL2 is very large, at almost 60 MW this is due to the large amounts of water that needs to be evaporated inorder to concerntrate AA to the required amount

Table 4.4: Final optimized column parameters for ECO route

Column	Stages	Diameter m	Pressure (bara)	Boiler duty (kW)	Condenser duty (kW)
1	15	2.0	1	4420	331
2	30	4.4	1	58267	33220

Table 4.5: ECO process HX parameters

Unit	Utility	Duty (kW)	Type	Material
31	WTR	876	Plate	cs
32	WTR	5548	Plate	ss
33	WTR	280	Shell	cs
35	WTR	23028	Plate	ss
41	-	45088	Shell	cs
42	-	46435	Shell	cs
43	WTR	3090	Shell	cs
44	-	9831	Shell	cs
45	WTR	47056	Shell	cs
46	WTR	443	Shell	cs
47	-	478	Plate	cs
48	LPS	1627	Shell	cs
49	WTR	2157	Shell	cs

4.1.3. Biomass Based Route

The process flowsheet results for the biomass based t3HDA production route is discussed below.

Process Flow Diagrams

The process design for the ECH of MA to t3HDA is shown in Figure 4.9. As discussed in Section 3.4.3, the fermentation of muconic acid is not modeled and the final clarified fermentation broth composition is attained from Dell'Anna et al. [19] and the broth cost is estimated from Mokwatlo et al. [56].

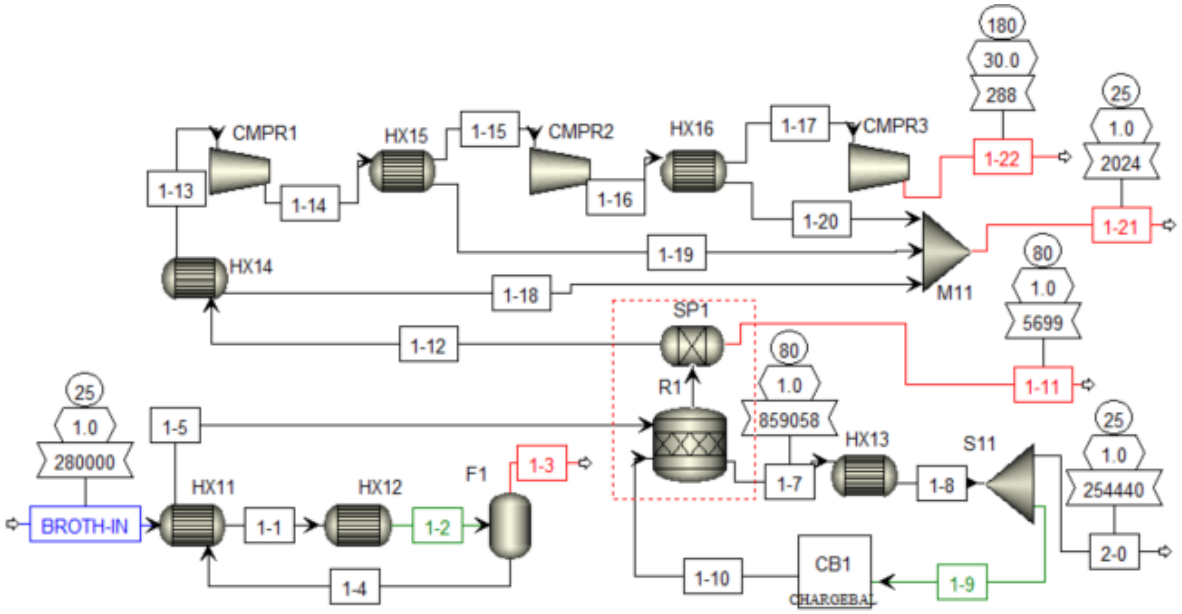

Figure 4.9: Flowsheet electrochemical oxidation of MA

The first step in the process, as shown with HX11, HX12 and F1, is to flash any dissolved gases which may be present in the broth. The broth temperature is raised to almost boiling temperature in HX 12, 95°C, the dissolved gasses are then removed before the heat in the broth is recovered in HX11. This gas removal is important as it ensures the oxygen and any produced hydrogen can be recovered with minimal impurities at the anode and cathode, respectively.

Once incondensables have been removed, the broth enters the ECH reactor shown with the red dotted rectangle. Similar to the ECO reactor, the ECH is modeled with a $RStoic$ and Sep unit. The electrical duty as well as reaction extends of R1 are controlled by a calculator block which has been programmed to model the experimental results of Dell'Anna et al. [19]. The final duty is 69 MW with a reaction extent of 90.6 kmol/hr of t3HDA and 136 kmol/hr of H_2. An example is shown in Appendix A. The broth is circulated through HX13 which cools the broth to 25°C from 80°C, by removing 52.6 MW of heat with CW. A portion of the stream is then recycled through the reactor to maintain a reactor outlet temperature of 80°C. Note that CB1 is a $Chargeball$ block. This block does not effect the steady state stream result and is used to allow for charge balancing during the numerical iterations before steady state is reached. Because the results reached convergence, CB1 can be ignored.

The H_2 and O_2 produced in this reactor is assumed to not leak through the membrane and thus SP1 simply splits the O_2 and H_2 ideally. Other evaporated compounds are split 50/50. The O_2 stream, 1-11, is not further processed and, along with stream 1-3, is assumed to be returned to the fermentation process to be bubbled through the fermentation tanks to oxygenate the broth and recover any valuable evaporated compounds. The H_2 stream, 1-12, is then compressed to 30 bar through a multistage compression and inter cooling process. The condensate is recovered and also assumed to be sent back to the fermentation tanks, while the the H_2 can be purified, pressurized and sold depending on downstream usage.

The economic value of the 273 kg/h H_2 production is \$954/h (based on the price of 3.49 as shown in Table 3.3). There is the potential to conventionally hydrogenate t3HDA to AA. Based on the results by

Mokwatlo et al. and ignoring the hydrogen requirements, the cost of t3HDA to AA hydrogenation would be around $160 per ton of AA [56]. Based on these figures, the total cost increase per kg of AA, if the t3HDA was hydrogenated to AA, would be roughly $0.7, when accounting for lost revenue due to H_2 usage.

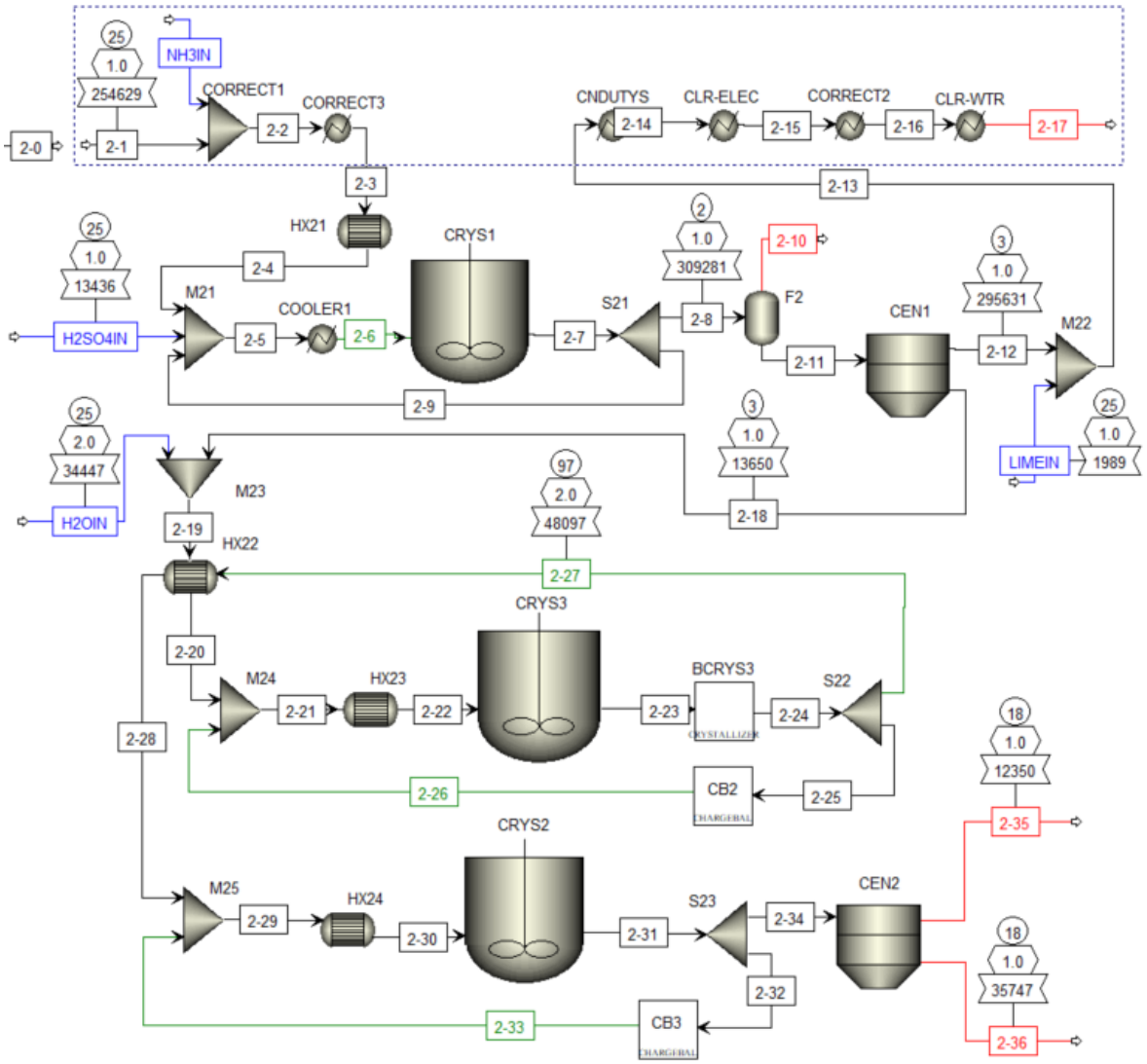

Figure 4.10: Flowsheet of t3HDA separation

Once the broth has been passed through the ECH reactor, the t3HDA need to be separated from the broth. This is shown in Figure 4.10. There are several things to note about this flowsheet, one of which is the blocks in the blue dotted box are non-physical and are simply used to correct for certain effects.

- NH3IN, CORRECT1 and CORRECT3 are used to correct the pH to its expected level. As discussed in Section 3.3.1, t3HDA and MA, and their ionic forms, do not have comprehensive property models. For this reason the ECH reactor was modeled using the JOBACK property estimation method for MA and t3HDA enthalpy of formation. However it becomes important to model ionic behavior for the broth separation. Therefore the switch between the t3HDA with JOBACK estimated properties and the t3HDA with assumed AA properties happens from streams 2-0 and 2-1. As the broth pH is meant to be neutral, ammonia is added to ensure pH = 7 and a dumby cooler is used to set the temperature of stream 2-3 to that of 2-0. This is not a realistic situation as this ammonia would have in fact been added to the fermentation tanks, therefor this NH3 is not considered an additional cost.
- Similar to the other two flowsheets, CNDUTYS is there to account for centrifuge duties as utility

specification is not possible within the $CFuge$ block.

- CLR-ELEC, CORRECT2 and CLR-WTR are used to account for electricity and CW usage of the chiller units as discussed in Section 3.3.11 and below.

After pH correction the broth is dosed with H_2SO_4 to bring the pH to 1.5. This pH drop as well as 2°C temperature brings the solubility of the t3HDA and unreacted MA to almost zero where it is recovered at 96% which is inline with previous studies [56].

After this the solid t3HDA and unwanted solid MA is dissolved and the t3HDA recrystallized.

Equipment Parameters

The HX requirements for the biomass based process are shown in Table 4.6. It can be seen that HX13, which is responsible for the removal of process heat from the ECH reactor, was a very large duty requirement. This is due to the large ohmic heating within the ECH reactor.

Table 4.6: Biomass based process HX parameters

Unit	Utility	Duty (kW)	Type	Material
11	-	19057	Plate	cs
12	LPS	11035	Shell	cs
13	WTR	52594	Plate	cs
14	WTR	1439	Plate	cs
15	WTR	243	Plate	cs
16	WTR	172	Plate	cs
21	WTR	3310	Shell	ss
22	-	3288	Shell	cs
23	LPS	1009	Shell	cs
24	WTR	1211	Shell	cs

4.2. Techno-Economic Assessment and Emissions Results

In order to assess the profitability, emissions and material efficiency KPIs set out in Section 3.2, the TEA for each process was carried out using the approach detailed in Section 3.4. The results of the TEAs are shown here.

4.2.1. Conventional Route Techno Economic Assessment Results

In the conventional AA production process, it can be seen in Figure 4.11 and Figure B.1 that the majority of AA cost is derived from the raw materials and specifically BEN feedstock. This is a common property of high energy petroleum processes as these materials generally require less external utility and specialized equipment to react. The total expected cost of AA is **$1.58 per kg**

A comparison of the AA MSP against real life market prices is not straightforward. There are several key geopolitical events that have disrupted supply chains and cause price volatility. This includes energy price fluctuations due to conflict in Eastern Europe, tariff uncertainty in the American market and an AA anti-dumping investigation by the EU against AA from China. Global prices vary from $1.03 to $2.05 /kg depending on region. The 2025 Q2 AA price estimates for Europe range between $1.4/kg [117] and $1.8/kg [118]. This work's MSP estimate of $1.58/kg is in the middle of this range.

The largest three feedstock expenses in the conventional process, which account for $1.06 per kg of AA, are BEN, H_2 and HNO_3, whilst reactors, crystallizers, columns and heat exchangers form the majority of CAPEX, as shown in Figure B.2. The total capital expenditure, when accounting for working capital and contingency is estimated to be $84 million. Finally the largest utility cost is LPS, as shown in Figure B.1, and is primarily due to the large duty of COL2. MPS is generated in after R1 and R5 in this process and this is sufficient to supply MPS needed in COL1. It can be seen that electrical power generation from the turbine after N_xO_x decomposition is minimal.

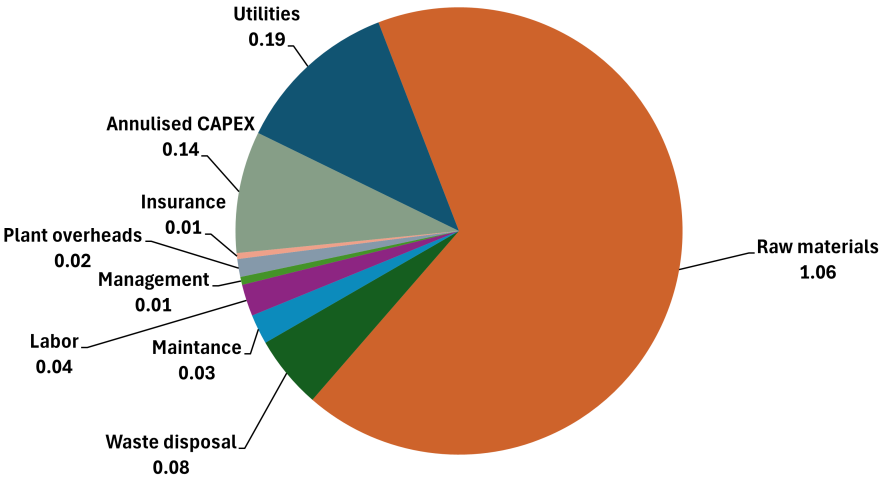

Figure 4.11: Conventional AA total cost breakdown ($/kg AA)

4.2.2. ECO Route Techno Economic Assessment Results

The predicted cost of AA form ECO is **$2.33 per kg**. The cost structure of the ECO route, shown in Figure 4.12, shows that the feedstock costs of the ECO route is $0.66/kg, or 40% lower than that of the conventional route. This is due to the hydrogen being supplied by the ECO reactor and the removed need for HNO_3. The largest cost component for the ECO becomes the utilities. Specifically the electricity costs at $0.77 per kg, as shown in Figure B.3. Waste disposal costs are only marginally higher for the ECO route because, although the amount of removed waste is larger, the treatment costs of HNO_3 containing streams are higher.

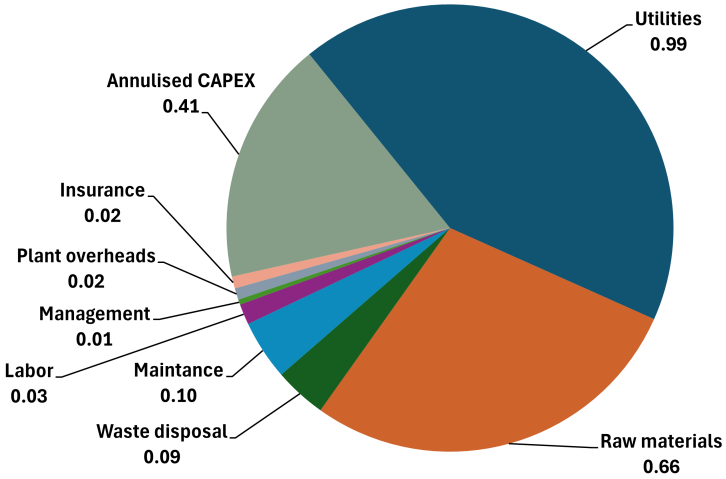

Figure 4.12: ECO AA total cost breakdown ($/kg AA)

Looking at the ECO CAPEX breakdown shown in Figure B.4, it can be seen that the reactors and ED setup are the most costly items. Based on the approach set out in Section 3.4.2, the 32 MW ECO reactor is expected to have an installed price of $59 million dollars. This estimate is on the higher side of similar power commercial water electrolysis units, however with lower current density and lower FE, this estimate is reasonable.

4.2.3. Biomass Based Route Techno Economic Assessment Results

The total cost breakdown for the biomass based route is shown in Figure 4.13 and predicted total cost of t3HDA is **$3.97 per kg**. As is typical for biomass based processes, the feedstock cost constitutes the majority of t3HDA cost, at $2.05 per kg. [78, 20, 19]. The largest utility cost of biomass based t3HDA production is electricity as seen in Figure 4.13. The lack of major amounts of process steam is understandable in this case as pH change and chillers were used as the primary means of product recovery. The ECH uses the majority of the electrical utility at 69 MW, with the hydrogen compression and chiller units using around 500 kW and 6 MW, respectively.

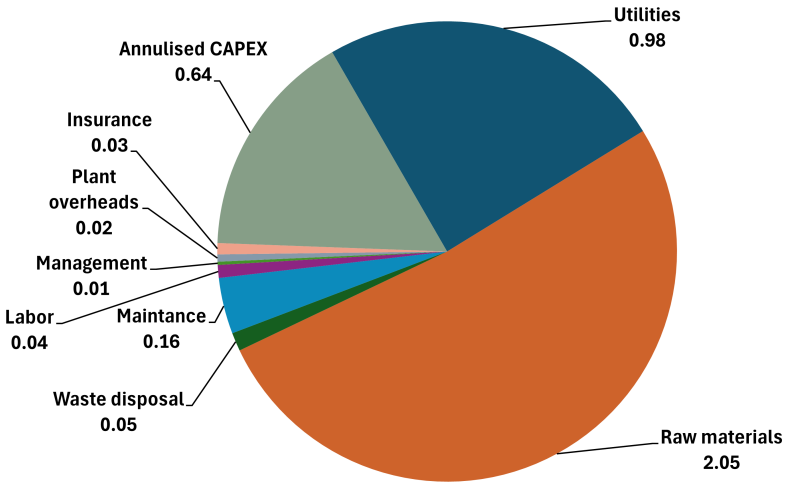

Figure 4.13: Biomass based t3HDA total cost breakdown ($/kg t3HDA)

4.2.4. KPI Comparisons

When comparing the results between the three studied processes, several noteworthy trends can be seen. First, as shown in Figure 4.14, it is clear to see that under current achievable current densities, FEs and product concentrations, ECO and ECH are not cost competitive with the conventional route. Secondly the ECO route and the biomass based route are significantly less CO_2 intensive than the conventional route, as shown by Figure 4.15. Finally, the material efficiency of all three processes is fairly reasonable for industrial processes.

KP1 Results: Profitability

ECO offers the closest MSP to the incumbent, however without cheaper electrical utility costs and ECO reactor and ED equipment, the use of ECO is $0.75 per kg (48%) more expensive than the conventional route. Notably, if low cost electricity can be used to lower the ECO utility cost, it is likely that this would also allow for lower feedstock H_2 cost in the conventional route, thus it is unclear if the conventional route cost would be static either. Another way in which the the cost of all processes can be reduced is with a lower expected rate of return (currently set at 15%). This is especially true in the case of ECO and biomass processes where annualized CAPEX is $0.41 per kg and $0.63 per kg, respectively. If a expected rate of return of 7.5% was used, annualized and thus product cost would decrease by $0.16 and $0.25 per kg, respectively.

The biomass based route is the most expensive process for a number of reasons. Firstly, comparatively to fossil derived BEN and hydrogen, feedstock costs of the MA in the fermentation broth is large. As discussion in Section 3.4.3, this cost estimate was based on the work of Mokwatlo et al. [56]. Secondly, the FE of the ECH reactor is low, at 40%, based of the experimental results of Dell'Anna [19]. This results in excessive H_2 production at high voltage, 5.7 volts and thus leads to high electrical utility consumption for a relatively low value by product. Finally, as discussed previously and shown in Figure B.6, the CAPEX of the Biomass based route is large due to the ECH reactor, coolers and crystallizers.

It is clear from Figure 4.14 that the Biomass based route is unlikely to become cost competitive to the conventional process unless t3HDA can demand a substantial price premium or several things occur:

- The cost of feedstock can reduce by significant amounts.
- The electrical efficiency of the ECH reactor increases.
- The CAPEX of the ECH decreases.

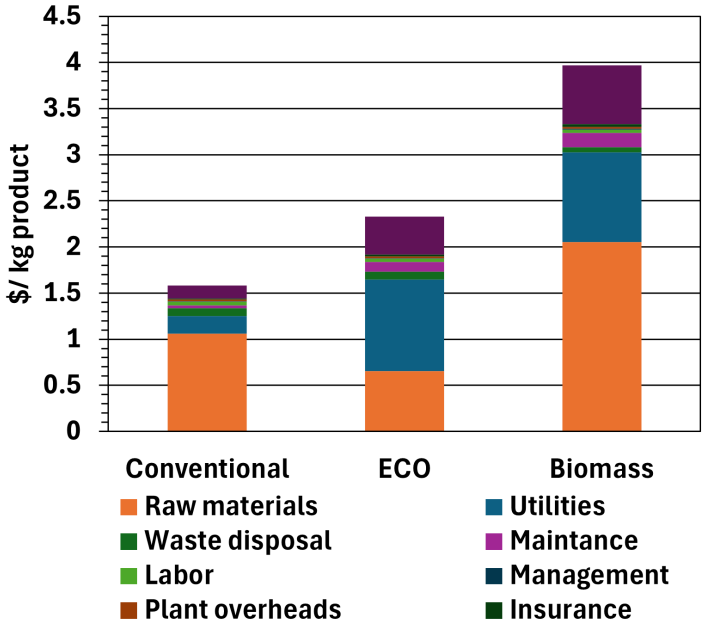

Figure 4.14: Overall cost comparison

KP2 Results: Emissions

When looking at the emissions of the three processes shown in Figure 4.15, it is clear to see the ECO and biomass based routes are significantly less emitting than that of the conventional route. Note that "Materials" accounts for input feedstocks and output streams.

As shown in Figure B.1, the main source of CO_{2eq} for the conventional route is the HNO_3 feedstock, at 3 kg CO_{2eq} per kg AA with the total CO_{2eq} being **4.79 kg CO_{2eq} per kg AA** . It is worth noting that the emissions from HNO_3 production can vary widely depending on process and emission controls used. The value of 3.9 kg CO_{2eq} per kg HNO_3 at 60% is the industrial average [7]. If HNO_3 is sourced from a plant with good abatement technology, the CO_{2eq} of HNO_3 could drop to 0.5 kg [119] and the CO_{2eq} of AA to 2.3 kg, therefore bringing the conventional route inline with the ECO route. This is discussed further in Section 4.4. H_2 feedstock only accounts for 0.3 kg CO_{2eq} per kg AA due the assumed use of green H_2.

AA from the ECO route is predicted to have a CO_{2eq} of **2.2 kg CO_{2eq} per kg AA**. The main reduction in CO_{2eq} is due to the removal of HNO_3 from the process. However, due to the low solubility of KA oil in the electrolyte solution, large amounts of LPS is needed for AA concentration and this results in 0.95 kg CO_{2eq} per kg AA. Further work to increase the final concentration of AA after ECO would be highly beneficial in reducing CO_{2eq}. The BEN feedstock accounts for about 0.8 kg CO_{2eq} per kg AA for the ECO route and conventional route.

The CO_{2eq} of biomass based t3HDA production is comparatively low, at **1.18 kg CO_{2eq} per kg t3HDA**. The main sources of CO_{2eq} are MA feedstock, electrical utility and LPS at 0.41, 0.29 and 0.20 kg CO_{2eq} per kg, respectively. This is shown in Figure B.5. The MA feedstock CO_{2eq} is again based on the work by Mokwatlo et al. [56]. There are minor amounts of CO_{2eq} from the H_2SO_4 and lime used in the acid dosing.

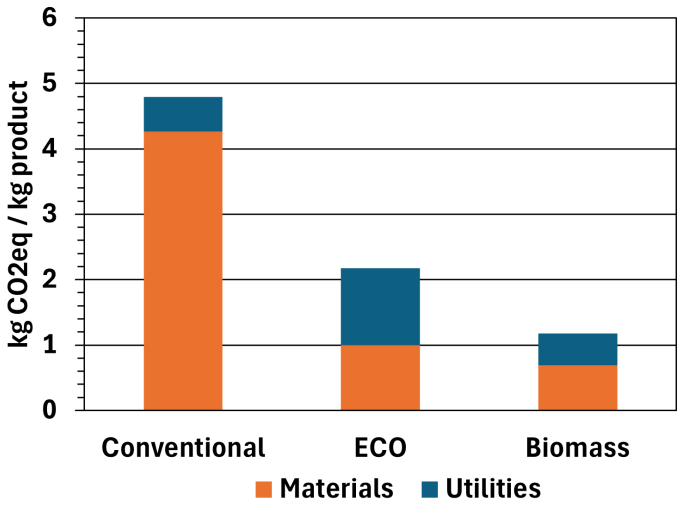

Figure 4.15: Overall CO_2 emissions comparison

KP3 Results: Material efficiency
Material efficiency is difficult to quantify as there are many different types of inlet and outlet streams of varying degrees of cost and environmental impact. It is therefore difficult to provide a single number as with MSP and CO_{2eq}. One way we can assess material efficiency of the processes is by looking at the excess of the main feedstock. It this case BEN or MA. This comparison is shown in Figure 4.16 and shows that BEN excess for the conventional and ECO route are similar, with the ECO route having slightly lower excess due to the recycling of unreacted KA oil to the ECO reactor. The conventional route would benefit from the addition of a small recovery column after HX48, shown in Figure 4.4, to recover KA oil and improve conversion efficiency. The biomass based route shows the best conversion ratio of feedstock to product at 1.09, however it is worth noting that this number ignores the fermentation process which is likely to have far higher production of unwanted byproducts [20, 19, 23].

Another important consideration is water consumption. Unsurprisingly the biomass based approach uses significant amounts of water for fermentation, about 300 tons/h. This water is likely to be treated and reused multiple times but still represents a large water treatment and top up requirement. ECO and the conventional process do not use excessive amounts of water.

4.3. Results Validation

4.3.1. Conventional Route Validation

Due to the conventional process being fairly well documented the validation of these results is straight forward. Overall conversion percentages, reactor temperatures and pressures, selectivity and excess feed ratios of all sections of the process were compared to various sources to ensure all results fell into common ranges. The final MSP of AA, which is discussed further in Section 4.2, was found to be $1.58 per kg AA which is in the middle of the range discussed in the literature review.

4.3.2. ECO Route Validation

The two largest CAPEX and utility expenses within the ECO process are the ECO reactor and ED KOH recovery. The electrical utility and CAPEX calculated in this project were compared to other work to judge if the results are reasonable.

- **ECO reactor CAPEX:** The calculated equipment cost of $1503 per kg/h AA was again compared to the estimate by Liu et al., which was found to be $1500 per kg/h AA [11]. This close estimate is surprising as, compared to the approach laid out in Section 3.4.2, Liu employed completely different set of assumptions and approaches to estimate the ECO reactor cost and arrived at a very similar result.

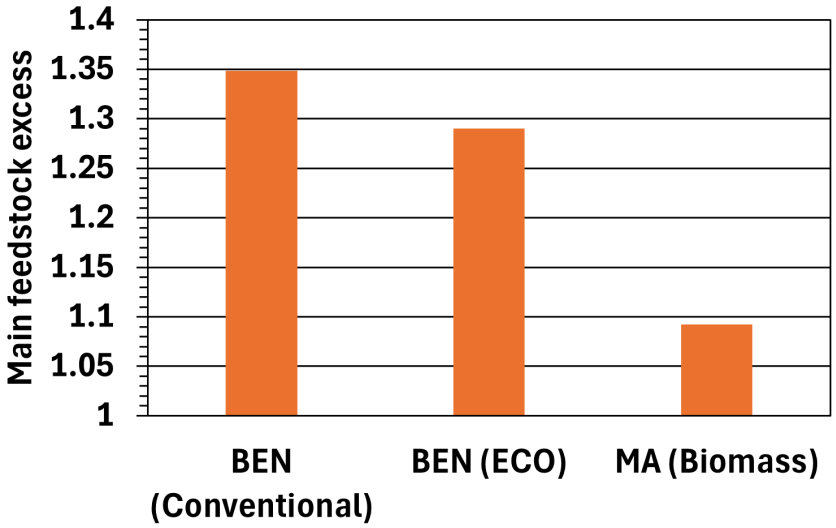

Figure 4.16: Overall main feedstock molar excess comparison. (Normalized by reaction stoichiometry and mole of AA/t3HDA produced)

- **ED CAPEX:** The ED setup installed cost of $169 000 per kmol/h KOH was compared to the work by Ramdin et al.[44]. When adjusted for current density, these authors calculated an installed ED CAPEX cost of 145 000 per kmol/h Formic acid. It is not clear how much of an impact the adjustment for current density and the differences in product properties will have on price, but it clear to see that these estimates are reasonable.
- **ECO reactor utility:** The calculated utility of 2.57 kWh/kg AA was compared to the techno economic assessment by Liu et al., which found a power requirement of 2.4 kWh/kg AA [11]. It is unsurprising that these results are similar as they are based on the same experimental data. The 7% difference is due to the slightly adjusted cell voltage because of the higher cell operating pressure.
- **ED utility:** As discussed previously, the electrical utility of ED was estimated based on the experimental work of Wisniewski et al. [43]. The final electrical utility was 106 kWh per kmol. When compared to the work by Ferrer et al. [120] and Ramdim et al. [44] which predicted a electrical utility of roughly 115 kWh per kmol of recovered NaOH, the 106 kWh per kmol of KOH found here seems reasonable.

4.3.3. Biomass Based Route Validation

The two largest CAPEX items in the biomass based route are the ECH reactor and the first crystallizer. The following approach was used to validate the the cost estimates for each:

- **ECH reactor CAPEX:** The equipment cost estimate for the ECH reactor was done based on the method set out in Section 3.4.2 and gave a final equipment cost of $800.0 per kW, when including the cost of HX13. Dell'Anna et al. [19] used an estimate for cost of ECH reactor per unit area of $10 000 by Matthiesen et al. [20], and a current density equal to 200 mA/cm^2 (same as this work) to find a final cost of $983.2 per kW. These two estimates are based on two different approaches and yet are reasonably close to the one another.
- **CRYS 1 CAPEX:** The total CAPEX cost of the first crystalizer stage is $9014 per (kg/h) of solid 3tHDA product. This includes the cost of CRYS1, prepackaged COOLER1 and HX21. Mokwatlo et al. employed a similar technique in the separation of MA from a fermentation broth and found a total CAPEX of $8 520 per (kg/h) [56]. t3HDA and MA should have similar solubility and the titers of the broths were similar, 44.6 and 47.2, respectively. Therefore the similarities of these results indicates a reasonable CAPEX estimation.

4.4. Sensitivity Analysis

The results of the sensitivity analysis, which method was laid out in Section 3.4.4, are shown in Figure 4.17, 4.18 and 4.19. Overall the results are as expected.

4.4.1. Conventional Route Sensitivity

The conventional route MSP shows the most sensitivity to its largest component cost, BEN feedstock. If BEN was priced at 1.39$/kg as in mid 2022, the MSP of AA would increase by 23%. As discussed previously, the majority of emissions from the conventional route (57%) could be avoided if the nitric acid supply is sourced from a cleaner producer which employees N_XO_X reduction technology.

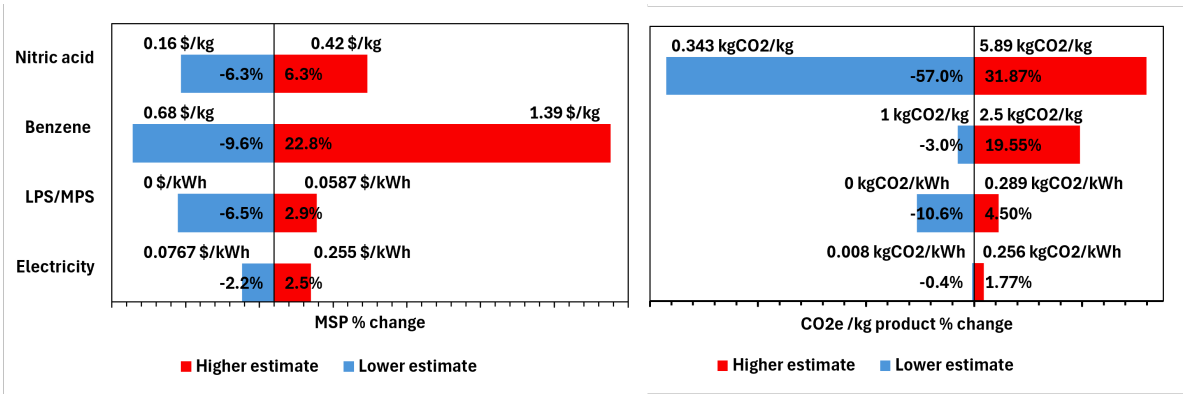

Figure 4.17: Sensitivity assessment of conventional AA route

4.4.2. ECO Route Sensitivity

Unsurprisingly, the ECO MSP is most sensitive to the electricity price, as shown in Figure 4.18. This is due to the large duty of the ECO reactor and ED system. BEN feedstock plays a similar role in ECO route MSP as in the conventional route, note the slightly lower % sensitivity to BEN price is largely due the MSP of the ECO route being slightly higher. In absolute terms, the BEN price sensitivity is likely the same as in the conventional route. MSP is sensitive to the ECO reactor costs but due to the large number of cost items in this model, the net effect on MSP is diluted.

Looking at emissions sensitivity, it can be seen that the use of waste heat can remove 43% of total emissions in the ECO route. This is due to the large amount of process steam needed to concentrate the dilute AA solution. If grid electricity, which averages 0.256 kg CO_2/kWh in the Netherlands, is used instead of green electricity in the ECO process, 45% increase in process emissions can be expected. Note again the effects of lower process emissions resulting in larger % changes for the BEN feedstock.

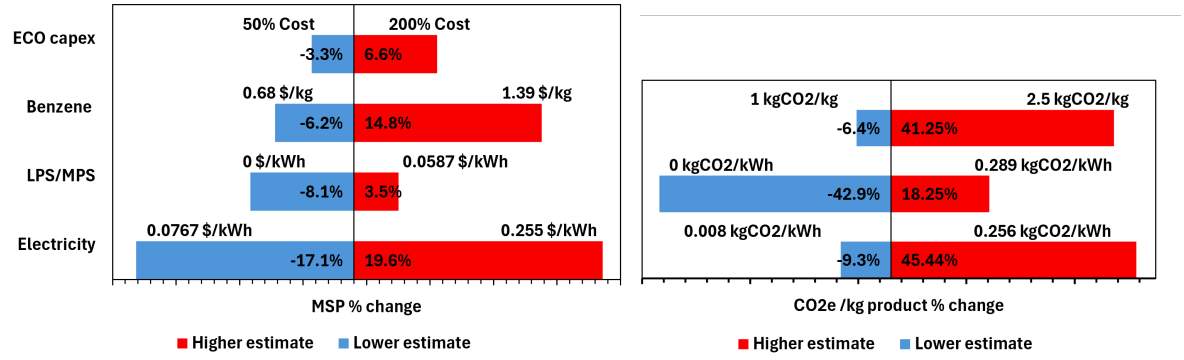

Figure 4.18: Sensitivity assessment of ECO AA route

4.4.3. Biomass Route Sensitivity

Looking at Figure 4.19, it can be seen that the biomass based t3HDA production route shares similar sensitivity results to that of the ECO route. The MSP and emissions of the biomass route are sensitivity to the FE of the ECH reactor due to electricity being the major utility of the process. This shows ECH FE sensitivity indicates the benefit for improved optimization and is discussed further in Section 6.2.

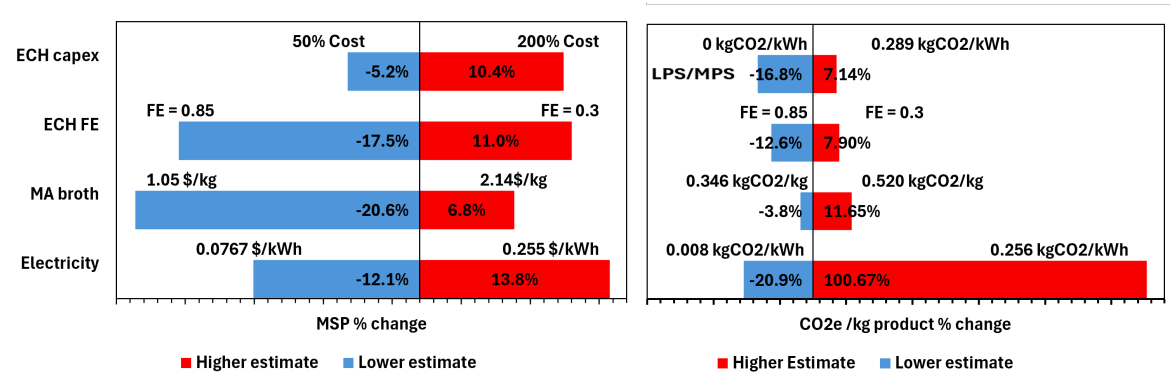

Figure 4.19: Sensitivity assessment of biomass based t3HDA route

5
Conclusion

The aim of this thesis was to compare the feasibility of two electrochemical based alternatives to current AA production process on an economic and emissions basis. To achieve this, the process systems modeling prospective was used to evaluate three key performance indicators for each of the three modeled processes. MSP, process CO_{2eq} emissions and material efficiency were calculated and it was found that although the two electrochemical based alternatives may be capable of significantly reducing emission impacts of AA production, they are not yet cost competitive with the incumbent AA production process. There are several important takeaways from the results presented in this report.

- **CO_{2eq}** The emission KPI results show that the biomass and ECO alternative processes are the better AA production processes. A large portion of the ECO route emissions is due to the large amount of LPS needed to concentrate the dilute AA solution after the KA oil oxidation. If this concentration can be increased before separation or if waste heat with a lower CO_{2eq} can be used, the ECO route CO_{2eq} would be similar to that of the biomass route of around 1.3 kg CO_{2eq} per kg AA.
- **N_2O abatement:** When looking at the emission results of the conventional production process, it is clear that should the HNO_3 supplier implement N_2O abatement and other emission reducing technology, the emission impact of the conventional process would be somewhat comparable to that of the ECO route. It is unclear what additional costs this cleaner supply of HNO_3 would entail for the conventional process, but it is likely that the ECO route will become a less attractive alternative to the conventional process if emission rates were the same.
- **MSP:** At a MSP of $1.58 per kg AA, it is clear that the conventional production process remains the best economic option when compared to $2.33 and $3.97 for the ECO and biomass route, respectively. Low-cost waste heat from an outside source would decrease the MSP of all processes by a small amount, while cheaper electricity prices have the possibility to significantly reduce the MSP of electrochemical alternatives.
- **ECH necessity:** The high MSP of t3HDA from the biomass route indicates that unless a premium is placed on t3HDA, there is likely no reason to perform ECH on MA. Instead, it is more reasonable to simply recover the MA from the fermentation broth and conventionally hydrogenate it to AA. Process modeling results by Mokwatlo et al. show that even with H_2 from CO_2 intense SMR, a MSP of $2.6 and emission KPI of 1.2 kg CO_{2eq} per kg AA is possible [56].
- **Sensitivity of electrified processes:** The MSP and CO_{2eq} of both of the studied electrochemical based alternatives are highly dependent on electricity prices and performance of the ECO reactor, ECH reactor or ED system. These technologies are also mostly untested on a large scale. For these reasons, the uncertainty of these results is large and more work would be needed to validate the results presented here.

The models and results presented within this report indicate the complexity of modeling comprehensive reaction and downstream processes, but it also highlights the importance of doing so. Too often downstream separation is an afterthought in the search for novel approaches to chemical production. The capital and operational costs of the downstream separation should be a major consideration when making design decisions for new electrochemical reactors.

6 Recommendations

6.1. General Recommendations

The following recommendations apply broadly to all of the modeled processes.

6.1.1. Water Purification

Within this project, water purification and pretreatment was not assessed. Water of high purity is required in the production of AA or t3HDA due to the high purity requirements of downstream nylon production. Water purification steps can be included in the model or the associated cost accounted for in water feedstock prices.

6.1.2. Heat Exchanger Sizing

As discussed in Section 3.4.2, the heat transfer coefficients, used in the calculation of required surface areas of heat exchangers, were taken from literature on general heat transfer coefficients for various combinations of fluid types. This approach is not as accurate as using actual heat transfer properties of the fluids involved and the geometry of the HX. Further work should incorporate the fluid properties and HX geometry of each HX into the area calculations.

6.1.3. Electrical Price Intermittency

The price of electricity within this project was assumed to be steady. If renewable electricity sources are to be used, it would be beneficial to incorporate the transient behavior of the studied processes in order to understand the transient effects of process parameters. This would highlight the economic value of each process in a frequently price varying energy market.

6.1.4. Material Properties

As discussed in Section 3.3.1, several EOS types were used in various sections of the modeled processes and there were some material properties that had to be estimated or approximated due to the lack of empirical material properties. Experimental work to validate these estimations and approximations would be beneficial in providing more certainty of the model results.

6.1.5. Pumping Requirements

Liquid pumping requirements as well as equipment pressure drops are not considered in this project due to the low power requirements compared to that of the compressors, reactors and chillers. This simplification may be too simplistic for liquid streams with large flow rates such as in the biomass based route or gas recycle streams such as the H_2 circulation within the BEN hydrogenation step. Realistic pressure drops and pressure increasing equipment should be added to the models to account for this effect.

6.1.6. Heat Integration

While some effort to apply heat integration throughout the various processes can be seen in the flowsheets, a complete pinch analysis is likely to offer additional insight into possible avenues for reducing utility usage. Additionally, techniques such as vapor compression could be investigated to improve energy efficiency of separation processes.

6.1.7. Improved Membrane and Catalyst Modeling

Within this project, catalyst and membrane costs for many reactors have been treated as a once off CAPEX cost. This ignores the not insignificant OPEX costs associated with frequent replacement or renewal. Further work would benefit from incorporating accurate catalyst and membrane usage data in each reactor, as well as any downstream effects of leached catalyst.

6.2. Process Specific Modeling Recommendations

The recommendations presented here at specific to each process and are generally recommendations on the optimization or reorganization of various sections of the flowsheets.

6.2.1. Conventional Route

- The oxidation of KA oil with HNO_3 is generally performed with excess HNO_3, as discussed in Section 2.1. This is done to ensure complete oxidation of KA oil but mostly to control reaction temperature [8]. R3 could be split into multiple smaller reactors which could be connected in series with inter coolers to allow for staged addition of HNO_3 and thus minimize excess required. This would lower downstream separation requirements.
- The modeling of the N_2O decomposition reactors is very simplistic, with $RStoic$ reaction extents set to achieve outlet temperatures specified in literature. A more detailed and realistic $Rplug$ model could be used to approximate the reactor behavior [4].
- The unreacted KA oil which, in the current model, is ejected with the excess water after HX48, could be recovered with another smaller distillation column and recycled back to the oxidation reactor. This would recover a noticeable amount of valuable intermediate product.

6.2.2. ECO Route

- The electrical utility requirement of the ED is a function of the KOH concentration of the concentrated return stream. Therefor the more water run through the ED setup, the less energy is required. There is scope for optimization of the flowsheet configuration of the ECO route in order to maximize the amount of return liquid that enters the ED setup.
- The ECO experimental results on which the constructed model is based does not state wether it may be possible to further concentrate the AA in solution by recycling the mixture through the ECO reactor and continually adding KA oil to maintain the KA oil at the solubility limit. Experiments should be conducted to see if this is the case. If this is the case, the downstream separation and overall AA production costs and emissions could be significantly reduced.

6.2.3. Biomass Based Route

- The ECH reactor was modeled at the optimal operating point found by a simplified TEA of the process [19]. After further investigation, it was found that this TEA does not account for the increased electrical utility due to the FE being less than 1. Therefore, although the ECH reactor in this project is modeled correctly, the operating point may not be the most economically or environmentally optimal. This should be assessed by varying of the operating conditions to assess for optimal conditions.
- The size of the chiller unit used to cool CRYS1 to 2°C could be greatly reduced if a HX is used to precool the warmer liquid entering the crystallization loop with the colder liquid exiting the centrifuge after crystallization.

References

[1] *Adipic Acid Market Size, Share & Trends Analysis Report, 2030 — grandviewresearch.com*. [Accessed 27-01-2025].

[2] Yingshuai Jia et al. “Directional Electrosynthesis of Adipic Acid and Cyclohexanone by Controlling the Active Sites on NiOOH”. In: *Journal of the American Chemical Society* 146.2 (2023), pp. 1282–1293.

[3] A Shimizu, K Tanaka, and M Fujimori. “Abatement technologies for N2O emissions in the adipic acid industry”. In: *Chemosphere-global change science* 2.3-4 (2000), pp. 425–434.

[4] Dong He et al. “Conceptual design of a fixed bed N2O decomposition reactor with a heat pipe heat exchanger”. In: *International Journal of Chemical Reactor Engineering* 22.5 (2024), pp. 547–557.

[5] David Miller, Katy Armstrong, and Peter Styring. “Assessing methods for the production of renewable benzene”. In: *Sustainable Production and Consumption* 32 (2022), pp. 184–197.

[6] Amela Ajanovic, Marlene Sayer, and Reinhard Haas. “On the future relevance of green hydrogen in Europe”. In: *Applied Energy* 358 (2024), p. 122586. ISSN: 0306-2619.

[7] CarbonCloud. *Nitric Acid, 70 percent in H2O, HNO3*. 2025. URL: `https://apps.carboncloud.com/climatehub/product-reports/id/2198404469941#:~:text=%E2%80%9DNitric%20Acid%2C%2070%25%20in,match%20the%20latest%20climate%20science.` (visited on 03/11/2025).

[8] Michael Tuttle Musser. “Adipic Acid”. In: *Ullmann’s encyclopedia of industrial chemistry*. Weinheim, Germany: Wiley-VCH, 2000.

[9] Thomas Schaub. “Producing adipic acid without the nitrous oxide”. In: *Science* 366.6472 (2019), pp. 1447–1447.

[10] Yiqiang Wen et al. “A large-scale continuous-flow process for the production of adipic acid via catalytic oxidation of cyclohexene with H 2 O 2”. In: *Green Chemistry* 14.10 (2012), pp. 2868–2875.

[11] Xiang Liu et al. “Electrosynthesis of adipic acid with high faradaic efficiency within a wide potential window”. In: *Nature Communications* 15.1 (2024), p. 7685.

[12] Zhenhua Li et al. “Electrocatalytic synthesis of adipic acid coupled with H2 production enhanced by a ligand modification strategy”. In: *Nature Communications* 13.1 (2022), p. 5009.

[13] Ran Wang et al. “Electrifying Adipic Acid Production: Copper-Promoted Oxidation and C- C Cleavage of Cyclohexanol”. In: *Angewandte Chemie* 134.50 (2022), e202214977.

[14] Li Liu et al. “Self-supported bimetallic array superstructures for high-performance coupling electrosynthesis of formate and adipate”. In: *Exploration* 4.3 (2024), p. 20230043.

[15] Fulai Liu et al. “Graphdiyne as an electron modifier for boosting electrochemical production of adipic acid”. In: *Advanced Functional Materials* 34.6 (2024), p. 2310274.

[16] Fulai Liu et al. “Sustainable adipic acid production via paired electrolysis of lignin-derived phenolic compounds with water as hydrogen and oxygen sources”. In: *Journal of the American Chemical Society* 146.22 (2024), pp. 15275–15285.

[17] Shariful Kibria Nabil et al. “Acid–base chemistry and the economic implication of electrocatalytic carboxylate production in alkaline electrolytes”. In: *Nature Catalysis* 7.3 (2024), pp. 330–337.

[18] Sampath Gunukula and Robert P Anex. “Techno-economic analysis of multiple bio-based routes to adipic acid”. In: *Biofuels, Bioproducts and Biorefining* 11.5 (2017), pp. 897–907.

[19] Marco Nazareno Dell’Anna et al. “Electrochemical hydrogenation of bioprivileged cis, cis-muconic acid to trans-3-hexenedioic acid: from lab synthesis to bench-scale production and beyond”. In: *Green Chemistry* 23.17 (2021), pp. 6456–6468.

[20] John E Matthiesen et al. “Electrochemical conversion of biologically produced muconic acid: key considerations for scale-up and corresponding technoeconomic analysis”. In: *ACS Sustainable Chemistry & Engineering* 4.12 (2016), pp. 7098–7109.

[21] John E Matthiesen et al. “Electrochemical conversion of muconic acid to biobased diacid monomers”. In: *ACS Sustainable Chemistry & Engineering* 4.6 (2016), pp. 3575–3585.

[22] Derek R Vardon et al. “Adipic acid production from lignin”. In: *Energy & Environmental Science* 8.2 (2015), pp. 617–628.

[23] Deep M Patel et al. “Structure sensitivity of the electrochemical hydrogenation of cis, cis-muconic acid to hexenedioic acid and adipic acid”. In: *Green Chemistry* 26.8 (2024), pp. 4506–4517.

[24] Robin Smith. *Chemical Process Design and Integration*. West Sussex, England: John Wiley and Sons, 2005.

[25] Jeovanna Rios et al. “A critical review on the progress and challenges to a more sustainable, cost competitive synthesis of adipic acid”. In: *Green Chemistry* 23.9 (2021), pp. 3172–3190.

[26] A Castellan, Joannes Christiaan Josephus Bart, and Stefano Cavallaro. “Industrial production and use of adipic acid”. In: *Catalysis Today* 9.3 (1991), pp. 237–254.

[27] Jan CJ Bart and Stefano Cavallaro. “Transiting from adipic acid to bioadipic acid. 1, petroleum-based processes”. In: *Industrial & Engineering Chemistry Research* 54.1 (2015), pp. 1–46.

[28] H.J. Arpe K. Weissermel. *Industrial Organic Chemistry*. 3th ed. John Wiley & Sons, Ltd, 2003.

[29] M. Larry Campbell. “Cyclohexane”. In: *Ullmann’s encyclopedia of industrial chemistry*. Weinheim, Germany: Wiley-VCH, 2000.

[30] H ILLIS O. FOLKINS. “Benzene”. In: *Ullmann’s encyclopedia of industrial chemistry*. Weinheim, Germany: Wiley-VCH, 2000.

[31] Ahmed Abutaleb and Mohammad Ashraf Ali. “A comprehensive and updated review of studies on the oxidation of cyclohexane to produce ketone-alcohol (KA) oil”. In: *Reviews in Chemical Engineering* 38.7 (2022), pp. 769–797.

[32] Hui Li, Yuanbin She, and Tao Wang. “Advances and perspectives in catalysts for liquid-phase oxidation of cyclohexane”. In: *Frontiers of Chemical Science and Engineering* 6 (2012), pp. 356–368.

[33] Michael Tuttle Musser. “Cyclohexanol and Cyclohexanone”. In: *Ullmann’s encyclopedia of industrial chemistry*. Weinheim, Germany: Wiley-VCH, 2000.

[34] Sira Suren et al. “Measurement on the solubility of adipic acid in various solvents at high temperature and its thermodynamics parameters”. In: *Fluid Phase Equilibria* 360 (2013), pp. 332–337.

[35] Qi Wang et al. “Life cycle assessment for the direct synthesis of adipic acid in microreactors and benchmarking to the commercial process”. In: *Chemical engineering journal* 234 (2013), pp. 300–311.

[36] Caliane BB Costa, Aline C da Costa, and Rubens Maciel Filho. “Mathematical modeling and optimal control strategy development for an adipic acid crystallization process”. In: *Chemical Engineering and Processing: Process Intensification* 44.7 (2005), pp. 737–753.

[37] BASF et al. *Method of removing nitrogen oxides from a gas flow*. WO97/10042. 1997.

[38] Lambert Schneider, Michael Lazarus, and Anja Kollmuss. “Industrial N2O projects under the CDM: Adipic acid-A case of carbon leakage”. In: *Stockholm: Stockholm Environmental Institute* (2010).

[39] Gavin Towler and Ray Sinnott. *Chemical Engineering Design. Principles, Practice and Economics of Plant and Process Design*. Third Edition. Oxford, England: Butterworth-Heinemann, Elsevier, 2022.

[40] EU. *Greenhouse gas emission intensity of electricity generation in Europe*. Oct. 2024. URL: https://www.eea.europa.eu/en/analysis/indicators/greenhouse-gas-emission-intensity-of-1?activeAccordion=ecdb3bcf-bbe9-4978-b5cf-0b136399d9f8 (visited on 03/11/2025).

[41] BV Lyalin and VA Petrosyan. “Electrosynthesis of adipic acid by undivided cell electrolysis”. In: *Russian chemical bulletin* 53 (2004), pp. 688–692.

[42] aspentech. *Aspen Plus*. Version V12.0. Feb. 7, 2025. URL: https://www.aspentech.com/en/products/engineering/aspen-plus.

[43] J Wiśniewski, Grażyna Wiśniewska, and Tomasz Winnicki. “Application of bipolar electrodialysis to the recovery of acids and bases from water solutions”. In: *Desalination* 169.1 (2004), pp. 11–20.

[44] Mahinder Ramdin et al. “High-pressure electrochemical reduction of CO2 to formic acid/formate: effect of pH on the downstream separation process and economics”. In: *Industrial & Engineering Chemistry Research* 58.51 (2019), pp. 22718–22740.

[45] Thomas Francis Fuller and John Naim Harb. *Electrochemical engineering*. Hoboken, NJ, USA: Wiley, 2018.

[46] Mohd Nur Ikhmal Salehmin et al. “High-pressure PEM water electrolyser: A review on challenges and mitigation strategies towards green and low-cost hydrogen production”. In: *Energy Conversion and Management* 268 (2022), p. 115985.

[47] Mohd Adnan Khan et al. “The techno-economics of hydrogen compression”. In: *Transition Accelerator Technical Briefs* 1.1 (2021), pp. 1–36.

[48] CarbonCloud. *Potassium hydroxide (KOH). E525*. 2025. URL: https://apps.carboncloud.com/climatehub/product-reports/id/1394351136979#:~:text=%E2%80%9DPotassium%20hydroxide%20(KOH).,match%20the%20latest%20climate%20science. (visited on 03/11/2025).

[49] CarbonCloud. *Sulfuric acid (H2SO4). E513*. 2025. URL: https://apps.carboncloud.com/climatehub/product-reports/id/1266801278346#:~:text=%E2%80%9DSulfuric%20acid%20(H2SO4).,match%20the%20latest%20climate%20science. (visited on 03/11/2025).

[50] Todd Werpy and Gene Petersen. *Top value added chemicals from biomass: volume I–results of screening for potential candidates from sugars and synthesis gas*. Tech. rep. National Renewable Energy Lab.(NREL), Golden, CO (United States), 2004.

[51] Miguel Suastegui et al. “Combining metabolic engineering and electrocatalysis: application to the production of polyamides from sugar”. In: *Angewandte Chemie International Edition* 55.7 (2016), pp. 2368–2373.

[52] John Edward Matthiesen et al. *Functionalization of trans-3-hexenedioic acid for the production of hydrophobic polyamides and chemical resistance thereof*. US Patent App. 16/192,937. 2019.

[53] Karen M Draths and John W Frost. “Environmentally compatible synthesis of adipic acid from D-glucose”. In: *Journal of the American Chemical Society* 116.1 (1994), pp. 399–400.

[54] Han-Na Lee et al. “Corynebacterium cell factory design and culture process optimization for muconic acid biosynthesis”. In: *Scientific reports* 8.1 (2018), p. 18041.

[55] Thomas Nicolai et al. “In-situ muconic acid extraction reveals sugar consumption bottleneck in a xylose-utilizing Saccharomyces cerevisiae strain”. In: *Microbial Cell Factories* 20.1 (2021), p. 114.

[56] Sekgetho C Mokwatlo et al. “Bioprocess development and scale-up for cis, cis-muconic acid production from glucose and xylose by Pseudomonas putida”. In: *Green Chemistry* 26.19 (2024), pp. 10152–10167.

[57] He Liu et al. “Engineering Pseudomonas putida for lignin bioconversion into cis-cis muconic acid”. In: *Chemical Engineering Journal* 495 (2024), p. 153375.

[58] Xiaowen Chen et al. “DMR (deacetylation and mechanical refining) processing of corn stover achieves high monomeric sugar concentrations (230 g L- 1) during enzymatic hydrolysis and high ethanol concentrations (> 10% v/v) during fermentation without hydrolysate purification or concentration”. In: *Energy & Environmental Science* 9.4 (2016), pp. 1237–1245.

[59] Arthur J. Ragauskas et al. “Lignin Valorization: Improving Lignin Processing in the Biorefinery”. In: *Science* 344.6185 (2014), p. 1246843.

[60] Byeongchan Ahn et al. “Integrated process design and analysis for co-production of biofuels with adipic acid and tetrahydrofuran”. In: *Industrial Crops and Products* 200 (2023), p. 116830.

[61] Nobuji Yoshikawa et al. “Microbial production of cis, cis-muconic acid”. In: *Journal of biotechnology* 14.2 (1990), pp. 203–210.

[62] Chun-Ming Wu et al. “Microbial synthesis of cis, cis-muconic acid from benzoate by Sphingobacterium sp. mutants”. In: *Biochemical engineering journal* 29.1-2 (2006), pp. 35–40.

[63] chemanalyst. *Sodium Benzoate Prices, News, Monitor, Analysis & Demand*. 2025. URL: https://www.chemanalyst.com/Pricing-data/sodium-benzoate-1185 (visited on 01/10/2025).

[64] Robert S Nelson et al. “Muconic acid production from algae hydrolysate as a high-value coproduct of an algae biorefinery”. In: *Algal Research* 75 (2023), p. 103300.

[65] Komakazu Gomi and Sadayuki Horiguchi. “Purification and Characterization of Pyrocatechase from the Catechol-assimilating Yeast Candida maltosa”. In: *Agricultural and biological chemistry* 52.2 (1988), pp. 585–587.

[66] Haoran Zhang et al. “Engineering E. coli–E. coli cocultures for production of muconic acid from glycerol”. In: *Microbial cell factories* 14 (2015), pp. 1–10.

[67] Calvin A Henard et al. “Muconic acid production from methane using rationally-engineered methanotrophic biocatalysts”. In: *Green Chemistry* 21.24 (2019), pp. 6731–6737.

[68] Ryan Davis et al. *Process design and economics for the conversion of lignocellulosic biomass to hydrocarbons: dilute-acid and enzymatic deconstruction of biomass to sugars and biological conversion of sugars to hydrocarbons*. Tech. rep. National Renewable Energy Lab.(NREL), Golden, CO (United States), 2013.

[69] chemanalyst. *Benzoic Acid Prices, News, Monitor, Analysis & Demand — chemanalyst.com*. https://www.chemanalyst.com/Pricing-data/benzoic-acid-1146. [Accessed 28-01-2025]. 2025.

[70] Mike. *Glycerol price index - businessanalytiq — businessanalytiq.com*. https://businessanalytiq.com/procurementanalytics/index/glycerol-price-index/. [Accessed 28-01-2025]. 2025.

[71] EIA. *United States Natural Gas Industrial Price (Dollars per Thousand Cubic Feet) — eia.gov*. https://www.eia.gov/dnav/ng/hist/n3035us3m.htm. [Accessed 28-01-2025]. 2025.

[72] Thomas J Schwartz et al. “Bridging the chemical and biological catalysis gap: challenges and outlooks for producing sustainable chemicals”. In: *Acs Catalysis* 4.6 (2014), pp. 2060–2069.

[73] Derek R Vardon et al. “cis, cis-Muconic acid: separation and catalysis to bio-adipic acid for nylon-6, 6 polymerization”. In: *Green Chemistry* 18.11 (2016), pp. 3397–3413.

[74] George Mwangi and Gbekeloluwa Oguntimein. “Study of an activated carbon system for the treatment of fermentation wastewater from a bioethanol production process”. In: *West Indian Journal of Engineering* (2013).

[75] Amy E Settle et al. “Enhanced catalyst durability for bio-based adipic acid production by atomic layer deposition”. In: *Joule* 3.9 (2019), pp. 2219–2240.

[76] Sofia Capelli et al. “Bio Adipic Acid Production from Sodium Muconate and Muconic Acid: A Comparison of Two Systems”. In: *ChemCatChem* 11.13 (2019), pp. 3075–3084.

[77] Lijuan Zhang et al. “A review of thermal catalytic and electrochemical hydrogenation approaches for converting biomass-derived compounds to high-value chemicals and fuels”. In: *Fuel Processing Technology* 226 (2022), p. 107097.

[78] Gayle J Bentley et al. “Engineering glucose metabolism for enhanced muconic acid production in Pseudomonas putida KT2440”. In: *Metabolic engineering* 59 (2020), pp. 64–75.

[79] Chen Ling et al. “Muconic acid production from glucose and xylose in Pseudomonas putida via evolution and metabolic engineering”. In: *Nature Communications* 13.1 (2022), p. 4925.

[80] Toray Industries, Inc. *Toray and PTT Global Chemical Agree to Explore Mass Production Technology to Build Supply Structure for Non-Edible Biomass-Derived Nylon*. 2024. URL: https://www.toray.com/global/news/article.html?contentId=x1tdy8vx (visited on 02/21/2025).

[81] Carl-Fredrik Lindberg et al. “Key performance indicators improve industrial performance”. In: *Energy procedia* 75 (2015), pp. 1785–1790.

[82] Volker H. Hoffmann and Timo Busch. “Corporate Carbon Performance Indicators”. In: *Journal of Industrial Ecology* 12.4 (2008), pp. 505–520.

[83] U.S. Environmental Protection Agency. *BACKGROUND REPORT,AP-42 SECTION 6.2, ADIPIC ACID PRODUCTION*. Report. Research Triangle Park, NC 27711: U.S. Environmental Protection Agency, 1994.

[84] Iris Vural-Gürsel et al. “Improving energy efficiency of process of direct adipic acid synthesis in flow using pinch analysis”. In: *Industrial & Engineering Chemistry Research* 52.23 (2013), pp. 7827–7835.

[85] E.A. Polman et al. *A follow-up study into the hydrogen quality requirements*. Tech. rep. Dutch Ministry of Economic Affairs and Climate Policy, 2023.

[86] Santanu Kumar Dash, Suprava Chakraborty, and Devaraj Elangovan. “A Brief Review of Hydrogen Production Methods and Their Challenges”. In: *Energies* 16.3 (2023). ISSN: 1996-1073. URL: https://www.mdpi.com/1996-1073/16/3/1141.

[87] Parnian Alikhani et al. “Marginal emission factors in power systems: The case of the Netherlands”. In: *12th International Conference on Smart Cities and Green ICT Systems, SMARTGREENS 2023*. SCITEPRESS. 2023, pp. 50–57.

[88] IPCC. *RENEWABLE ENERGY SOURCES*.

[89] FW Winn. “New relative volatility method for distillation calculations”. In: *Petrol. Refin* 37.5 (1958), pp. 216–218.

[90] S. Jooria, L. Wong Sak Hoi, and K. T. K. F Kong Win Chang. *Power consumption of batch v/s continuous centrifugals*. 2002. (Visited on 06/19/2025).

[91] BMA. *Südzucker – a long-term partner in the development of BMA centrifugals*. 2025. URL: https://www.bma-america.us/news-1-1/news/detail?cHash=a270c0ed0bc1b0b768b4002e42c529c5&tx_news_pi1%5Baction%5D=detail&tx_news_pi1%5Bcontroller%5D=News&tx_news_pi1%5Bnews%5D=2993 (visited on 06/19/2025).

[92] Tsukishima Kikai. *Fully Automatic Batch type Centrifugal*. 2025. (Visited on 06/19/2025).

[93] P Marchal et al. “Crystallization and precipitation engineering—I. An efficient method for solving population balance in crystallization with agglomeration”. In: *Chemical Engineering Science* 43.1 (1988), pp. 59–67.

[94] Samantha LY Tang, Richard L Smith, and Martyn Poliakoff. “Principles of green chemistry: PRODUCTIVELY”. In: *Green Chemistry* 7.11 (2005), pp. 761–762.

[95] Ajay Kumar Ray. *Coulson and Richardson’s Chemical Engineering*. Oxford, UK: Butterworth-Heinemann, Elsevier, 2023.

[96] chemengonline. *The Chemical Engineering Plant Cost Index*. 2025. URL: https://www.chemengonline.com/pci-home (visited on 03/10/2025).

[97] Georg A Buchner et al. “Techno-economic assessment framework for the chemical industry—based on technology readiness levels”. In: *Industrial & Engineering Chemistry Research* 57.25 (2018), pp. 8502–8517.

[98] Oxford University Press. *Oxford English Dictionary*. Accessed: 2025-02-25. 2025. URL: https://www.oed.com/.

[99] purchasing.com. *Air Compressor Comparisons; Purchasing*. 2025. URL: https://www.purchasing.com/construction-equipment/air-compressors/air-compressor-comparison/index.html (visited on 06/25/2025).

[100] Adrián García, Pablo Marín, and Salvador Ordóñez. “Hydrogenation of liquid organic hydrogen carriers: Process scale-up, economic analysis and optimization”. In: *International Journal of Hydrogen Energy* 52 (2024), pp. 1113–1123.

[101] Bloom Tech. *Cyclohexanol Liquid CAS 108-93-0*. 2025. URL: https://www.bloomtechz.com/basic-chemicals/raw-materials/cyclohexanol-liquid-cas-108-93-0.html (visited on 06/25/2025).

[102] Emanuele Taibi et al. *Green hydrogen cost reduction*. Tech. rep. International Renewable Energy Agency, 2020.

[103] Minsu Kim et al. "Techno-economic analysis of anion exchange membrane electrolysis process for green hydrogen production under uncertainty". In: *Energy Conversion and Management* 302 (2024), p. 118134.

[104] Sahil R Shah, Natasha C Wright, Patrick A Nepsky, et al. "Cost-optimal design of a batch electrodialysis system for domestic desalination of brackish groundwater". In: *Desalination* 443 (2018), pp. 198–211.

[105] Ionomr Innovations Inc. *Hydrogen Production Cost by AEM Water Electrolysis*. Tech. rep. Ionomr Innovations Inc., 2020.

[106] Richard Turton et al. *Analysis, synthesis and design of chemical processes*. Pearson Education, 2008.

[107] business analytiq. *Benzene price index*. 2025. URL: https://businessanalytiq.com/procurementanalytics/index/benzene-price-index/ (visited on 03/12/2025).

[108] European Hydrogen Observatory. *Cost of hydrogen production*. 2025. URL: https://observatory.clean-hydrogen.europa.eu/index.php/hydrogen-landscape/production-trade-and-cost/cost-hydrogen-production (visited on 03/12/2025).

[109] Waternet. *Tap water rates for homes with a water meter*. 2025. URL: https://www.waternet.nl/en/service-and-contact/tap-water/costs/rates-with-a-water-meter/ (visited on 03/12/2025).

[110] business analytiq. *Nitric Acid price index*. 2025. URL: https://businessanalytiq.com/procurementanalytics/index/nitric-acid-price-index/ (visited on 03/12/2025).

[111] business analytiq. *Potassium Hydroxide price index*. 2025. URL: https://businessanalytiq.com/procurementanalytics/index/potassium-hydroxide-price-index/ (visited on 03/12/2025).

[112] business analytiq. *Sulfuric acid price index*. 2025. URL: https://businessanalytiq.com/procurementanalytics/index/sulfuric-acid-price-index/ (visited on 03/12/2025).

[113] Mike. *Calcium Hydroxide price index*. 2025. URL: https://businessanalytiq.com/procurementanalytics/index/calcium-hydroxide-price-index/ (visited on 06/25/2025).

[114] IPCC. *emissions factor database*. 2025. URL: https://www.ipcc-nggip.iges.or.jp/efdb/find_ef.php?ipcc_code=2.A.2&ipcc_level=2 (visited on 06/25/2025).

[115] IEA ETSAP. *Industrial Combustion Boilers. Technology Brief I01 – May 2010*.

[116] B Neuffer, N Frank, and M Desai. "Available and emerging technologies for reducing greenhouse gas emissions from the nitric acid production industry". In: *Report of the Office of Air and Radiation, US Environmental Protection Agency, Research Triangle Park, NC* (2010).

[117] IMARC Group. *Adipic Acid Prices*. 2025. URL: https://www.imarcgroup.com/adipic-acid-pricing-report (visited on 06/19/2025).

[118] Business Analytiq. *Adipic Acid price index*. 2025. URL: https://businessanalytiq.com/procurementanalytics/index/adipic-acid-price-index/ (visited on 06/19/2025).

[119] Heike Mainhardt and Dina Kruger. "N2O emissions from adipic acid and nitric acid production". In: *IPCC good practice guidance and uncertainty management in national greenhouse gas inventories* (2001).

[120] Jesus Salavador Jaime-Ferrer et al. "Three-compartment bipolar membrane electrodialysis for splitting of sodium formate into formic acid and sodium hydroxide: Role of diffusion of molecular acid". In: *Journal of Membrane Science* 325.2 (2008), pp. 528–536.

[121] Matthias Bohnet. *Ullmann's encyclopedia of industrial chemistry*. Weinheim, Germany: Wiley-VCH, 2000.

A

Electrochemical Reactor Duty Calculations

Electrocatalytic Oxidation Duty

As discussed in Section 2.2.2, the electrical duty required for the ECO was calculated based on the work by Liu et al. [11] and modified to allow for a higher operating pressure. The calculation was setup to run automatically within Aspen Plus, however an example calculation is shown below.

$$Total\ current = (AA_{out} - AA_{in}) \times \frac{zC}{FE} \tag{A.1}$$

$$Total\ current = (25mol/s - 0.3mol/s) \times \frac{6 * 96485}{0.82} = 17.4\ MA \tag{A.2}$$

$$Total\ duty = Total\ current \times Cell\ voltage \tag{A.3}$$

$$Total\ duty = 17.4\ MA \times (1.76V + 0.05V) = 32\ MW \tag{A.4}$$

Electrochemical hydrogenation

The electrical duty required for the ECH was calculated based on the work by Dell'Anna et al. [19]. Similarly to ECO, the calculation was setup to run automatically within Aspen Plus, however an example calculation is shown below.

$$Total\ current = (25mol/s - 0mol/s) \times \frac{2 * 96485}{0.4} = 12.0\ MA \tag{A.5}$$

$$Total\ duty = 12.0\ MA \times (5.7V) = 69\ MW \tag{A.6}$$

B

Techno-economic results

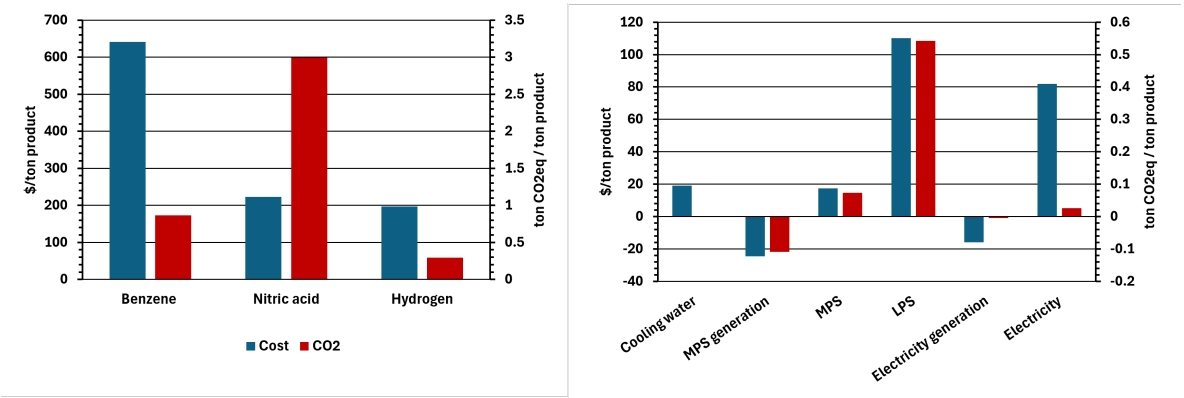

Figure B.1: Conventional AA feedstock and utility cost breakdown

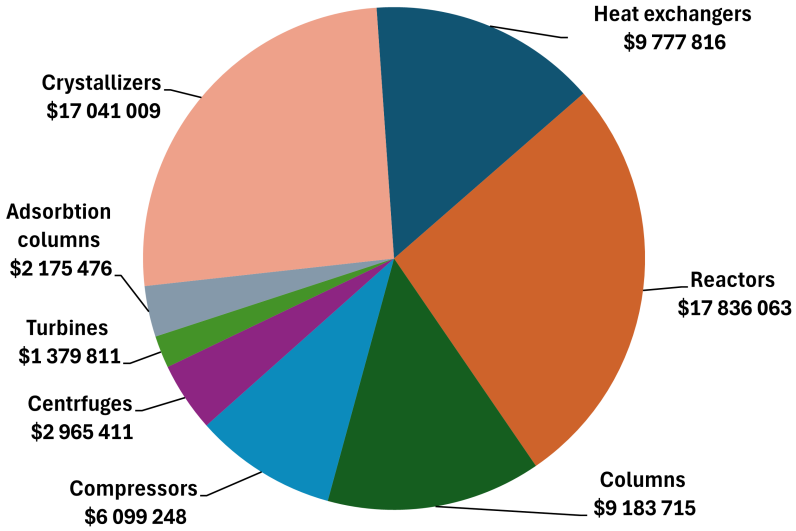

Figure B.2: Conventional AA CAPEX cost breakdown

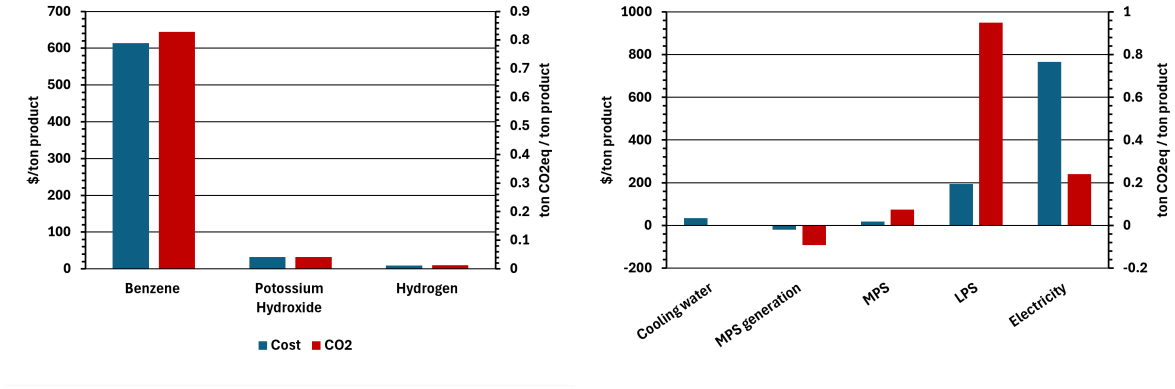

Figure B.3: ECO AA feedstock and utility cost breakdown

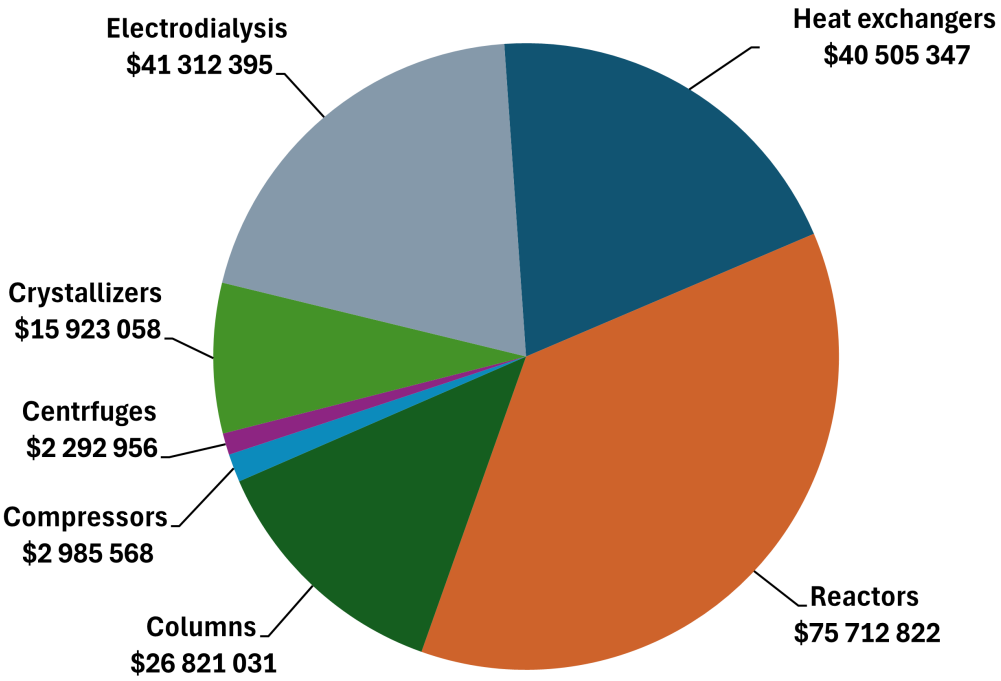

Figure B.4: ECO AA CAPEX cost breakdown

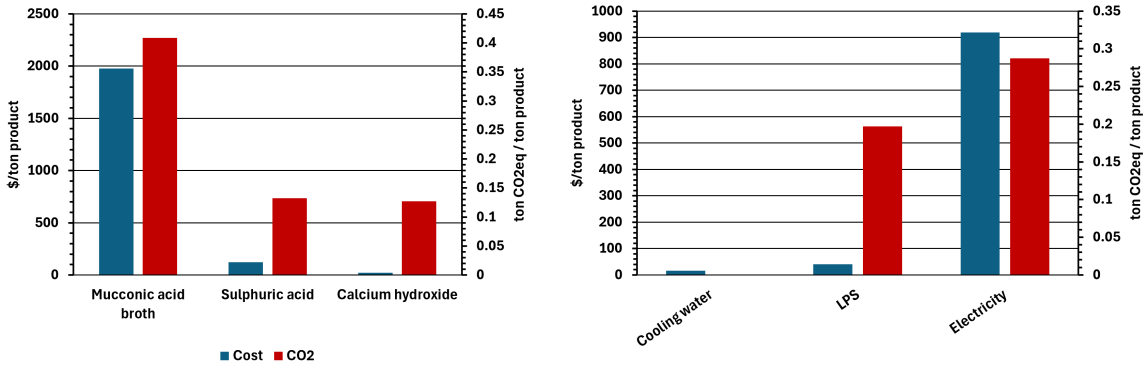

Figure B.5: Biomass based t3HDA feedstock and utility cost breakdown

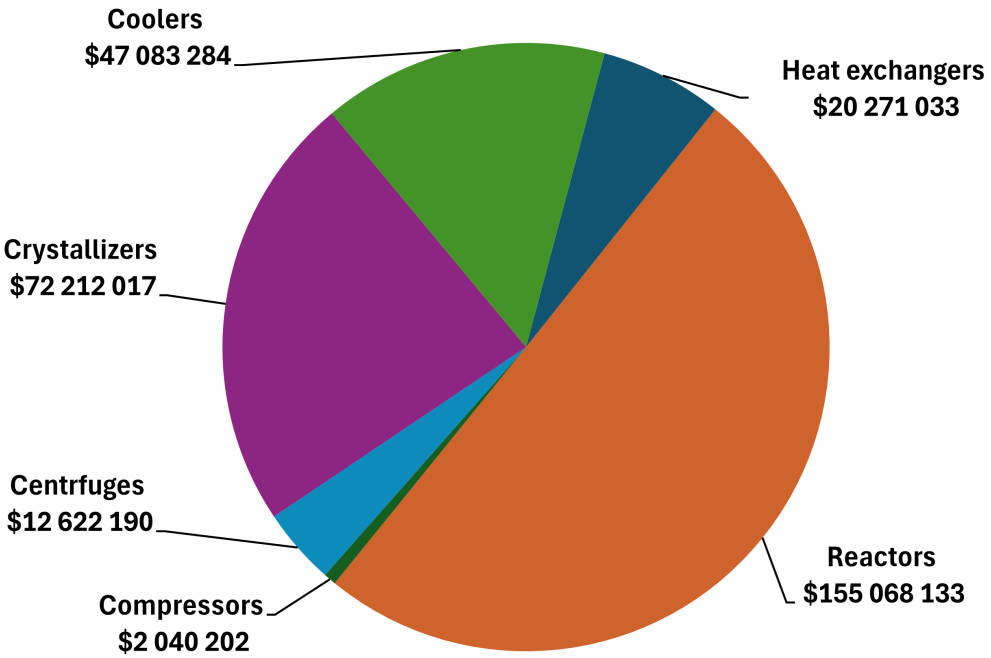

Figure B.6: Biomass based t3HDA CAPEX cost breakdown

C

Stream Results

C.1. Conventional Process Stream Results

Name	-	01-02	01-03	01-04	01-05	01-06	2-0	02-01	02-02	02-03	02-04
Temperature	(°C)	641	185	35	35	35	35	128	128	128	40
Pressure	(bar)	50	50	50	50	50	50	15	15	15	15
Liquid fraction	-	0	0	0	0	0	1	1	0.99	1	1
Vapor fraction	-	1	1	1	1	1	0	0	0.01	0	0
Solid fraction	-	0	0	0	0	0	0	0	0	0	0
Mass flow	(kg/h)	10336	10336	856	848	9	9480	54423	51739	2683	51739
H2	(kg/h)	669.7	669.7	669.7	663	6.7	0	0	0	0	0
N2	(kg/h)	0	0	0	0	0	0	985.1	985.1	0	985.1
O2	(kg/h)	0	0	0	0	0	0	393	393	0	393
AR	(kg/h)	43.2	43.2	40.1	39.7	0.4	3.1	18.9	18.9	0	18.9
CO2	(kg/h)	0	0	0	0	0	0	222.9	222.9	0	222.9
N2O	(kg/h)	0	0	0	0	0	0	0	0	0	0
NO2	(kg/h)	0	0	0	0	0	0	0	0	0	0
NO	(kg/h)	0	0	0	0	0	0	0	0	0	0
H2O	(kg/h)	0	0	0	0	0	0	2289.1	2289.1	0	2289.1
HNO3	(kg/h)	0	0	0	0	0	0	0	0	0	0
BEN	(kg/h)	0	0	0	0	0	0	0	0	0	0
TOLUENE	(kg/h)	0	0	0	0	0	0	0	0	0	0
ANE	(kg/h)	9613.1	9613.1	146.4	144.9	1.5	9466.7	37447.6	37447.6	0	37447.6
MTHYLANE	(kg/h)	9.9	9.9	0.1	0.1	0	9.8	132	132	0	132
CXPROX	(kg/h)	0	0	0	0	0	0	9437.5	9437.5	0	9437.5
CHA	(kg/h)	0	0	0	0	0	0	182.7	182.7	0	182.7
CHN	(kg/h)	0	0	0	0	0	0	630.6	630.6	0	630.6
GA	(kg/h)	0	0	0	0	0	0	2683.5	0	2683.5	0
AA	(kg/h)	0	0	0	0	0	0	0	0	0	0
AA(S)	(kg/h)	0	0	0	0	0	0	0	0	0	0
NO3-	(kg/h)	0	0	0	0	0	0	0	0	0	0
H3O+	(kg/h)	0	0	0	0	0	0	0	0	0	0
OH-	(kg/h)	0	0	0	0	0	0	0	0	0	0

Name	-	02-05	02-06	02-07	02-08	02-09	02-10	02-11	02-12	02-13	02-14	02-15	02-16	02-17
Temperature	(°C)	100	108	108	73	128	20	20	145	20	74	35	19	224
Pressure	(bar)	15	15	15	1	15	15	15	5	15	1	1	1	4
Liquid fraction	-	1	1	1	0	0	0	1	0.01	0	0	0.94	0.93	0
Vapor fraction	-	0	0	0	1	1	1	0	0.99	1	1	0.06	0.07	1
Solid fraction	-	0	0	0	0	0	0	0	0	0	0	0	0	0
Mass flow	(kg/h)	51739	49568	2172	40663	75637	25240	50398	561	24679	41223	41223	91621	28959
H2	(kg/h)	0	0	0	0	0	0	0	0	0	0	0	0	0
N2	(kg/h)	985.1	963.1	22	963.1	25746.8	21862.4	3884.3	0	21862.4	963.1	963.1	4847.7	21884.1
O2	(kg/h)	393	386.1	6.9	386.1	2593.7	1497.4	1096.3	0	1497.4	386.1	386.1	1482.5	6703.7
AR	(kg/h)	18.9	18.4	0.5	18.4	470.8	374.1	96.7	0	374.1	18.4	18.4	115.1	371.5
CO2	(kg/h)	222.9	218	4.9	218	2337.4	889	1448.4	0	889	218	218	1666.4	0
N2O	(kg/h)	0	0	0	0	0	0	0	0	0	0	0	0	0
NO2	(kg/h)	0	0	0	0	0	0	0	0	0	0	0	0	0
NO	(kg/h)	0	0	0	0	0	0	0	0	0	0	0	0	0
H2O	(kg/h)	3569.8	1584	1985.8	1584	4585.4	26.8	4558.6	0	26.8	1584	1584	6142.7	0
HNO3	(kg/h)	0	0	0	0	0	0	0	0	0	0	0	0	0
BEN	(kg/h)	0	0	0	0	0	0	0	0	0	0	0	0	0
TOLUENE	(kg/h)	0	0	0	0	0	0	0	0	0	0	0	0	0
ANE	(kg/h)	36592.8	36592.3	0.5	36557.6	39477.2	589.6	38887.7	560.1	29.5	37117.6	37117.6	76005.3	0
MTHYLANE	(kg/h)	132	132	0	122.2	84.6	0.4	84.2	0.4	0	122.6	122.6	206.8	0
CXPROX	(kg/h)	0	0	0	0	231	0	231	0	0	0	0	231	0
CHA	(kg/h)	2217.1	2208.6	8.5	182.7	11	0	11	0	0	182.7	182.7	193.7	0
CHN	(kg/h)	7607.7	7465.2	142.5	630.6	99.2	0	99.2	0	0	630.6	630.6	729.8	0
GA	(kg/h)	0	0	0	0	0.3	0	0.3	0	0	0	0	0.3	0
AA	(kg/h)	0	0	0	0	0	0	0	0	0	0	0	0	0
AA(S)	(kg/h)	0	0	0	0	0	0	0	0	0	0	0	0	0
NO3-	(kg/h)	0	0	0	0	0	0	0	0	0	0	0	0	0
H3O+	(kg/h)	0	0	0	0	0	0	0	0	0	0	0	0	0
OH-	(kg/h)	0	0	0	0	0	0	0	0	0	0	0	0	0

Name	-	02-18	02-19	3-0	03-01	03-02	03-03	03-04	03-05	03-06	03-08	4-0	04-01	04-02
Temperature	(°C)	35	229	154	30	70	176	70	65	46	25	52	52	52
Pressure	(bar)	4	15	1	1	3	3	3	1	0.3	0.3	1	1	0.3
Liquid fraction	-	0	0	1	1	1	0	0	0	1	1	1	1	1
Vapor fraction	-	1	1	0	0	0	1	1	1	0	0	0	0	0
Solid fraction	-	0	0	0	0	0	0	0	0	0	0	0	0	0
Mass flow	(kg/h)	28959	28959	8905	8905	67336	7544	2443	12261	45216	45216	62620	62620	62620
H2	(kg/h)	0	0	0	0	0	0	0	0	0	0	0	0	0
N2	(kg/h)	21884.1	21884.1	0	0	0	5701.1	0	5619.6	32	32	81.5	81.5	81.5
O2	(kg/h)	6703.7	6703.7	0	0	0	1746.4	0	1656.7	24.8	24.8	89.8	89.8	89.8
AR	(kg/h)	371.5	371.5	0	0	0	96.8	0	94.7	1.3	1.3	2.1	2.1	2.1
CO2	(kg/h)	0	0	0	0	0	0	0	0	0	0	0	0	0
N2O	(kg/h)	0	0	0	0	541.8	0	2151.1	541.8	42.5	42.5	0	0	0
NO2	(kg/h)	0	0	0	0	2667	0	147.8	1974.8	15.8	15.8	0	0	0
NO	(kg/h)	0	0	0	0	0	0	0	150.5	0.4	0.4	0	0	0
H2O	(kg/h)	0	0	0	0	26271.2	0	78.1	1291.8	17766.1	17766.1	24889.1	21701.1	21699.5
HNO3	(kg/h)	0	0	0	0	24905.8	0	52.7	873.9	27169.1	27169.1	24664.1	13513.3	13508
BEN	(kg/h)	0	0	0	0	0	0	0	0	0	0	0	0	0
TOLUENE	(kg/h)	0	0	0	0	0	0	0	0	0	0	0	0	0
ANE	(kg/h)	0	0	34.7	34.7	23.9	0	10.8	23.9	11.5	11.5	0	0	0
MTHYLANE	(kg/h)	0	0	9.8	9.8	8.1	0	1.7	8.1	5.1	5.1	0	0	0
CXPROX	(kg/h)	0	0	0	0	0	0	0	0	0	0	0	0	0
CHA	(kg/h)	0	0	2025.9	2025.9	101	0	0.3	5.4	34.9	34.9	95.6	95.6	95.6
CHN	(kg/h)	0	0	6834.6	6834.6	340.8	0	1	18.1	72.7	72.7	322.7	322.7	322.7
GA	(kg/h)	0	0	0	0	0	0	0	0	0	0	0	0	0
AA	(kg/h)	0	0	0	0	12476.3	0	0.1	1.4	39.7	39.7	12474.8	12474.8	12474.8
AA(S)	(kg/h)	0	0	0	0	0	0	0	0	0	0	0	0	0
NO3-	(kg/h)	0	0	0	0	0	0	0	0	0	0	0	10972.5	10977.8
H3O+	(kg/h)	0	0	0	0	0	0	0	0	0	0	0	3366.3	3367.9
OH-	(kg/h)	0	0	0	0	0	0	0	0	0	0	0	0	0

Name	-	04-03	04-04	04-05	04-06	04-07	04-08	04-09	04-10	04-11	04-12	04-13	04-14	04-15
Temperature	(°C)	69	40	40	94	24	15	17	17	17	19	19	19	87
Pressure	(bar)	0.3	0.3	0.3	0.3	25	25	1	1	1	1	0.3	1	0.3
Liquid fraction	-	0	0	1	1	0.95	0.8	0.94	0.94	0.94	1	1	0	0
Vapor fraction	-	1	1	0	0	0	0	0	0	0	0	0	0	1
Solid fraction	-	0	0	0	0	0.05	0.2	0.06	0.06	0.06	0	0	1	0
Mass flow	(kg/h)	8855	215	8640	53764	617177	617177	617209	563412	53797	41722	41722	12074	37075
H2	(kg/h)	0	0	0	0	0	0	0	0	0	0	0	0	0
N2	(kg/h)	81.5	81.5	0	0	0	0	0	0	0	0	0	0	0
O2	(kg/h)	89.8	89.7	0	0	0	0	0	0	0	0	0	0	0
AR	(kg/h)	2.1	2	0.1	0	0	0	0	0	0	0	0	0	0
CO2	(kg/h)	0	0	0	0	0	0	0	0	0	0	0	0	0
N2O	(kg/h)	0	0	0	0	0	0	0	0	0	0	0	0	0
NO2	(kg/h)	0	0	0	0	0	0	0	0	0	0	0	0	0
NO	(kg/h)	0	0	0	0	0	0	0	0	0	0	0	0	0
H2O	(kg/h)	8258.5	34.1	8199.1	13441.1	159216.6	158679.9	158773.7	144936.4	13839.1	13849.5	13849.6	0	15090.8
HNO3	(kg/h)	88.6	0	0.1	13419.4	171465.1	169588.1	169914.9	155110.7	14810.6	14846.9	14847.1	0	21870.8
BEN	(kg/h)	0	0	0	0	0	0	0	0	0	0	0	0	0
TOLUENE	(kg/h)	0	0	0	0	0	0	0	0	0	0	0	0	0
ANE	(kg/h)	0	0	0	0	0	0	0	0	0	0	0	0	0
MTHYLANE	(kg/h)	0	0	0	0	0	0	0	0	0	0	0	0	0
CXPROX	(kg/h)	0	0	0	0	0	0	0	0	0	0	0	0	0
CHA	(kg/h)	66.2	3.4	62.8	29.4	337.4	337.4	337.4	308	29.4	29.4	29.4	0	27.2
CHN	(kg/h)	268.9	4.6	264.2	53.8	618	618	618	564.1	53.9	53.9	53.9	0	51.1
GA	(kg/h)	0	0	0	0	0	0	0	0	0	0	0	0	0
AA	(kg/h)	0	0	0	12474.8	16673.2	16673.2	4599.2	4198.3	400.9	400.9	400.9	0	35.1
AA(S)	(kg/h)	0	0	0	0	126455.3	126455.3	138529.7	126455.3	12074.5	0	0	12074.5	0
NO3-	(kg/h)	0	0	87	10977.8	108977.8	110824.9	110527.7	100888.1	9633.2	9597.5	9597.3	0	0
H3O+	(kg/h)	0	0	26.7	3367.9	33433.3	34000	33908.8	30951.5	2955.4	2944.4	2944.4	0	0
OH-	(kg/h)	0	0	0	0	0	0	0	0	0	0	0	0	0

Name	-	04-16	04-17	04-18	04-19	04-20	04-21	04-22	04-23	04-24	04-25	04-26	04-28	04-29
Temperature	(°C)	87	45	15	17	17	17	19	19	87	87	87	45	40
Pressure	(bar)	0.3	1	1	1	1	1	1	0.3	0.3	0.3	0.3	0.3	0.3
Liquid fraction	-	1	0.99	0.95	0.98	0.98	0.98	1	1	0	1	0	1	0
Vapor fraction	-	0	0	0	0	0	0	0	0	1	0	1	0	1
Solid fraction	-	0	0.01	0.05	0.02	0.02	0.02	0	0	0	0	0	0	0
Mass flow	(kg/h)	4648	13279	13279	13279	8631	4648	4318	4318	3855	464	40930	40930	215
H2	(kg/h)	0	0	0	0	0	0	0	0	0	0	0	0	0
N2	(kg/h)	0	0	0	0	0	0	0	0	0	0	0	0	81.5
O2	(kg/h)	0	0	0	0	0	0	0	0	0	0	0	0	89.7
AR	(kg/h)	0	0	0	0	0	0	0	0	0	0	0	0	2
CO2	(kg/h)	0	0	0	0	0	0	0	0	0	0	0	0	0
N2O	(kg/h)	0	0	0	0	0	0	0	0	0	0	0	0	0
NO2	(kg/h)	0	0	0	0	0	0	0	0	0	0	0	0	0
NO	(kg/h)	0	0	0	0	0	0	0	0	0	0	0	0	0
H2O	(kg/h)	1330.9	3680.9	3618.3	3621.8	2354.2	1267.6	1268.8	1268.8	1398.5	127.5	16489.3	13896.3	34.1
HNO3	(kg/h)	1973	5211.1	4992.3	5004.5	3252.9	1751.6	1755.8	1755.7	2448.3	207	24319.1	15249.4	0
BEN	(kg/h)	0	0	0	0	0	0	0	0	0	0	0	0	0
TOLUENE	(kg/h)	0	0	0	0	0	0	0	0	0	0	0	0	0
ANE	(kg/h)	0	0	0	0	0	0	0	0	0	0	0	0	0
MTHYLANE	(kg/h)	0	0	0	0	0	0	0	0	0	0	0	0	0
CXPROX	(kg/h)	0	0	0	0	0	0	0	0	0	0	0	0	0
CHA	(kg/h)	2.2	6.2	6.2	6.2	4	2.2	2.2	2.2	2	0.2	29.2	29.2	3.4
CHN	(kg/h)	2.8	8	8	8	5.2	2.8	2.8	2.8	2.7	0.2	53.7	53.7	4.6
GA	(kg/h)	0	0	0	0	0	0	0	0	0	0	0	0	0
AA	(kg/h)	365.8	434	434	104.9	68.2	36.7	36.7	36.7	3.2	33.5	38.2	38.2	0
AA(S)	(kg/h)	0	611.2	611.2	940.3	611.2	329.1	0	0	0	0	0	0	0
NO3-	(kg/h)	744.4	2546.1	2761.4	2749.4	1787.1	962.3	958.2	958.2	0	73.1	0	8924.6	0
H3O+	(kg/h)	228.4	781.1	847.2	843.5	548.3	295.2	294	294	0	22.4	0	2738	0
OH-	(kg/h)	0	0	0	0	0	0	0	0	0	0	0	0	0

Name	-	04-30	4-31	4-32	4-33	4-34	4-35	4-36	4-37	4-38	4-39	4-40	4-41	4-42
Temperature	(°C)	199	45	19	23	94	99	99	50	19	15	17	17	17
Pressure	(bar)	1	0.3	1	1	1	1	1	1	1	1	1	1	1
Liquid fraction	-	0	1	0	0.34	0.34	0.34	1	1	0.37	0.37	0.81	0.35	0.35
Vapor fraction	-	1	0	0	0	0	0	0	0	0	0	0	0	0
Solid fraction	-	0	0	1	0.66	0.66	0.66	0	0	0.63	0.63	0.19	0.65	0.65
Mass flow	(kg/h)	215	40930	329	18667	18667	18667	18667	18667	531190	531190	531152	512523	18629
H2	(kg/h)	0	0	0	0	0	0	0	0	0	0	0	0	0
N2	(kg/h)	81.5	0	0	0	0	0	0	0	0	0	0	0	0
O2	(kg/h)	89.7	0	0	0	0	0	0	0	0	0	0	0	0
AR	(kg/h)	2	0	0	0	0	0	0	0	0	0	0	0	0
CO2	(kg/h)	0	0	0	0	0	0	0	0	0	0	0	0	0
N2O	(kg/h)	0	0	0	0	0	0	0	0	0	0	0	0	0
NO2	(kg/h)	0	0	0	0	0	0	0	0	0	0	0	0	0
NO	(kg/h)	0	0	0	0	0	0	0	0	0	0	0	0	0
H2O	(kg/h)	34.1	16489.3	0	6263.8	6263.8	6263.8	6263.8	6263.8	178396.2	178396.2	178389	172132.4	6256.6
HNO3	(kg/h)	0	24319.1	0	0	0	0	0	0	0	0	0	0	0
BEN	(kg/h)	0	0	0	0	0	0	0	0	0	0	0	0	0
TOLUENE	(kg/h)	0	0	0	0	0	0	0	0	0	0	0	0	0
ANE	(kg/h)	0	0	0	0	0	0	0	0	0	0	0	0	0
MTHYLANE	(kg/h)	0	0	0	0	0	0	0	0	0	0	0	0	0
CXPROX	(kg/h)	0	0	0	0	0	0	0	0	0	0	0	0	0
CHA	(kg/h)	3.4	29.2	0	0	0	0	0	0	0	0	0	0	0
CHN	(kg/h)	4.6	53.7	0	0	0	0	0	0	0	0	0	0	0
GA	(kg/h)	0	0	0	0	0	0	0	0	0	0	0	0	0
AA	(kg/h)	0	38.2	0	0	0	0	12403.6	12403.6	17392.5	17392.5	5170.2	4988.9	181.3
AA(S)	(kg/h)	0	0	329.1	12403.6	12403.6	12403.6	0	0	335401.6	335401.6	347592.6	335401.6	12191
NO3-	(kg/h)	0	0	0	0	0	0	0	0	0	0	0	0	0
H3O+	(kg/h)	0	0	0	0	0	0	0	0	0	0	0	0	0
OH-	(kg/h)	0	0	0	0	0	0	0	0	0	0	0	0	0

Name	-	4-43	4-44	4-45	5-0	05-01	05-02	05-03	05-04	05-05	05-06	05-07	05-08	05-09
Temperature	(°C)	18	18	29	66	576	217	35	60	58	20	20	20	566
Pressure	(bar)	1	1	1	1	30	30	30	30	30	30	30	30	30
Liquid fraction	-	1	0	1	0	0	0	0.3	1	0	0	1	0	0
Vapor fraction	-	0	0	0	1	1	1	0.7	0	1	1	0	1	1
Solid fraction	-	0	1	0	0	0	0	0	0	0	0	0	0	0
Mass flow	(kg/h)	6438	12191	6438	14704	14704	14704	14704	4286	10647	10647	42	10605	10605
H2	(kg/h)	0	0	0	0	0	0	0	0	0	0	0	0	0
N2	(kg/h)	0	0	0	5619.6	5619.6	5619.6	5619.6	32	5589.1	5589.1	1.4	5587.6	5587.6
O2	(kg/h)	0	0	0	1656.7	1656.7	1656.7	1656.7	24.8	1633.2	1633.2	1.3	1631.9	1631.9
AR	(kg/h)	0	0	0	94.7	94.7	94.7	94.7	1.3	93.5	93.5	0	93.4	93.4
CO2	(kg/h)	0	0	0	0	0	0	0	0	0	0	0	0	0
N2O	(kg/h)	0	0	0	2692.9	2692.9	2692.9	2692.9	42.5	2650.6	2650.6	0.3	2650.4	2650.4
NO2	(kg/h)	0	0	0	2122.5	2122.5	2122.5	2122.5	15.8	0.1	0.1	0	0.1	0.1
NO	(kg/h)	0	0	0	150.5	150.5	150.5	150.5	0.4	608.2	608.2	0.1	608.1	608.1
H2O	(kg/h)	6256.6	0	6256.6	1369.8	1369.8	1369.8	1369.8	1276.8	43.5	43.5	37.7	5.9	5.9
HNO3	(kg/h)	0	0	0	926.5	926.5	926.5	926.5	2850	0.9	0.9	0.9	0.1	0.1
BEN	(kg/h)	0	0	0	0	0	0	0	0	0	0	0	0	0
TOLUENE	(kg/h)	0	0	0	0	0	0	0	0	0	0	0	0	0
ANE	(kg/h)	0	0	0	34.7	34.7	34.7	34.7	11.5	23.3	23.3	0.1	23.3	23.3
MTHYLANE	(kg/h)	0	0	0	9.8	9.8	9.8	9.8	5.1	4.8	4.8	0	4.7	4.7
CXPROX	(kg/h)	0	0	0	0	0	0	0	0	0	0	0	0	0
CHA	(kg/h)	0	0	0	5.7	5.7	5.7	5.7	5.7	0	0	0	0	0
CHN	(kg/h)	0	0	0	19	19	19	19	19	0.1	0.1	0.1	0	0
GA	(kg/h)	0	0	0	0	0	0	0	0	0	0	0	0	0
AA	(kg/h)	181.3	0	181.3	1.5	1.5	1.5	1.5	1.5	0	0	0	0	0
AA(S)	(kg/h)	0	12191	0	0	0	0	0	0	0	0	0	0	0
NO3-	(kg/h)	0	0	0	0	0	0	0	0	0	0	0	0	0
H3O+	(kg/h)	0	0	0	0	0	0	0	0	0	0	0	0	0
OH-	(kg/h)	0	0	0	0	0	0	0	0	0	0	0	0	0

Name	-	05-10	05-11	05-12	05-13	05-14	05-15	AIR-IN	AIR-IN-2	BEN-IN	H2-IN	H2O-IN2	H20-IN	HNO3-IN
Temperature	(°C)	570	804	800	280	616	192	25	25	25	210	25	25	25
Pressure	(bar)	30	30	30	30	30	1	1	1	50	50	1	30	1
Liquid fraction	-	0	0	0	0	0	0	0	0	1	0	1	1	1
Vapor fraction	-	1	1	1	1	1	1	1	1	0	1	0	0	0
Solid fraction	-	0	0	0	0	0	0	0	0	0	0	0	0	0
Mass flow	(kg/h)	10605	10605	10605	10605	10605	10605	28959	7544	8797	691	6264	188	60874
H2	(kg/h)	0	0	0	0	0	0	0	0	0	687.7	0	0	0
N2	(kg/h)	5587.6	6566	6566	6566	7558.4	7558.4	21884.1	5701.1	0	0	0	0	0
O2	(kg/h)	1631.9	2190.7	2190.7	2190.7	2919.6	2919.6	6703.7	1746.4	0	0	0	0	0
AR	(kg/h)	93.4	93.4	93.4	93.4	93.4	93.4	371.5	96.8	0	3.5	0	0	0
CO2	(kg/h)	0	0	0	0	0	0	0	0	0	0	0	0	0
N2O	(kg/h)	2650.4	1113.3	1113.3	1113.3	0	0	0	0	0	0	0	0	0
NO2	(kg/h)	0.1	0.1	0.1	0.1	0.1	0.1	0	0	0	0	0	0	0
NO	(kg/h)	608.1	608.1	608.1	608.1	0	0	0	0	0	0	0	0	0
H2O	(kg/h)	5.9	5.9	5.9	5.9	5.9	5.9	0	0	0	0	6263.8	187.8	24349.7
HNO3	(kg/h)	0.1	0	0	0	0	0	0	0	0	0	0	0	36524.6
BEN	(kg/h)	0	0	0	0	0	0	0	0	8787.8	0	0	0	0
TOLUENE	(kg/h)	0	0	0	0	0	0	0	0	9.2	0	0	0	0
ANE	(kg/h)	23.3	23.3	23.3	23.3	23.3	23.3	0	0	0	0	0	0	0
MTHYLANE	(kg/h)	4.7	4.7	4.7	4.7	4.7	4.7	0	0	0	0	0	0	0
CXPROX	(kg/h)	0	0	0	0	0	0	0	0	0	0	0	0	0
CHA	(kg/h)	0	0	0	0	0	0	0	0	0	0	0	0	0
CHN	(kg/h)	0	0	0	0	0	0	0	0	0	0	0	0	0
GA	(kg/h)	0	0	0	0	0	0	0	0	0	0	0	0	0
AA	(kg/h)	0	0	0	0	0	0	0	0	0	0	0	0	0
AA(S)	(kg/h)	0	0	0	0	0	0	0	0	0	0	0	0	0
NO3-	(kg/h)	0	0	0	0	0	0	0	0	0	0	0	0	0
H3O+	(kg/h)	0	0	0	0	0	0	0	0	0	0	0	0	0
OH-	(kg/h)	0	0	0	0	0	0	0	0	0	0	0	0	0

C.2. Electrochemical approach Process Stream Results

Name	-	3-0	03-01	03-02	03-03	03-04	03-05	03-06	03-07	03-08
Temperature	(°C)	96	25	85	44	25	113	113	113	164
Pressure	(bar)	1	1	1	1	1	50	50	50	20
Liquid fraction	-	0.92	1	1	1	1	1	1	1	1
Vapor fraction	-	0.08	0	0	0	0	0	0	0	0
Solid fraction	-	0	0	0	0	0	0	0	0	0
Mass flow	(kg/h)	11089	11089	82990	268217	268217	267177	13033	254144	254144
H2	(kg/h)	0	0	0	0	0	0.1	0	0.1	0.1
N2	(kg/h)	27.4	27.4	28.4	28.4	28.4	13.4	0	13.4	13.4
O2	(kg/h)	8.4	8.4	32.9	32.9	32.9	141.7	0	141.7	141.7
AR	(kg/h)	0.5	0.5	0.5	0.5	0.5	0.3	0	0.3	0.3
CO2	(kg/h)	4.3	4.3	42.3	42.3	42.3	191.8	0	191.8	191.8
H2O	(kg/h)	1988	1988	73199.3	244527.5	244527.5	238996.8	0	238996.8	238996.8
BEN	(kg/h)	0	0	0	0	0	0	0	0	0
TOLUENE	(kg/h)	0	0	0	0	0	0	0	0	0
ANE	(kg/h)	35.5	35.5	35.5	35.5	35.5	0	0	0	0
MTHYLANE	(kg/h)	9.8	9.8	9.8	9.8	9.8	0.4	0	0.4	0.4
CXPROX	(kg/h)	0	0	0	0	0	0	0	0	0
CHA	(kg/h)	2035.1	2035.1	2035.1	2035.1	2035.1	0	0	0	0
CHN	(kg/h)	6979.6	6979.6	7605.9	7609	7609	646.3	0	646.3	646.3
GA	(kg/h)	0	0	0	2.2	2.2	422.8	0	422.8	422.8
AA	(kg/h)	0	0	0	174.8	174.8	13044.5	0	13044.5	13044.5
AA(S)	(kg/h)	0	0	0	0	0	0	0	0	0
KOH	(kg/h)	0	0	0	13719.4	13719.4	13719.4	13033.4	686	686

Name	-	03-10	03-11	03-12	03-13	03-14	03-16	03-17	03-18	4-0	04-01	04-02	04-03	04-04
Temperature	(°C)	113	113	113	45	45	100	25	80	164	100	100	94	94
Pressure	(bar)	50	50	50	50	50	1	1	1	20	1	1	0.8	0.8
Liquid fraction	-	0	0.19	0	0	1	0.94	1	1	1	1	0	0.99	1
Vapor fraction	-	1	0.81	1	1	0	0.06	0	0	0	0	1	0.01	0
Solid fraction	-	0	0	0	0	0	0	0	0	0	0	0	0	0
Mass flow	(kg/h)	1040	232	808	661	147	184545	184545	184545	254291	180432	73859	180432	107015
H2	(kg/h)	648.6	0	648.6	648.6	0	0	0	0	0.1	0	0.1	0	0
N2	(kg/h)	15	15	0	0	0	0	0	0	13.4	0	13.4	0	0
O2	(kg/h)	61	61	0	0	0	0	0	0	141.7	0	141.7	0	0
AR	(kg/h)	0.2	0.2	0	0	0	0	0	0	0.3	0	0.3	0	0
CO2	(kg/h)	101.8	101.8	0	0	0	0	0	0	191.8	0	191.8	0	0
H2O	(kg/h)	202.3	43.1	159.2	12.3	146.9	171328.1	171328.1	171328.1	239143.7	166275.8	72868	166275.8	92861
BEN	(kg/h)	0	0	0	0	0	0	0	0	0	0	0	0	0
TOLUENE	(kg/h)	0	0	0	0	0	0	0	0	0	0	0	0	0
ANE	(kg/h)	0	0	0	0	0	0	0	0	0	0	0	0	0
MTHYLANE	(kg/h)	9.4	9.4	0	0	0	0	0	0	0.4	0	0.4	0	0
CXPROX	(kg/h)	0	0	0	0	0	0	0	0	0	0	0	0	0
CHA	(kg/h)	0	0	0	0	0	0	0	0	0	0	0	0	0
CHN	(kg/h)	1.6	1.6	0	0	0	3.1	3.1	3.1	646.3	3.2	643.1	3.2	1
GA	(kg/h)	0	0	0	0	0	2.2	2.2	2.2	422.8	422.8	0	422.8	422.7
AA	(kg/h)	0	0	0	0	0	174.8	174.8	174.8	13044.5	13044.5	0	13044.5	13044.4
AA(S)	(kg/h)	0	0	0	0	0	0	0	0	0	0	0	0	0
KOH	(kg/h)	0	0	0	0	0	13036.8	13036.8	13036.8	686	686	0	686	686

Name	-	04-05	04-06	04-07	04-08	04-09	04-10	04-11	04-12	04-13	04-14	04-15	04-16	04-17
Temperature	(°C)	94	97	86	88	94	88	24	15	17	17	17	18	18
Pressure	(bar)	0.8	1	0.6	0.6	0.8	0.6	0.6	0.6	1	1	1	1	1
Liquid fraction	-	0	0.97	0.99	1	1	0	0.65	0.65	0.62	0.62	0.62	1	0.01
Vapor fraction	-	1	0.03	0.01	0	0	1	0	0	0	0	0	0	0
Solid fraction	-	0	0	0	0	0	0	0.35	0.35	0.38	0.38	0.38	0	0.99
Mass flow	(kg/h)	73417	73859	107015	32784	73417	74231	397671	397671	397683	364887	32796	20177	12619
H2	(kg/h)	0	0.1	0	0	0	0	0	0	0	0	0	0	0
N2	(kg/h)	0	13.4	0	0	0	0	0	0	0	0	0	0	0
O2	(kg/h)	0	141.7	0	0	0	0	0	0	0	0	0	0	0
AR	(kg/h)	0	0.3	0	0	0	0	0	0	0	0	0	0	0
CO2	(kg/h)	0	191.8	0	0	0	0	0	0	0	0	0	0	0
H2O	(kg/h)	73414.7	72868	92861	18631.6	73414.7	74229.4	225905	225905	225903.1	207273.4	18629.7	18536.5	93.1
BEN	(kg/h)	0	0	0	0	0	0	0	0	0	0	0	0	0
TOLUENE	(kg/h)	0	0	0	0	0	0	0	0	0	0	0	0	0
ANE	(kg/h)	0	0	0	0	0	0	0	0	0	0	0	0	0
MTHYLANE	(kg/h)	0	0.4	0	0	0	0	0	0	0	0	0	0	0
CXPROX	(kg/h)	0	0	0	0	0	0	0	0	0	0	0	0	0
CHA	(kg/h)	0	0	0	0	0	0	0	0	0	0	0	0	0
CHN	(kg/h)	2.3	643.1	1	0.1	2.3	0.8	1.3	1.3	1.3	1.2	0.1	0.1	0
GA	(kg/h)	0	0	422.7	422.7	0	0.1	5129.7	5129.7	5130.1	4707	423.1	421	2.1
AA	(kg/h)	0.1	0	13044.4	13044	0.1	0.3	19035	19035	6529.4	5991	538.5	535.8	2.7
AA(S)	(kg/h)	0	0	0	0	0	0	139274.7	139274.7	151792.7	139274.7	12518	0	12518
KOH	(kg/h)	0	0	686	686	0	0	8325.6	8325.6	8326.3	7639.6	686.6	683.2	3.4

Name	-	04-18	04-20	04-21	04-22	04-23	04-24	04-25	04-26	04-27	04-28	04-29	04-30	4-31
Temperature	(°C)	18	77	86	77	58	15	17	17	17	18	18	76	76
Pressure	(bar)	0.395	0.395	0.6	0.395	0.395	0.395	1	1	1	1	1	0.395	0.395
Liquid fraction	-	1	1	0.21	0	0.98	0.98	0.95	0.95	0.95	1	0	0.17	1
Vapor fraction	-	0	0	0.79	1	0	0	0	0	0	0	0	0.83	0
Solid fraction	-	0	0	0	0	0.02	0.02	0.05	0.05	0.05	0	1	0	0
Mass flow	(kg/h)	20177	6961	74231	13216	10396	10396	10395	3435	6960	6578	382	87446	87446
H2	(kg/h)	0	0	0	0	0	0	0	0	0	0	0	0	0
N2	(kg/h)	0	0	0	0	0	0	0	0	0	0	0	0	0
O2	(kg/h)	0	0	0	0	0	0	0	0	0	0	0	0	0
AR	(kg/h)	0	0	0	0	0	0	0	0	0	0	0	0	0
CO2	(kg/h)	0	0	0	0	0	0	0	0	0	0	0	0	0
H2O	(kg/h)	18536.5	5321	74229.4	13215.5	7946.5	7946.5	7945.9	2625.5	5320.3	5320.3	0	87445	87445
BEN	(kg/h)	0	0	0	0	0	0	0	0	0	0	0	0	0
TOLUENE	(kg/h)	0	0	0	0	0	0	0	0	0	0	0	0	0
ANE	(kg/h)	0	0	0	0	0	0	0	0	0	0	0	0	0
MTHYLANE	(kg/h)	0	0	0	0	0	0	0	0	0	0	0	0	0
CXPROX	(kg/h)	0	0	0	0	0	0	0	0	0	0	0	0	0
CHA	(kg/h)	0	0	0	0	0	0	0	0	0	0	0	0	0
CHN	(kg/h)	0.1	0	0.8	0.1	0	0	0	0	0	0	0	0.9	0.9
GA	(kg/h)	421	420.9	0.1	0	628.6	628.6	628.6	207.7	420.9	420.9	0	0.1	0.1
AA	(kg/h)	535.8	535.8	0.3	0	611.7	611.7	229.7	75.9	153.8	153.8	0	0.4	0.4
AA(S)	(kg/h)	0	0	0	0	188.5	188.5	570.4	188.5	382	0	382	0	0
KOH	(kg/h)	683.2	683.2	0	0	1020.4	1020.4	1020.3	337.1	683.2	683.2	0	0	0

Name	-	4-32	4-33	4-34	4-35	4-36	4-37	4-38	4-39	4-40	4-41	4-42	4-43	4-44
Temperature	(°C)	93	92	95	105	99	99	99	26	13	17	17	17	19
Pressure	(bar)	1	2	2	2	2	2	2	1	1	1	1	1	1
Liquid fraction	-	1	1	0.92	0.92	0.99	0.99	0.99	0.38	0.38	0.33	0.33	0.33	0
Vapor fraction	-	0	0	0	0	0	0	0	0	0	0	0	0	0
Solid fraction	-	0	0	0.08	0.08	0.01	0.01	0.01	0.62	0.62	0.67	0.67	0.67	1
Mass flow	(kg/h)	71901	6063	167570	167570	167570	148505	19064	251943	251943	251953	232879	19074	12738
H2	(kg/h)	0	0	0	0	0	0	0	0	0	0	0	0	0
N2	(kg/h)	1	0	0	0	0	0	0	0	0	0	0	0	0
O2	(kg/h)	24.5	0	0	0	0	0	0	0	0	0	0	0	0
AR	(kg/h)	0	0	0	0	0	0	0	0	0	0	0	0	0
CO2	(kg/h)	38	0	0	0	0	0	0	0	0	0	0	0	0
H2O	(kg/h)	71211.3	6063	54110.3	54110.3	54110.2	47954.2	6156.1	81277.3	81277.3	81274.1	75121.2	6152.9	0
BEN	(kg/h)	0	0	0	0	0	0	0	0	0	0	0	0	0
TOLUENE	(kg/h)	0	0	0	0	0	0	0	0	0	0	0	0	0
ANE	(kg/h)	0	0	0	0	0	0	0	0	0	0	0	0	0
MTHYLANE	(kg/h)	0	0	0	0	0	0	0	0	0	0	0	0	0
CXPROX	(kg/h)	0	0	0	0	0	0	0	0	0	0	0	0	0
CHA	(kg/h)	0	0	0	0	0	0	0	0	0	0	0	0	0
CHN	(kg/h)	626.3	0	0	0	0	0	0	0	0	0	0	0	0
GA	(kg/h)	0	0	18.6	18.6	18.6	16.5	2.1	27.9	27.9	27.9	25.8	2.1	0
AA	(kg/h)	0	0	99493.4	99493.4	112262.7	99490.7	12772	14943.3	14943.3	2349.1	2171.3	177.8	0
AA(S)	(kg/h)	0	0	13917.3	13917.3	1148	1017.4	130.6	155649.4	155649.4	168256.7	155518.8	12737.9	12737.9
KOH	(kg/h)	0	0	30.2	30.2	30.2	26.7	3.4	45.3	45.3	45.3	41.9	3.4	0

Name	-	4-45	4-46	4-47	4-48	4-49	AIR-IN	BEN-IN	H2-IN	H2OIN1	H2OIN2	KOHIN
Temperature	(°C)	19	81	27	96	81	25	210	210	25	25	25
Pressure	(bar)	1	1	1	1	1	1	50	50	50	2	50
Liquid fraction	-	1	1	1	0.98	1	0	1	0	1	1	1
Vapor fraction	-	0	0	0	0.02	0	1	0	1	0	0	0
Solid fraction	-	0	0	0	0	0	0	0	0	0	0	0
Mass flow	(kg/h)	6336	165973	6578	73859	167200	28959	8797	684	5539	6063	683
H2	(kg/h)	0	0	0	0.1	0	0	0	681	0	0	0
N2	(kg/h)	0	0	0	13.4	0	21884.1	0	0	0	0	0
O2	(kg/h)	0	0	0	141.7	0	6703.7	0	0	0	0	0
AR	(kg/h)	0	0	0	0.3	0	371.5	0	3.4	0	0	0
CO2	(kg/h)	0	0	0	191.8	0	0	0	0	0	0	0
H2O	(kg/h)	6152.9	165789.6	5320.3	72868	167012.6	0	0	0	5538.5	6063	0
BEN	(kg/h)	0	0	0	0	0	0	8787.8	0	0	0	0
TOLUENE	(kg/h)	0	0	0	0	0	0	9.2	0	0	0	0
ANE	(kg/h)	0	0	0	0	0	0	0	0	0	0	0
MTHYLANE	(kg/h)	0	0	0	0.4	0	0	0	0	0	0	0
CXPROX	(kg/h)	0	0	0	0	0	0	0	0	0	0	0
CHA	(kg/h)	0	0	0	0	0	0	0	0	0	0	0
CHN	(kg/h)	0	3.1	0	643.1	3.2	0	0	0	0	0	0
GA	(kg/h)	2.1	2.2	420.9	0	2.3	0	0	0	0	0	0
AA	(kg/h)	177.8	174.8	153.8	0	178.3	0	0	0	0	0	0
AA(S)	(kg/h)	0	0	0	0	0	0	0	0	0	0	0
KOH	(kg/h)	3.4	3.4	683.2	0	3.4	0	0	0	0	0	682.6

C.3. Biomass Based Process Stream Results

Name	-	01-01	01-02	01-03	01-04	01-05	01-06	01-07	01-08	01-09	01-10
Temperature	(°C)	82	95	95	95	30	80	80	25	25	25
Pressure	(bar)	1	1	1	1	1	1	1	1	1	1
Liquid fraction	-	0.98	0.94	0	1	1	0	1	1	1	1
Vapor fraction	-	0.02	0.06	1	0	0	1	0	0	0	0
Solid fraction	-	0	0	0	0	0	0	0	0	0	0
Mass flow	(kg/h)	280000	280000	17547	262453	262453	8011	859058	859058	604616	604616
MA	(kg/h)	13118.4	13118.4	0.1	13118.3	13118.3	0	803.1	803.1	565.2	565.2
MAA(S)	(kg/h)	0	0	0	0	0	0	0	0	0	0
MAA(AQ)	(kg/h)	0	0	0	0	0	0	0	0	0	0
MAA-	(kg/h)	0	0	0	0	0	0	0	0	0	0
MAA-2	(kg/h)	0	0	0	0	0	0	0	0	0	0
GLUCOSE	(kg/h)	854	854	0	854	854	0	2883.4	2883.4	2029.4	2029.4
H2O	(kg/h)	261075.9	261138.9	13106.7	248032.3	248034.9	4049.4	810012.6	810019.2	570102.1	570102.1
H2	(kg/h)	0	0	0	0	0	273.6	1.7	1.7	1.2	1.2
T3HDA	(kg/h)	0	0	0	0	0	0	44104.4	44104.4	31041.2	31041.2
T3A(S)	(kg/h)	0	0	0	0	0	0	0	0	0	0
T3A(AQ)	(kg/h)	0	0	0	0	0	0	0	0	0	0
T3A-	(kg/h)	0	0	0	0	0	0	0	0	0	0
T3A-2	(kg/h)	0	0	0	0	0	0	0	0	0	0
H+	(kg/h)	0	0	0	0	0	0	0	0	0	0
OH-	(kg/h)	0.2	0.4	0	0.4	0.4	0	1.8	1.5	1.1	1.1
AR	(kg/h)	0	0	0	0	0	0	0	0	0	0
NH4+	(kg/h)	120	53.2	0	53.2	66.3	0	133.3	171.3	120.5	120.5
H2SO4	(kg/h)	0	0	0	0	0	0	0	0	0	0
SALT4	(kg/h)	0	0	0	0	0	0	0	0	0	0
SALT1	(kg/h)	0	0	0	0	0	0	0	0	0	0
HSO4-	(kg/h)	0	0	0	0	0	0	0	0	0	0
SO4--	(kg/h)	0	0	0	0	0	0	0	0	0	0
O2	(kg/h)	4018.2	4018.2	4016.7	1.5	1.5	3624.2	8.7	8.7	6.1	6.1
CO2	(kg/h)	176.1	336.3	334.9	1.3	0	36.6	1.1	0	0	0
SALT2	(kg/h)	0	0	0	0	0	0	0	0	0	0
HCO3-	(kg/h)	378.1	168.5	0	168.5	117.1	0	395.2	245.7	172.9	172.9
CO3--	(kg/h)	7.2	2.9	0	2.9	44.7	0	17.7	143.8	101.2	101.2
N2	(kg/h)	1.3	1.3	1.3	0	0	0	0	0	0	0
NH3	(kg/h)	238.6	303.8	87.6	216.2	200.9	27.2	682.2	640	450.4	450.4
SALT3	(kg/h)	0	0	0	0	0	0	0	0	0	0
NH2COO-	(kg/h)	12	4	0	4	14.6	0	12.8	35.2	24.8	24.8
LIME	(kg/h)	0	0	0	0	0	0	0	0	0	0

Name	-	01-11	01-12	01-13	01-14	01-15	01-16	01-17	01-18	01-19	01-20	01-21	01-22	2-0
Temperature	(°C)	80	80	25	204	25	172	25	25	25	25	25	180	25
Pressure	(bar)	1	1	1	3.5	3.5	10	10	1	3.5	10	1	30	1
Liquid fraction	-	0.03	0	0	0	0	0	0	1	1	1	1	0	1
Vapor fraction	-	0.97	1	1	1	1	1	1	0	0	0	0	1	0
Solid fraction	-	0	0	0	0	0	0	0	0	0	0	0	0	0
Mass flow	(kg/h)	5699	2312	362	362	303	303	288	1950	59	15	2024	288	254440
MA	(kg/h)	0	0	0	0	0	0	0	0	0	0	0	0	237.9
MAA(S)	(kg/h)	0	0	0	0	0	0	0	0	0	0	0	0	0
MAA(AQ)	(kg/h)	0	0	0	0	0	0	0	0	0	0	0	0	0
MAA-	(kg/h)	0	0	0	0	0	0	0	0	0	0	0	0	0
MAA-2	(kg/h)	0	0	0	0	0	0	0	0	0	0	0	0	0
GLUCOSE	(kg/h)	0	0	0	0	0	0	0	0	0	0	0	0	854
H2O	(kg/h)	2024.7	2024.7	80.6	80.6	22.5	22.5	7.8	1944	58.1	14.7	2016.8	7.8	239915.5
H2	(kg/h)	0	273.6	273.6	273.6	273.6	273.6	273.6	0	0	0	0	273.6	0.5
T3HDA	(kg/h)	0	0	0	0	0	0	0	0	0	0	0	0	13063.1
T3A(S)	(kg/h)	0	0	0	0	0	0	0	0	0	0	0	0	0
T3A(AQ)	(kg/h)	0	0	0	0	0	0	0	0	0	0	0	0	0
T3A-	(kg/h)	0	0	0	0	0	0	0	0	0	0	0	0	0
T3A-2	(kg/h)	0	0	0	0	0	0	0	0	0	0	0	0	0
H+	(kg/h)	0	0	0	0	0	0	0	0	0	0	0	0	0
OH-	(kg/h)	0	0	0	0	0	0	0	0.1	0	0	0.1	0	0.4
AR	(kg/h)	0	0	0	0	0	0	0	0	0	0	0	0	0
NH4+	(kg/h)	0	0	0	0	0	0	0	0.1	0	0	0.1	0	50.7
H2SO4	(kg/h)	0	0	0	0	0	0	0	0	0	0	0	0	0
SALT4	(kg/h)	0	0	0	0	0	0	0	0	0	0	0	0	0
SALT1	(kg/h)	0	0	0	0	0	0	0	0	0	0	0	0	0
HSO4-	(kg/h)	0	0	0	0	0	0	0	0	0	0	0	0	0
SO4–	(kg/h)	0	0	0	0	0	0	0	0	0	0	0	0	0
O2	(kg/h)	3624.2	0	0	0	0	0	0	0	0	0	0	0	2.6
CO2	(kg/h)	36.6	0	0	0	0	0	0	0	0	0	0	0	0
SALT2	(kg/h)	0	0	0	0	0	0	0	0	0	0	0	0	0
HCO3-	(kg/h)	0.1	0	0	0	0	0	0	0	0	0	0	0	72.8
CO3–	(kg/h)	0	0	0	0	0	0	0	0	0	0	0	0	42.6
N2	(kg/h)	0	0	0	0	0	0	0	0	0	0	0	0	0
NH3	(kg/h)	13.6	13.6	7.4	7.4	6.8	6.8	6.4	6.1	0.6	0.4	7.1	6.4	189.5
SALT3	(kg/h)	0	0	0	0	0	0	0	0	0	0	0	0	0
NH2COO-	(kg/h)	0	0	0	0	0	0	0	0	0	0	0	0	10.4
LIME	(kg/h)	0	0	0	0	0	0	0	0	0	0	0	0	0

Name	-	02-01	02-02	02-03	02-04	02-05	02-06	02-07	02-08	02-09	02-10	02-11	02-12	02-13
Temperature	(°C)	25	30	25	15	20	2	2	2	0	0	2	3	3
Pressure	(bar)	1	1	1	1	1	1	1	1			1	1	1
Liquid fraction	-	0.95	1	1	1	0.96	0.96	0.96	0.96	0	0	0.96	1	1
Vapor fraction	-	0	0	0	0	0	0	0	0	0	0	0	0	0
Solid fraction	-	0.05	0	0	0	0.04	0.04	0.04	0.04	0	0	0.04	0	0
Mass flow	(kg/h)	254629	295846	295846	295846	309281	309281	309281	309281	0	0	309281	295631	297620
MA	(kg/h)	0	0	0	0	0	0	0	0	0	0	0	0	0
MAA(S)	(kg/h)	0	0	0	0	231.6	241.7	241.7	241.7	0	0	241.7	0	0
MAA(AQ)	(kg/h)	0	0	0	0	0	0	0	0	0	0	0	0	0
MAA-	(kg/h)	233.6	0.9	0.7	0.4	12.9	2.9	2.9	2.9	0	0	2.9	2.9	2.9
MAA-2	(kg/h)	9.3	240.3	240.5	240.8	0	0	0	0	0	0	0	0	0
GLUCOSE	(kg/h)	854	854	854	854	854	854	854	854	0	0	854	852.1	852.1
H2O	(kg/h)	239950	278184	278184	278183	279840	279840	279840	279840	0	0	279840	279226	279226
H2	(kg/h)	0.5	0.5	0.5	0.5	0.5	0.5	0.5	0.5	0	0	0.5	0.5	0.5
T3HDA	(kg/h)	0	0	0	0	0	0	0	0	0	0	0	0	0
T3A(S)	(kg/h)	11497.1	0	0	0	13232.8	13242.8	12758.2	12758.2	0	0	12758.2	0	0
T3A(AQ)	(kg/h)	0	0	0	0	0	0	484.6	484.6	0	0	484.6	483.6	483.6
T3A-	(kg/h)	1669.7	49.8	39.8	23.7	12.9	2.9	2.9	2.9	0	0	2.9	2.9	2.9
T3A-2	(kg/h)	66.5	13013.7	13023.6	13039.6	0	0	0	0	0	0	0	0	0
H+	(kg/h)	0.1	0	0	0	16.3	21.1	21.1	21.2	0	0	21.2	20.9	20.3
OH-	(kg/h)	0	0	0	0	0	0	0	0	0	0	0	0	0
AR	(kg/h)	0	0	0	0	0	0	0	0	0	0	0	0	0
NH4+	(kg/h)	254.6	3359.2	3360.8	3363.5	3376.2	3376.2	3376.2	3376.2	0	0	3376.2	3368.8	3368.8
H2SO4	(kg/h)	0	0	0	0	0	0	0	0	0	0	0	0	0
SALT4	(kg/h)	0	0	0	0	0	0	0	0	0	0	0	0	0
SALT1	(kg/h)	0	0	0	0	0	0	0	0	0	0	0	0	0
HSO4-	(kg/h)	0	0	0	0	3663.7	3189.2	3189.2	3183.1	0	0	3183.1	3200.9	3252.9
SO4–	(kg/h)	0	0	0	0	7947.1	8416.6	8416.6	8422.7	0	0	8422.7	8379.7	8328.3
O2	(kg/h)	2.6	2.6	2.6	2.6	2.6	2.6	2.6	2.6	0	0	2.6	2.6	2.6
CO2	(kg/h)	91.1	5.4	4.5	3	91.4	91.4	91.4	91.4	0	0	91.4	91.2	91.2
SALT2	(kg/h)	0	0	0	0	0	0	0	0	0	0	0	0	0
HCO3-	(kg/h)	0.4	117.8	119	120.8	0	0	0	0	0	0	0	0	0
CO3–	(kg/h)	0	0.3	0.4	0.5	0	0	0	0	0	0	0	0	0
N2	(kg/h)	0	0	0	0	0	0	0	0	0	0	0	0	0
NH3	(kg/h)	0	15.8	14.2	11.6	0	0	0	0	0	0	0	0	0
SALT3	(kg/h)	0	0	0	0	0	0	0	0	0	0	0	0	0
NH2COO-	(kg/h)	0	1	1	1.2	0	0	0	0	0	0	0	0	0
LIME	(kg/h)	0	0	0	0	0	0	0	0	0	0	0	0	1989

Name	-	02-14	02-15	02-16	02-17	02-18	02-19	02-20	02-21	02-22	02-23	02-24	02-25	02-26
Temperature	(°C)	4	1	80	59	3	22	92	96	100	97	97	97	97
Pressure	(bar)	1	1	1	1	1	2	2	2	2	2	2	2	2
Liquid fraction	-	1	1	1	1	0.05	0.73	0.73	0.94	0.94	1	1	1	1
Vapor fraction	-	0	0	0	0	0	0	0	0	0	0	0	0	0
Solid fraction	-	0	0	0	0	0.95	0.27	0.27	0.06	0.06	0	0	0	0
Mass flow	(kg/h)	297620	297620	297620	297620	13650	48097	48097	240485	240485	240485	240485	192388	192388
MA	(kg/h)	0	0	0	0	0	0	0	0	0	0	0	0	0
MAA(S)	(kg/h)	0	0.2	0	0	241.7	233.5	233.5	233.5	172.6	172.6	0	0	0
MAA(AQ)	(kg/h)	0	0	0	0	0	0	0	690.2	690.2	690.2	862.8	690.2	690.2
MAA-	(kg/h)	2.9	2.7	2.9	2.9	0	8.1	8.1	282.7	343.2	343.2	343.2	274.6	274.6
MAA-2	(kg/h)	0	0	0	0	0	0	0	0.1	0.1	0.1	0.1	0.1	0.1
GLUCOSE	(kg/h)	852.1	852.1	852.1	852.1	1.9	1.9	1.9	9.4	9.4	9.4	9.4	7.5	7.5
H2O	(kg/h)	279226	279226	279226	279226	613.9	35061	35061	175305	175305	175305	175305	140244	140244
H2	(kg/h)	0.5	0.5	0.5	0.5	0	0	0	0	0	0	0	0	0
T3HDA	(kg/h)	0	0	0	0	0	0	0	0	0	0	0	0	0
T3A(S)	(kg/h)	0	0.2	0	0	12758.2	12750	12750	13569.2	13508.2	1024	1024	819.2	819.2
T3A(AQ)	(kg/h)	483.6	483.6	483.6	483.6	1.1	1.1	1.1	49942.3	49942.3	62426.6	62426.6	49941.2	49941.2
T3A-	(kg/h)	2.9	2.7	2.9	2.9	0	8.1	8.1	282.7	343.2	343.2	343.2	274.6	274.6
T3A-2	(kg/h)	0	0	0	0	0	0	0	0.1	0.1	0.1	0.1	0.1	0.1
H+	(kg/h)	20	20.7	4.7	7.5	0	0.2	0.2	3.5	4.2	4.2	4.2	3.3	3.3
OH-	(kg/h)	0	0	0	0	0	0	0	0	0	0	0	0	0
AR	(kg/h)	0	0	0	0	0	0	0	0	0	0	0	0	0
NH4+	(kg/h)	3368.8	3368.8	3368.8	3368.8	7.4	7.4	7.4	37	37	37	37	29.6	29.6
H2SO4	(kg/h)	0	0	0	0	0	0	0	0	0	0	0	0	0
SALT4	(kg/h)	0	0	0	0	0	0	0	0	0	0	0	0	0
SALT1	(kg/h)	0	0	0	0	0	0	0	0	0	0	0	0	0
HSO4-	(kg/h)	3281.9	3213.1	4756.3	4490.9	7	5.2	5.2	96	113.5	113.5	113.5	90.8	90.8
SO4–	(kg/h)	8299.6	8367.6	6840.4	7103.1	18.4	20.3	20.3	32	14.6	14.6	14.6	11.7	11.7
O2	(kg/h)	2.6	2.6	2.6	2.6	0	0	0	0	0	0	0	0	0
CO2	(kg/h)	91.2	91.2	91.2	91.2	0.2	0.2	0.2	1	1	1	1	0.8	0.8
SALT2	(kg/h)	0	0	0	0	0	0	0	0	0	0	0	0	0
HCO3-	(kg/h)	0	0	0	0	0	0	0	0	0	0	0	0	0
CO3–	(kg/h)	0	0	0	0	0	0	0	0	0	0	0	0	0
N2	(kg/h)	0	0	0	0	0	0	0	0	0	0	0	0	0
NH3	(kg/h)	0	0	0	0	0	0	0	0	0	0	0	0	0
SALT3	(kg/h)	0	0	0	0	0	0	0	0	0	0	0	0	0
NH2COO-	(kg/h)	0	0	0	0	0	0	0	0	0	0	0	0	0
LIME	(kg/h)	1989	1989	1989	1989	0	0	0	0	0	0	0	0	0

Name	-	02-27	02-28	2-29	2-30	2-31	2-32	2-33	2-34	2-35	2-36	BROTH-IN	H2OIN	H2SO4IN
Temperature	(°C)	97	30	19	15	17	17	17	17	18	18	25	25	25
Pressure	(bar)	2	2	2	2	2	2	2	2	1	1	1	2	1
Liquid fraction	-	1	1	0.78	0.78	0.74	0.74	0.74	0.74	0	1	0.99	1	1
Vapor fraction	-	0	0	0	0	0	0	0	0	0	0	0.01	0	0
Solid fraction	-	0	0	0.22	0.22	0.26	0.26	0.26	0.26	1	0	0	0	0
Mass flow	(kg/h)	48097	48097	332613	332613	332613	284516	284516	48097	12350	35747	280000	34447	13436
MA	(kg/h)	0	0	0	0	0	0	0	0	0	0	13118.4	0	0
MAA(S)	(kg/h)	0	0	0	0	0	0	0	0	0	0	0	0	0
MAA(AQ)	(kg/h)	172.6	172.6	1193.3	1193.3	1193.3	1020.7	1020.7	172.6	0	172.6	0	0	0
MAA-	(kg/h)	68.6	68.6	474.5	474.5	474.5	405.9	405.9	68.6	0	68.6	0	0	0
MAA-2	(kg/h)	0	0	0.1	0.1	0.1	0.1	0.1	0	0	0	0	0	0
GLUCOSE	(kg/h)	1.9	1.9	13	13	13	11.1	11.1	1.9	0	1.9	854	0	0
H2O	(kg/h)	35061	35061	242464	242464	242464	207403	207403	35061	0	35061	261017	34447	1620
H2	(kg/h)	0	0	0	0	0	0	0	0	0	0	0	0	0
T3HDA	(kg/h)	0	0	0	0	0	0	0	0	0	0	0	0	0
T3A(S)	(kg/h)	204.8	204.8	73263.2	73263.2	85408.8	73058.4	73058.4	12350.4	12350.4	0	0	0	0
T3A(AQ)	(kg/h)	12485.3	12485.3	14494.8	14494.8	2349.2	2009.5	2009.5	339.7	0	339.7	0	0	0
T3A-	(kg/h)	68.6	68.6	474.5	474.5	474.5	405.9	405.9	68.6	0	68.6	0	0	0
T3A-2	(kg/h)	0	0	0.1	0.1	0.1	0.1	0.1	0	0	0	0	0	0
H+	(kg/h)	0.8	0.8	5.8	5.8	5.8	4.9	4.9	0.8	0	0.8	0	0	121.6
OH-	(kg/h)	0	0	0	0	0	0	0	0	0	0	0.1	0	0
AR	(kg/h)	0	0	0	0	0	0	0	0	0	0	0	0	0
NH4+	(kg/h)	7.4	7.4	51.2	51.2	51.2	43.8	43.8	7.4	0	7.4	211	0	0
H2SO4	(kg/h)	0	0	0	0	0	0	0	0	0	0	0	0	0.1
SALT4	(kg/h)	0	0	0	0	0	0	0	0	0	0	0	0	0
SALT1	(kg/h)	0	0	0	0	0	0	0	0	0	0	0	0	0
HSO4-	(kg/h)	22.7	22.7	156.9	156.9	156.9	134.2	134.2	22.7	0	22.7	0	0	11668.7
SO4–	(kg/h)	2.9	2.9	20.2	20.2	20.2	17.3	17.3	2.9	0	2.9	0	0	25
O2	(kg/h)	0	0	0	0	0	0	0	0	0	0	4018.2	0	0
CO2	(kg/h)	0.2	0.2	1.4	1.4	1.4	1.2	1.2	0.2	0	0.2	3.3	0	0
SALT2	(kg/h)	0	0	0	0	0	0	0	0	0	0	0	0	0
HCO3-	(kg/h)	0	0	0	0	0	0	0	0	0	0	510.7	0	0
CO3–	(kg/h)	0	0	0	0	0	0	0	0	0	0	75	0	0
N2	(kg/h)	0	0	0	0	0	0	0	0	0	0	1.3	0	0
NH3	(kg/h)	0	0	0	0	0	0	0	0	0	0	142	0	0
SALT3	(kg/h)	0	0	0	0	0	0	0	0	0	0	0	0	0
NH2COO-	(kg/h)	0	0	0	0	0	0	0	0	0	0	49.5	0	0
LIME	(kg/h)	0	0	0	0	0	0	0	0	0	0	0	0	0

Name	-	LIMEIN	NH3IN
Temperature	(°C)	25	25
Pressure	(bar)	1	1
Liquid fraction	-	1	1
Vapor fraction	-	0	0
Solid fraction	-	0	0
Mass flow	(kg/h)	1989	41216
MA	(kg/h)	0	0
MAA(S)	(kg/h)	0	0
MAA(AQ)	(kg/h)	0	0
MAA-	(kg/h)	0	0
MAA-2	(kg/h)	0	0
GLUCOSE	(kg/h)	0	0
H2O	(kg/h)	0	38265
H2	(kg/h)	0	0
T3HDA	(kg/h)	0	0
T3A(S)	(kg/h)	0	0
T3A(AQ)	(kg/h)	0	0
T3A-	(kg/h)	0	0
T3A-2	(kg/h)	0	0
H+	(kg/h)	0	0
OH-	(kg/h)	0	3.4
AR	(kg/h)	0	0
NH4+	(kg/h)	0	3.6
H2SO4	(kg/h)	0	0
SALT4	(kg/h)	0	0
SALT1	(kg/h)	0	0
HSO4-	(kg/h)	0	0
SO4–	(kg/h)	0	0
O2	(kg/h)	0	0
CO2	(kg/h)	0	0
SALT2	(kg/h)	0	0
HCO3-	(kg/h)	0	0
CO3–	(kg/h)	0	0
N2	(kg/h)	0	0
NH3	(kg/h)	0	2943.8
SALT3	(kg/h)	0	0
NH2COO-	(kg/h)	0	0
LIME	(kg/h)	1989	0